Unified design and validation of an AEB and ACC system considering road conditions

Hegeman, J.J.J.

Award date:
2020

Technische Universiteit
Eindhoven
University of Technology

Declaration concerning the TU/e Code of Scientific Conduct for the Master's thesis

I have read the TU/e Code of Scientific Conduct[i].

I hereby declare that my Master's thesis has been carried out in accordance with the rules of the TU/e Code of Scientific Conduct

Date

10-04-2020

Name

Jesper Hegeman

ID-number

0866066

Signature

Submit the signed declaration to the student administration of your department.

[i] See: http://www.tue.nl/en/university/about-the-university/integrity/scientific-integrity/
The Netherlands Code of Conduct for Academic Practice of the VSNU can be found here also.
More information about scientific integrity is published on the websites of TU/e and VSNU

Eindhoven University of Technology
Department of Mechanical Engineering
Dynamics & Control

Unified design and validation of an AEB and ACC system considering road conditions

Master Thesis

J.J.J. Hegeman
s138711
DC report number: DC 2020.045

Supervisors:
A. Forrai (Siemens)
N. van de Wouw (TU/e)

Eindhoven, March 2020

Preface

This report is the result of a master thesis project at Siemens in Helmond in fulfillment of my graduation at the Eindhoven University of Technology,

I would like to thank Nathan van de Wouw at TU/e and Forrai Alexandru at Siemens for providing the oppurtunity of this master's project, their support, their guidance and criticism. Furthermore I would like to thank Igo Besselink and Emilia Silvas for participating in my graduation committee.

Further, I would like to thank my family, roommates and girlfriend for their mental support.

I hope you enjoy your reading.

Jesper Hegeman

Executive summary

Problem context

In the year 2000, more than 200,000 people were heavily injured and 40,000 people died in road traffic in the European Union. In 2001, these numbers have led the European Commission to define its new long term zero-vision, by setting a new goal to reduce all fatalities to a value close to zero by 2050 [4]. In 2017, 25,300 people died and 135,00 people were heavily injured, which is already a huge improvement [1]. In the last two decades, safer cars have been developed and new Advanced Driver Assistance Systems (ADAS) systems have been implemented in production cars, such as Autonomous Emergency Braking (AEB) and Adaptive Cruise Control (ACC), which have led to less collisions. In current production cars, the AEB and ACC systems are below SAE level 3. The SAE level is a measure which shows the level of driving automation. For ADAS systems below level 3, the driver is legally liable and has to adapt his driving style to the road conditions; therefore the driver can adapt certain ADAS settings. For example, the distance to other vehicles can be chosen in case of the ACC or the driver can set the intervention settings for an AEB system corresponding to the current road conditions.

The ADAS systems that are in current vehicles must be developed to achieve SAE level 3. For SAE level 3, the driver is not required to monitor the environment. Since the ADAS system will automatically adapt its behavior to the environment, for example to the road condition. This leads to the following problem statement for this research project:

Limited knowledge about the road conditions leads to a large amount of traffic accidents per year. The current AEB and ACC systems are less effective on slippery roads, since information about the road is not yet available to be included in the design.

Research goals and questions

In this research a practical goal is defined, which is derived from the problem statement and business scope. Furthermore a scientific goal is derived which encompasses the scientific contribution. The research practical goal is to provide an unified AEB and ACC system which is able to have robust performance considering the variation of the road conditions as encountered in practice. Therefore a non-linear tyre model which can simulate different road conditions must be modelled and validated with a vehicle model from Siemens Simcenter Amesim. The scientific goal is to provide scientific insights in the usage of a neural network to estimate the maximum road friction coefficient during driving and provide decision algorithms for the AEB and ACC systems which can use the estimated to improve the safety. This leads to a main research question:

How can we design an unified AEB and ACC system which is able to have robust performance considering the variation of the road conditions?

In order to answer this research question a vehicle model which is able to capture the vehicle behavior on different road surfaces is presented. Subsequently, a method to control the vehicle's acceleration with a slip controller by encompassing information about the road conditions is developed and discussed. Furthermore, a unified AEB and ACC system is developed which considers information about the road condition. Lastly, a neural network is trained to estimate the maximum road friction coefficient based on data obtained from a Pacejka tyre model.

Vehicle modelling

To test and validate the ADAS systems, a vehicle model is needed. A dynamic non-linear tyre model is needed to capture the behavior of the car on different road conditions. In this research, three different vehicle models are described. First, a model considering only longitudinal dynamics is described based on the vehicle models from [40] and [54]; thereafter the longitudinal model is

extended to a model considering longitudinal, lateral, roll and yaw dynamics based on the roll axis vehicle model from [49] and [23] . Finally, the single-corner vehicle model from [54] is presented, which is used to design a slip controller. To validate the vehicle behavior, the model is validated with a vehicle model from Simcenter Amesim, which is a good model to validate against since that model is validated with real vehicle measurements.

ADAS

In this research, an AEB and ACC system is developed which is able to have robust performance considering the variation of the road conditions.

Autonomous Emergency Braking is braking that is applied automatically by the vehicle in response to the detection of a likely collision. The primary goal of AEB technology is to prevent crashes by detecting a potential conflict and alerting the driver, and, in many systems, aiding in brake application or automatically applying the brakes [25]. A typical AEB system includes an environment perception system, an upper-level controller and a lower-level controller. The upper-level controller is a threat-assessment and decision-making algorithm. The threat-assessment algorithm decides if a situation is safe or unsafe, and can warn the driver or/and choose to perform an automatic emergency brake in critical hazardous situations, where the lower-level system controls the acceleration of the vehicle to the desired acceleration provided by the upper-level controller.

Adaptive Cruise Control originates from Cruise Control, which today is a widespread functionality in modern vehicles. CC regulates the vehicle speed actuating the throttle only, via tracking of speed v that is set by the driver. ACC automatically adapts the vehicle's speed depending on a predecessor's behavior, actuating the throttle as well as the brake system. The goal of ACC is partial automation of the longitudinal vehicle control and the reduction of the workload of the driver with the aim to support and relieve the driver in a convenient manner.

In this research, Time-to-Collision (TTC) is used to asses the threat. The activation times for the AEB are scaled proportionally with the road conditions. Therefore, the AEB system is braking earlier on slippery roads compared to high friction dry roads. Since information about the road conditions is needed, a maximum road friction estimator is designed. The unified AEB and ACC system can be seen as two independent systems running simultaneously. However, the system is optimized to work fluently by designing a smart state machine. Both systems have a positive influence on each other. The ACC system is maintaining the desired relative distance D_{ref} and tracks the preceding vehicle's speed v_p, therefore the ACC system can be seen as another pre-braking stage in some situations, which can lead to more comfort and less interventions from the AEB system. On the other hand the AEB system leads to a safer experience. Since the maximum deceleration of an ACC system is -2 [$ms^{-}2$], an ACC system could not always avoid a collision. An AEB system is aloud to brake with higher deceleration and, therefore, an AEB system increases the probability to avoid a collision.

The lower-level controller controls the acceleration via controlling the wheel slips. First a PID-controller is designed to control the linearized longitudinal vehicle dynamics with actuator dynamics and delay. It is concluded that the PID-controller can not ensure stability for all working conditions (low velocities or high slips). Thereafter a Youla parameterized controller is used to improve the stability and performance. This controller is able to stabilize the plant for low velocities, however the closed loop system is still not stable for high slip ratios. Therefore the maximum slip setpoint is limited to ensure stability, however the stable region is varying for different road conditions. It is concluded that a maximum road friction estimator could help to ensure stability.

Road friction estimator

A neural network is trained to estimate the maximum road friction coefficient . The estimated maximum road friction coefficient is later used in the upper-level controller and the lower-level controller. Over-estimation leads to smaller activation times (AEB) than required to avoid a collision and can also lead to unstable behavior, which is explained later. Under-estimation leads to earlier activation times than required to avoid a collision and leads to a lower maximum deceleration. The neural network is trained with simulation data obtained from a Pacejka tyre model. To obtain the data, a scenario is designed for every road condition where the vehicle is accelerating and decelerating with 600 random values on a straight road for a certain amount of time. The goal is to minimize the mean squared error between the estimated maximum road friction coefficient and the real value of the maximum road friction coefficient. It is concluded that a certain minimum deceleration or acceleration is needed to accurately estimate the maximum road friction coefficient, therefore a state machine is designed to improve the accuracy of the estimate.

Conclusions

In this research an unified AEB and ACC system is constructed which is able to have robust performance considering the variation of the road conditions in a simulation environment. Therefore a non-linear tyre model which can simulate different road conditions is modelled and validated with a vehicle model from Siemens Simcenter Amesim. Subsequently a slip controller which considers the delayed actuator dynamics is designed to control the acceleration of the vehicle. Furthermore a neural network is trained with simulation data to predict the maximum road friction coefficient. The predicted value of the maximum road friction coefficient is used in the upper-level controller of the AEB algorithm and is used in the slip control algorithm to determine a stable set point for the slip controller. It is concluded that adding information about the road conditions in the upper-level controller of the AEB has positive impact, since the brake actuators are activated earlier, and therefore, the number of collisions on low friction surfaces is decreased.

This research has multiple limitations. The first limitation is that the ADAS systems and the maximum road friction estimator are designed to work on straight roads only. The second limitation is that the neural network is trained and validated with simulation data only. Future research is needed to investigate if the estimator also work with real vehicle data. The third limitation is that closed-loop stability of the Youla parameterized controller can only guarantee stability if the accuracy of the maximum road friction estimator is high enough and the last limitation is that all systems are validated without any sensor or parameter uncertainty.

Table of Contents

List of Figures **xiii**

List of Tables **xvii**

List of Symbols **xix**

List of Abbreviations **xxi**

1 Introduction **1**

1.1 Problem analysis . . . 1

1.1.1 Problem statement . . . 2

1.2 Research goals . . . 2

1.2.1 Practical goal . . . 2

1.2.2 Scientific goal . . . 3

1.3 Research questions . . . 4

1.4 Outline . . . 4

2 Literature study **7**

2.1 AEB performance evaluation in literature . . . 7

2.1.1 Upper-level controller . . . 7

2.1.1.1 Conclusions upper-level controller . . . 10

2.1.2 Lower-level controller . . . 11

2.1.3 Vehicle dynamics . . . 12

2.1.3.1 Sensors . . . 13

2.1.4 Discussion lower-level controller and vehicle dynamics . . . 13

2.2 ACC . . . 14

2.2.1 Upper-level controller . . . 14

2.2.2 Lower-level controller . . . 15

2.2.3 Discussion on existing work on AEB and ACC . . . 16

2.3 Maximum road friction estimator . . . 16

2.3.1 Discussion . . . 18

2.4 Envisioned scientific contribution . . . 18

3 Vehicle modelling **19**

3.1 Longitudinal vehicle model . . . 19

3.1.1 Vehicle and wheel dynamics . . . 19

3.1.2 Longitudinal tyre model . . . 20
3.1.3 Rolling resistance and aerodynamic forces . . . 21
3.1.4 Normal load force . . . 21
3.1.5 Reset integrator friction model . . . 22
3.2 Roll axis vehicle model . . . 26
3.2.1 Vehicle body dynamics . . . 26
3.2.2 Combined longitudinal and lateral dynamics tyre model . . . 28
3.3 Control-oriented vehicle model . . . 29
3.3.1 Model analysis . . . 30
3.3.1.1 Equilibrium points . . . 30
3.3.2 Model linearisation . . . 31
3.3.2.1 Stability analysis . . . 32
3.3.2.2 Sensitivity analysis . . . 33
3.4 Conclusion . . . 34

4 Control system design **37**
4.1 Slip controller . . . 37
4.1.1 Motivation . . . 38
4.1.2 Single-corner model stability and uncertainty analysis . . . 39
4.1.2.1 Stability analysis plant without actuator dynamics . . . 40
4.1.2.2 Stability analysis plant with actuator dynamics . . . 40
4.1.2.3 Uncertainty analysis . . . 41
4.1.3 Youla parameterization . . . 42
4.1.3.1 Implementation . . . 43
4.1.4 Validation . . . 45
4.1.5 Conclusion . . . 49
4.2 Slip control algorithm . . . 50
4.3 Upper level controller . . . 51
4.3.1 Autonomous emergency braking . . . 52
4.3.2 Adaptive cruise control . . . 54
4.4 Conclusions . . . 54

5 Road friction estimator **57**
5.1 Neural Network . . . 58
5.1.1 Data generation . . . 58

5.1.2 Data interpretation . . . 59
5.1.3 Network architecture . . . 61
5.1.4 Analysis of training statistics . . . 62
5.2 Analysis of real-time results . . . 66
5.3 Discussion . . . 68

6 Validation of ADAS systems **69**
6.1 Euro NCAP AEB performance . . . 69
6.1.1 Car-to-Car Rear Stationary performance . . . 69
6.1.2 Car-to-Car Rear Braking performance . . . 70
6.2 ACC performance . . . 77
6.2.1 Situation 1 . . . 78
6.2.2 Situation 2 . . . 79
6.2.3 Situation 3 . . . 79
6.2.4 Situation 4 . . . 79
6.2.5 Situation 5 . . . 79
6.2.6 Situation 6 . . . 80
6.3 Discussion . . . 80

7 Conclusions and recommendations **81**
7.1 Research questions . . . 81
7.1.1 Vehicle model . . . 81
7.1.2 Vehicle control . . . 81
7.1.3 Unification of the AEB and ACC system . . . 82
7.1.4 Maximum road friction estimator . . . 82
7.1.5 Stability . . . 82
7.1.6 Impact . . . 83
7.2 Recommendations and limitations . . . 83
7.3 Future research . . . 84

Bibliography **85**

Appendix **91**

A Simulation results **91**
A.1 Amesim validation . . . 91

A.2 Control . . . 96
A.2.1 Open loop simulation . . . 96
A.2.2 PI control . . . 97
A.2.3 Validation . . . 100
A.3 Neural network . . . 102

B Parameters **104**
B.1 Magic formula 1989 . . . 104
B.2 Magic formula 2002 . . . 105
B.2.1 Longitudinal force F_x . . . 105
B.2.2 Longitudinal force F_y . . . 105
B.2.3 Self aligning moment M_z . . . 106

C requirements **108**
C.1 AEB . . . 108
C.1.1 Requirements . . . 108
C.1.1.1 Control strategy requirements . . . 108
C.1.1.2 General requirements . . . 108
C.1.1.3 Operational limit requirements . . . 109
C.1.1.4 Sensor system . . . 109
C.1.1.5 Performance . . . 109
C.2 ACC . . . 110
C.2.1 Requirements . . . 111
C.2.1.1 Control strategy requirements . . . 111
C.2.1.2 Following capability requirements . . . 112
C.2.1.3 Operational limit requirements . . . 113

List of Figures

1.1 Different SAE levels. 2

1.2 Final deliverable of this research project. 4

2.1 A typical schematic diagram of an AEB system model 7

2.2 Summary of threat-assessment metrices. 8

2.3 A schematic block diagram of an ACC system including the upper-level controller, the lower-level controller and the switching logic [56]. 15

2.4 Classification of the vehicle-fixed methods for determining the maximum road friction coefficient μ_{max} (friction potential) [66]. 17

3.1 Vehicle dynamics 19

3.2 Pacejka curve characteristics. 20

3.3 Friction torque as a function of the angular displacement for the reset integrator model. 22

3.4 The brake input signal T_b and the friction torque T_{frict} of the front wheel. 24

3.5 The front wheel rotational velocity 24

3.6 The stick displacement together with its displacement threshold. 25

3.7 Roll axis vehicle model [55]. 26

3.8 View from above of the roll axis vehicle model with dimensions [55]. 27

3.9 Magic Formula version 5.1: Inputs and Outputs. 28

3.10 Influence of the inclination angle γ, the longitudinal slip κ and the side slip angle α on the Pacejka curve characteristics. 29

3.11 Equilibrium points for the single-corner model in the (κ,T_b) plane (example with $F_z = mg$ and dry asphalt). 31

3.12 $\bar{\kappa}$ as a function of κ for $\bar{T_b} = 1000$. 32

3.13 Magnitude and phase Bode plots of the frequency response associated with $G_\kappa(s)$ are displayed for four different values of $\bar{u}$, with $F_z = mg$, $\bar{\kappa}$ around the peak friction on a dry asphalt. 33

3.14 Magnitude and phase Bode plots of the frequency response associated with $G_\kappa(s)$ are displayed for three different values of F_z, with $u = 25[m/s]$, $\bar{\kappa}$ around the peak friction on a dry asphalt. 34

3.15 Longitudinal force F_x as function of κ for $F_z = mg$ on a a dry asphalt for two different tyre models. 35

3.16 Velocity response from time simulation of double corner model and the roll axis vehicle model with poorly estimated tyre parameters. 35

4.1 The block diagram of full system. 37

4.2 The friction coefficient $\mu_x(\kappa)$ plotted against the longitudinal slip κ for different road conditions. The horizontal dashed line represents the setpoint κ. 38

4.3 The normalised wheel deceleration as function of κ for different road conditions. The horizontal dashed line represents the setpoint η and the vertical dashed line represents the setpoint κ. 39

4.4 Wheel slip closed-loop system with delay and sensor noise. 39

4.5 Stability analysis of closed loop system for different gain and velocities. Blue surface is unstable region and white surface is stable region. 41

4.6 Unity-feedback system. 42

4.7 Magnitude Bode plots of complementary sensitivity T and sensitivity S. 44

4.8 Bode plots of transfer function G_{delay} and open loop transfer function L. 45

4.9 Wheel slip closed-loop system with delay. 45

4.10 The friction coefficient μ as function of κ for different road conditions. 46

4.11 The velocity for different road conditions with initial velocity $u_{init} = 40$. Controller: K_1. Slip setpoint $\kappa = 20$. 46

4.12 The controlled front and rear wheel slip κ_f and κ_r for different road conditions with initial velocity $u_{init} = 40$. Controller: K_1. Slip setpoint $\kappa = 20$. 47

4.13 A zoomed version of Figure 4.12. 48

4.14 The controlled front and rear wheel slip κ_f and κ_r for different initial velocities on dry surface $\mu_{max} = 1$. Controller: K_1. Slip setpoint $\kappa = 20$. 48

4.15 The controlled front and rear wheel slip κ_f and κ_r for different road conditions with initial velocity $u_{init} = 40$. Controller: K_4. Slip setpoint $\kappa = 20$. 49

4.16 The controlled front and rear wheel slip κ_f and κ_r for different initial velocities on dry surface $\mu_{max} = 1$. Controller: K_4. Slip setpoint $\kappa = 20$. 50

4.17 A slip control algorithm to determine a stable wheel-slip setpoint corresponding to the desired acceleration. 50

4.18 The states and transitions of the unified AEB and ACC. Solid line: controllable event Dashed line: uncontrollable. event 52

4.19 Schematic side view of AEB system with inputs. 53

5.1 Tolerable deviation $\Delta\mu_{max}$ in dependence on the real value μ_{max} of the maximum road friction coefficient for different initial longitudinal speeds [41]. 57

5.2 A general workflow for the design of a Neural Network adapted for our use case. . 58

5.3 Block diagram of the proposed estimator. 58

5.4 Simulation results of the acceleration $\dot{u}$ and the front wheel slip κ_f for two different values of μ_{max} over time. 59

5.5 A scatter plot is shown which is taken from the acceleration for different wheel slips for two different values of μ_{max} 60

5.6 The training data with all the unwanted data filtered out. 61

5.7 Neural network architecture [52]. 61

5.8 A performance plot which shows the Mean Squared Error during training for the training, validation and test data. 63

5.9 Regression plot which shows the target and output values of μ_{max} for the training, simulation and test data. 64

5.10 A histogram which shows the error of the estimated μ_{max} for all samples. 64

5.11 A simulation with a test data set which is not used during training of the neural network. 65

5.12 Acceleration during a scenario simulation to validate the neural network. 66

5.13 The estimated and real values of μ_{max} during a scenario as shown in Figure 5.12. . 67

5.14 The estimated and real values of μ_{max} during a scenario as shown in Figure 5.12 with the inclusion of a state machine. 67

6.1 Test scenarios [26]. 70

6.2 Performance rating for every initial velocity for CCRs scenarios [26]. 72

6.3 Two CCRs scenario on a snowy road with an initial velocity of 40 km/h. In the upper plot an AEB with pre-braking phases is used and in the lower plot an AEB system without pre-braking phases is used. 73

6.4 CCR test scenario according to Euro NCAP [26]. 74

6.5 Simulation results CCR braking Scenario 1. 74

6.6 Simulation results CCR braking Scenario 2. 75

6.7 Simulation results CCR braking Scenario 3. 75

6.8 Simulation results CCR braking Scenario 4. 76

6.9 Simulation results of unified AEB and ACC CCR braking Scenario 4. 76

6.10 The desired velocity and the actual velocity during the simulation scenario. 78

6.12 The desired distance and actual distance during the simulation scenario. 78

6.11 The acceleration and jerk during the simulation scenario. 79

A.1 Input signal for a Amesim and Simulink validation. 91

A.2 Comparison of braking torque after friction model between Amesim and Simulink model. 92

A.3 Comparison of velocity between Amesim and Simulink model. 92

A.4 Comparison of front and rear wheel rotational velocity ω_f and ω_r between Amesim and Simulink model. 93

A.5 Comparison of front and rear wheel slips κ_f and κ_r between Amesim and Simulink model. 93

A.6 Comparison of front and rear longitudinal forces F_{x_f} and F_{x_r} between Amesim and Simulink model. 94

A.7 A zoomed plot from Figure A.5 94

A.8 Comparison of front and rear vertical forces F_{z_f} and F_{z_r} between Amesim and Simulink model. 95

A.9 Input torque of open loop simulation without controller on dry asphalt. 96

A.10 Velocity result of open loop simulation without controller on dry asphalt for different input torques. 96

A.11 Slip ratio result of open loop simulation without controller on dry asphalt for different input torques. 97

A.12 Acceleration result of open loop simulation without controller on dry asphalt for different input torques. 97

A.13 Slip ratio result of closed loop simulation with controller on dry asphalt for different velocities. 98

A.14 Slip ratio result of closed loop simulation with controller on different road conditions. 99

A.15 Nyquist diagram of $K(s)G_{actuator}(s)G_{\kappa}(s,u)$. 100

A.16 The controlled front and rear wheel slip κ_f and κ_r for different road conditions with initial velocity $u_{init} = 40$. Controller: K_2. Slip setpoint $\kappa = 20$. 101

A.17 The controlled front and rear wheel slip κ_f and κ_r for different initial velocities on dry surface $\mu_{max} = 1$. Controller: K_2. Slip setpoint $\kappa = 20$. 101

A.18 The controlled front and rear wheel slip κ_f and κ_r for different road conditions with initial velocity $u_{init} = 40$. Controller: K_3. Slip setpoint $\kappa = 20$. 102

A.19 The controlled front and rear wheel slip κ_f and κ_r for different initial velocities on dry surface $\mu_{max} = 1$. Controller: K_3. Slip setpoint $\kappa = 20$. 102

C.1 Test scenarios. [26] 110

C.2 Functional ACC elements[15] 110

C.3 ACC states and transitions. [a] is manual switching [15] 111

C.4 Illustration of clearance. [15] 112

C.5 Zones of detection. zone a: Detection not required, zone b: Detection of vehicles required and zone c: Determination of range required. [15] 112

C.6 Target detection. [15] 113

List of Tables

1.1 Criteria for the maximum road friction estimator. 3

3.1 Pacejka 1989 model parameters. 20

4.1 The desired deceleration for the different threat stages. 53

5.1 Data training parameters and space dimensions. 59

6.1 Results CCRs scenarios of AEB without road information. 71

6.2 Results CCRs scenarios of AEB with road information. 71

6.3 CCR Braking scenarios. 72

A.1 Root mean squared error for different configurations. 103

B.1 Magic formula 1989 parameters. 105

List of symbols

Symbol	Unit	Description
u	ms^{-1}	longitudinal speed of the vehicle centre of mass
ω_f	$rads^{-1}$	angular speed of the front wheel
ω_r	$rads^{-1}$	angular speed of the rear wheel
T_{bf}	Nm	Braking torque front wheel
T_{br}	Nm	Braking torque rear wheel
T_{ff}	Nm	driving torque front wheel
T_{fr}	Nm	driving torque rear wheel
T_{roll_f}	Nm	rolling resistance torque front wheel
T_{roll_r}	Nm	rolling resistance torque rear wheel
F_{xf}	N	front longitudinal tyre-road contact forces
F_{xr}	N	rear longitudinal tyre-road contact forces
J	kgm^2	inertia of the wheel
M	kg	the vehicle's mass
g	ms^-2	the gravitational coefficient
R	m	the wheel radius
D	-	The peak factor which is the maximum longitudinal force
BCD	-	The stiffness factor which is longitudinal slip stiffness (slope of Fx vs. κ curve at the origin)
E	-	The curvature factor which enables to fix the longitudinal slip where the longitudinal force is r
L	-	The asymptotic factor which is the longitudinal force asymptote at high longitudinal slip
S_h	-	The horizontal shift which fix the anti-symmetry center of the curve
S_v	-	The vertical shift which fix the anti-symmetry center of the curve
κ_D	-	The longitudinal slip peak antecedent which is the longitudinal slip related to the maximum lo
b_i	-	constant parameters which are related to specific tyre properties
F_z	-	the vertical force
λ_i	-	Scaling factors Magic formula parameters
$\lambda_{\mu x}$	-	the scaling factor corresponding to maximum road friction coefficient μ_{max}
μ_{max}	-	Maximum tyre-road friction coefficient
V_x	ms^-1	the vehicle velocity
V_{cmin}	-	the minimum velocity where slip equation is valid
R_c	-	the rolling resistance coefficient
ρ	kgm^-2	the air density
C_d	-	the drag coefficient
A	m^2	the maximum vehicle cross area
a	m	the distance from the center of gravity to the front wheel center
b	m	the distance from the center of gravity to the rear wheel center
θ	rad	road inclination angle
θ_w	rad	angular displacement
θ_{w0}	rad	stick displacement threshold
T_{frict}	Nm	Friction torque between tyre and road
T_s	Nm	stiction torque
k_{rel}	m	the stick stiffness
T_c	Nm	the Coulomb friction torque
σ_1	-	the damping coefficient tuned to avoid vibrations when the solids stick together
κ	-	longitudinal slip
F_x	N	longitudinal force acting on wheels
F_y	N	lateral force acting on wheels

M_z	Nm	the self aligning moment
V_{sx}	ms^{-1}	the longitudinal slip velocity
V_x	ms^{-1}	the forward vehicle velocity
$\mu_x(\kappa)$	-	the longitudinal friction coefficient
v	ms^{-1}	lateral velocity
r	$rads^{-1}$	yaw rate
s_1 and s_2	m	the vehicle half track widths
δ	rad	the steering angle

List of abbreviations

ABS	Anti Blocking System
ACC	Adaptive Cruise Control
ADAS	Advanced Driver Assistance Systems
AEB	Autonomous Emergency Braking
AFS	Active Front Steering
B-BAC	Balance-Based Adaptive Control
BTN	Break Threat Number
CC	Cruise Control
CCRs	Car-to-Car Rear stationary
CCRm	Car-to-Car Rear moving
CCRb	Car-to-Car Rear braking
DOF	Degrees Of Freedom
EACC	Enhanced Adaptive Cruise Control
ECU	Electronic Control Unit
ESC	Electronic Stability Control System
FCW	Forward Collision Warning
GVT	Global Vehicle Target
GS	Gain Scheduling
LQR	Linear–Quadratic Regulator
MAE	Mean Absolute Error
MPC	Model Predictive Control
MRAC	Model Reference Adaptive Control
MSD	Minimal Safe Distance
NCAP	New Car Assessment Programme
NHTSA	National Highway Traffic Safety Administration
NMPC	Non-linear Model Predictive Control
PID	Proportional–Integral–Derivative
PSTN	Predictive Steering Threat Number
RHP	Right Half Plane
RMSE	Root Mean Squared Error
SBTM	Single Behavior Threat Metrics
STN	Steering Threat Number
TSM	Terminal Sliding Mode
TTC	Time To Collision
th	time headway
T_{slb}	Time to last second braking
V2V	vehicle to Vehicle
V2I	Vehicle to Infrastructure

1. Introduction

With the development of intelligent techniques, autonomous vehicles have been studied a lot in recent years. Many advanced driver assistance systems (ADAS) have been applied in production cars, for example, the Anti Blocking System (ABS), Electronic Stability Control system (ESC), Active Front Steering (AFS), Forward Collision Warning (FCW), Adaptive Cruise Control (ACC), and Autonomous Emergency Brake (AEB). One of the key technologies of autonomous vehicles is longitudinal collision-avoidance control which can avoid or soften vehicle collision effectively via automated braking.

Siemens has developed PreScan, which is a physics-based simulation platform. PreScan is used in the automotive industry for the development of Advanced Driver Assistance Systems (ADAS) that are based on sensor technologies such as radar, laser/lidar, camera, and GPS. PreScan is also used for designing and evaluating vehicle-to-vehicle (V2V) and vehicle-to-infrastructure (V2I) communication applications as well as autonomous driving applications [57].

The engineering department of Siemens which is located in Helmond, is doing projects regarding ADAS all around the globe. To attract new collaborations with companies Siemens is always developing their current systems. Siemens desires an implementation of both a AEB and ACC system in PreScan, which is able to have robust performance considering the variation of the road conditions as encountered in practice.

1.1 Problem analysis

In the year 2000, more than 200,000 people were heavily injured and 40,000 people died in road traffic in the European Union. In 2001, these numbers have led the European Commission to define its new long term zero-vision, by setting a new goal to reduce all fatalities to a value close to zero by 2050 [4]. In 2017, 25,300 people died and 135,00 people were heavily injured, which is already a significant improvement [1]. In the last two decades, safer cars have been developed and new ADAS systems have been implemented in production cars, such as AEB and ACC, which have led to less collisions. In [3], a literature review was conducted on the causes of all traffic accidents in Germany in the year 2011. It showed that 27 % of all accidents involving personal injuries and passenger cars occurred on slippery roads, where ice was responsible for 5 % of all cases. Poor road conditions lead to a reduced maximum road friction coefficient μ_{max} between the tyre and the road. In most cases, the road surface conditions were not the main accident cause. However, improper driving in combination with a poor road condition was. Improper driving in combination with a slippery road could often not be corrected in time which lead to the accident. The studies show that accidents happen, since the longitudinal speed is not adequately adapted to the road conditions. The driver must use haptic and optical signals to estimate the road surface during driving since no direct measure is available. A robust and reliable estimate of the maximum road friction could be effective in assisting the driver.

Another already proven crucial factor to improve road safety and reduce the number of fatalities are ADAS systems, such as the AEB and ACC. The AEB system is one of the most efficient ways to lower the social cost of traffic accidents. Most rear-end collisions are caused by the distraction of drivers and can be prevented by warning for the danger of a collision and/or braking autonomously if necessary. AEB systems can reduce about 43% rear-end crashes and 50% of rear-end injuries at low-speed cases [14]. The AEB protocols released by Euro NCAP [25] are tested in average conditions to achieve objectivity and convenience of the assessment. It is assumed that the road friction coefficient is nearly 0.9, the road slope is less than 1% grade, and there are no objects interfering with sensor detection. However, the system is less effective on slippery roads [38]. To research this phenomenon, a vehicle model should be used, which includes the tyre-road friction nonlinear dynamics.

In Figure 1.1, the different SAE levels which are a used to measure the level of automation are shown.

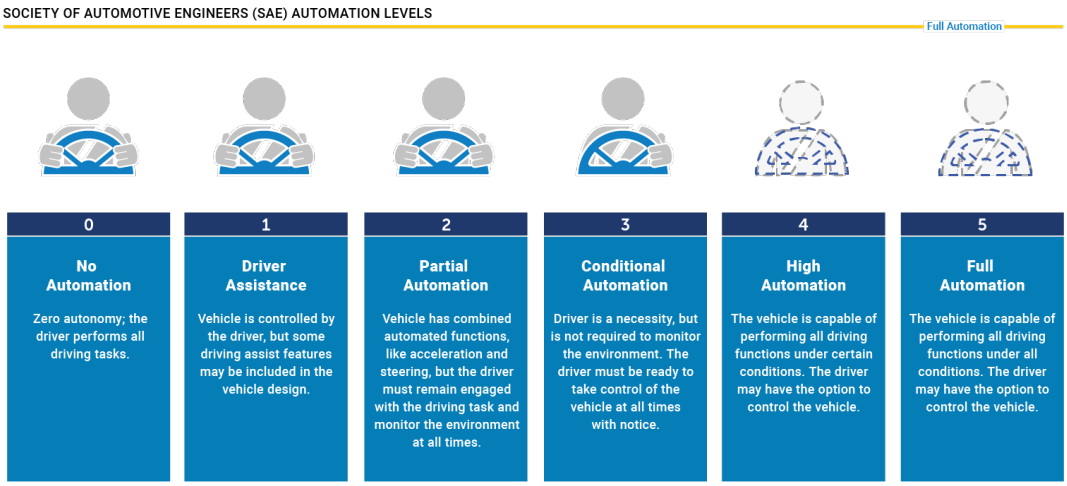

Figure 1.1: Different SAE levels.

In current production cars, the AEB and ACC systems are below SAE level 3. The SAE level is a measure which shows the level of driving automation. For ADAS systems below SAE level 3, the driver is legally liable and has to adapt his driving style to the road conditions; therefore the driver can adapt certain ADAS settings. For example, the distance to other vehicles can be chosen in case of the ACC or the driver can set the intervention settings for an AEB system corresponding to the current road conditions.

The ADAS systems that are in current vehicles must be developed to achieve SAE level 3. For SAE level 3 the driver is not required to monitor the environment, since the ADAS system will automatically adapt its behavior to the environment, for example the road condition. To improve the current AEB and ACC systems, a road friction estimator must be designed to estimate the road conditions. Paper [41] showed that a rough but reliable resolution of classifying three different road conditions is already valuable to improve the traffic safety.

1.1.1 Problem statement

As illustrated in the previous sections, there is a need to further develop the current AEB and ACC systems. This leads to the following problem statement for this research project:

Limited knowledge about the road conditions leads to a large amount of traffic accidents per year. The current AEB and ACC systems are less effective on slippery roads, since information about the road is not yet available to be included in the design.

1.2 Research goals

1.2.1 Practical goal

The practical (business) goal of this research is derived directly from the problem statement and business scope. The practical goal is formulated as follows:

The research should provide an AEB and ACC system which is able to have robust performance considering the variation of the road conditions as encountered in practice. The vehicle model that is used must be validated with a vehicle model from Siemens Simcenter Amesim.

From the literature study it is concluded that an unified AEB and ACC system could be beneficial. The main advantages of this unified strategy include two aspects: The first advantage is that

multiple driving modes can be introduced based on the level of danger. Each driving mode has its maximum acceleration and, therefore, the vehicle longitudinal control can be more intelligent and lead to a more comfortable experience.

The second potential advantage is the computational efficiency of the algorithm. For autonomous vehicles, the computer needs to calculate and process a large number of data, including environmental perception data, positioning data and vehicle driving data, etc. The unified framework design of the longitudinal control algorithm should reduce the complexity of the code and improve the efficiency of operation.

Therefore, the practical goal is extended with an extra preference namely, that the AEB and ACC system should be designed in a unified framework.

1.2.2 Scientific goal

It is apparent that there are multiple research and solution directions that address the identified practical goal. A first scientific goal is to develop a method to estimate the maximum road friction coefficient. Since this is very broad, an elaborate literature review is conducted in Chapter 2 that results in a more detailed explanation of the scientific contribution and relevance of the existing literature. In short, it is concluded that the current proposed road friction estimators do not manage to full-fill all the criteria. The criteria are stated in Table 1.1.

Criteria
No additional sensors needed
Applicability in ADAS
Active intervention not necessary for robust estimate
Online capability of the algorithm
Only longitudinal vehicle states must be used for the estimation
Must be able to detect the maximum road friction coefficient on low and high friction roads.

Table 1.1: Criteria for the maximum road friction estimator.

In [53] an artificial neural network is trained to estimate the maximum road friction coefficient based on the side slip angle α. The neural network had promising results, however a steering input was needed to accurately identify the maximum road friction coefficient. This makes us believe that a neural network could be trained to estimate the maximum road friction coefficient based on the longitudinal slip κ, therefore it is chosen as a further research topic.

Subsequently, the maximum road friction estimator could improve the robustness of the slip controller which will be designed to control the vehicle on different road conditions. Normally an ABS system will increase its braking torque on the wheels until the wheels starts to slip, thereafter the braking torque is limited. If the maximum road friction coefficient estimator can estimate the road friction coefficient accurately enough, the ABS could have a significant improvement in performance by the knowledge of the full vehicle states and operating conditions [58]. If the slip behavior is known, the braking torque can be increased to an optimum, which will be further addressed in Chapter 4.

Concluding, the practical goal can be addressed by estimating the maximum road friction coefficient, which eventually leads to a scientific goal:

Provide scientific insights in the usage of a neural network to estimate the maximum road friction coefficient μ_{max} during driving and provide decision algorithms for the AEB and ACC systems which can use the estimated μ_{max} to improve the safety.

1.3 Research questions

Based on the above discussion a set of research questions are defined. The research questions are both in line with the scientific and practical goal of this research. First, a primary research question is defined to guide this research:

How can we design an unified AEB and ACC system which is able to have robust performance considering the variation of the road conditions?

In support of the main research question, 6 sub-questions are identified.

- What controllers can be used to control the vehicle in order to satisfy our robustness, implementation, performance, and the vehicle operational limit requirements?
- How can we systematically unify the AEB and ACC systems?
- How can we model the vehicle behavior on different road surfaces?
- How can we estimate the maximum road friction coefficient?
- How to prove the stability of the closed-loop system?
- What is the impact of implementing information about the road condition in the threat assessment algorithm?

To complement these research questions, Figure 1.2 is introduced to provide the reader with an outlook of the final deliverable of this research project, where κ, μ_{max}, $\dot{u}$ and T_i are, respectively, the longitudinal slip ratio, the maximum road friction coefficient, the vehicle's acceleration and the input torques. Furthermore, the elements of the control loop that need to be developed are shown.

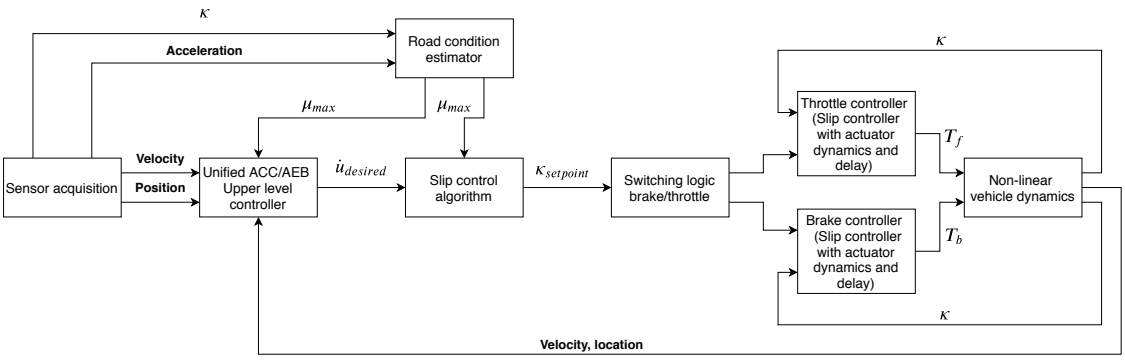

Figure 1.2: Final deliverable of this research project.

1.4 Outline

The structure of the thesis is now introduced. In Chapter 2, a literature study is performed that focuses on finding suitable approaches to control the vehicle, finding ways to simulate the vehicle behavior on different road surfaces, finding approaches to asses the threat level during ADAS scenarios and finally find a suitable method to estimate the maximum road friction coefficient. This subsequently leads to answering the first, third and fourth sub-question posted above. The chapter ends with a summarized explanation of the envisioned scientific contribution.

Chapter 3 describes three different vehicle models. A control-oriented vehicle model is presented which includes a Pacejka tyre model. This model is used to design a slip controller which is used to control the acceleration of the vehicle.

The design an evaluation of this slip controller is presented in Chapter 4, which aids in answering sub-question one. The roll axis vehicle model from [23] is used to validate the designed ADAS systems. The process of designing these ADAS systems is shown in Chapter 3, where sub-question two is answered.

The last sub-question is answered in Chapter 6 by evaluating the ADAS systems as discussed in Chapter 3. The roll axis vehicle model is also used to obtain training data, which is used to train a neural network for the estimation of the maximum road friction coefficient. The design and validation of the maximum road friction estimator is shown in Chapter 5, thus answering the fourth sub-question. Finally, the conclusions, the limitations of the current research and future research are provided in Chapter 7.

2. Literature study

2.1 AEB performance evaluation in literature

Autonomous Emergency Braking (AEB) is braking that is applied automatically by the vehicle in response to the detection of a likely collision. The primary goal of AEB technology is to prevent crashes by detecting a potential conflict and alerting the driver, and, in many systems, aiding in brake application or automatically applying the brakes [25]. Figure 2.1 shows a typical AEB system which includes an environment perception system, an upper-level controller and a lower-level controller. The upper-level controller is a threat-assessment and decision-making algorithm, where the lower-level system controls the acceleration of the vehicle to the desired acceleration provided by the upper-level controller. The upper-level controller calculates the desired acceleration to keep the host vehicle at a safe distance from an obstacle [38].

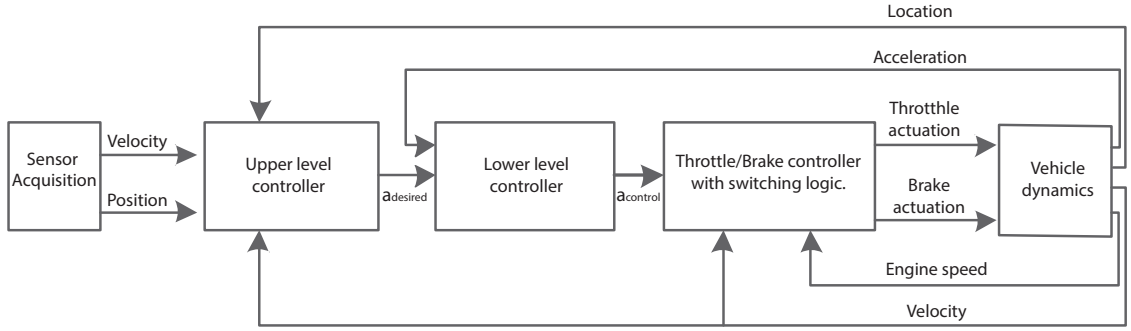

Figure 2.1: A typical schematic diagram of an AEB system model

2.1.1 Upper-level controller

A threat-assessment algorithm decides if a situation is safe or unsafe, and can warn the driver or/and choose to perform an automatic emergency brake in critical hazardous situations. In [17], a literature study on threat-assessment techniques is conducted. Methods found in the literature can be divided, on a higher level, into physical model-based methods and data-driven methods. The main difference between the two classes is that for physical model-based methods, threat-assessment and decision making is performed based on learning from real insights and models, while data-driven methods rely on data-based learning, i.e., black-box modeling. Physical model-based methods are divided into the following categories: Single Behavior Threat Metrics (SBTM), optimization-based methods, formal methods, and probabilistic methods which are discussed in the following sections.

Single Behavior Threat Metrics

In the presence of perfect measurements and comprehensive knowledge of the intention of each participant (e.g., its destination), it can be possible to accurately predict the position and velocity of a host and preceding car in order to assess the risk of collision. However, this is rarely the case in reality and, therefore, simplifications are introduced in the problem formulation. By using reasonable simplifications, one can specify the threat-assessment problem as being driven by threat metrics based on single future behaviors of the different traffic participants. The most popular SBTM methods are summarized in Figure 2.2 and discussed below.

(1) Time-to-Collision (TTC), which represents the time until a collision between two objects occurs. In [61], the optimal TTC threshold is studied under certain sensor uncertainties. However, TTC is not robust for every driving scenario. Let a situation consist of two vehicles traveling next to each other with approximately the same velocity. If only TTC is used, the threat level will

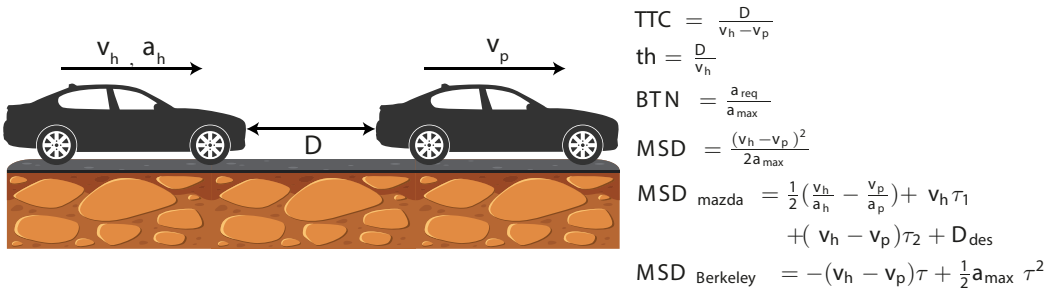

Figure 2.2: Summary of threat-assessment metrices.

be low even if the inter-vehicle distance decreases to a minimum. In [41] TTC is used as threat assessment, however the activation times are scaled with the maximum road friction coefficient to make the AEB system more robust for a variation in road conditions.

(2) Another related time-based measure is the time headway (th), which is calculated as the distance between the two vehicles divided by the following host vehicle speed. Time headway is essential because it specifies how much time the host vehicle's driver has to react in case the lead vehicle suddenly brakes at maximum deceleration level.

(3) Brake Threat Number (BTN) is defined as the ratio between the longitudinal acceleration required to avoid a collision, and the maximum longitudinal acceleration, respectively. In [47], they used BTN to investigate the fundamental limitations of collision-avoidance systems, subject to systematic measurement errors and unexpected future object motion. Specifically, they include the effects of sensor and actuator delays and derive closed-form expressions for performance with an emphasis on early and unnecessary interventions. The dimensionality of the input state space for collision avoidance functions is, in general, very large, making exhaustive evaluation by real vehicle test driving unfeasible. By theoretically assessing the worst-case performance for scenario subsets, the dimensionality of the input state space is efficiently handled. Recently, [35] proposed the notion of Predictive Steering Threat Number (PSTN), using a bicycle model with a time-varying lateral acceleration to represent the dynamics of the vehicle. The authors claimed to have a more realistic model when compared to commonly used models in STN-related works since earlier work consider the vehicle as a point mass. Also, in [11], it is mentioned that state-of-the-art threat assessment algorithms do not adequately take steering and braking dynamics into account. They proposed a so-called linear bicycle model, although they do not include sensor uncertainties.

(4) Minimal Safe Distance (MSD), defined as the minimum distance to be kept between the host and the obstacle.

In complex scenarios, a single SBTM may not be enough to characterize a situation thoroughly and, therefore, multiple SBTMs may be needed. The author of [48] proposed to use a combination of TMs (-e.g., TTC,th, MSD) to reflect the real threat level better. In [68], a new, improved multiple threat behavior method is proposed. Their goal was to improve algorithms in earlier work, including the Mazda algorithm, the Honda algorithm, Berkeley Algorithm, and National Highway Traffic Safety Administration's (NHTSA) algorithm. Most threat assessment algorithms used in automotive collision-avoidance systems are expressed in terms of range. The measured current range R is compared with the warning range R_w or overriding range R_o to decide if warning or braking is needed. It is difficult to clearly quantify the level of danger or threat from the comparison result, since the range criteria vary non-linearly under different dynamic conditions. Time-to-last-second-braking (T_{lsb}), is a new time-based measure proposed for rear-end collision

threat assessment. It is defined as the time remaining for the driver or the control system at the current situation to take the last extreme evasive action, e.g., braking at the maximum level, to avoid a rear-end collision. The main advantage of this method is that the estimation of the T_{lsb} measure takes into account all possible current information characteristics of the current dynamic situation (i.e., velocity, acceleration, distance between host and preceding vehicle, relative velocity, relative acceleration, max acceleration), while most previous algorithms only use partially updated information and assume that the rest of the state variables remain constant.

Optimization-based methods

The most popular optimization method for threat-assessment is Model Predictive Control (MPC). MPC consists of an optimization problem minimizing an objective cost function subject to constraints such as a dynamical model and constraints on the states and/or inputs. The optimization is performed over a finite-time horizon, and the optimal solution yields the best control law for the given cost function. MPC is of particular interest for safety-critical and time-critical constrained applications such as automotive threat-assessment algorithms. The benefit of using MPC in the upper-level controller is that safety and comfort constraints can easily be integrated within the controller. In [20], the authors claim that the current MPC ACC focuses entirely on a onefold driving scene, such as tracking a desired spacing from a preceding vehicle or tracking a desired speed. Current MPC systems cannot autonomously adapt to different driving scenes. In this paper, they merge an AEB and ACC system in the upper-level controller. The Enhanced Adaptive Cruise Control (EACC) system proposed in this paper, can realize conventional ACC, speed tracking, and autonomous emergency braking (AEB). EACC does not merely combine three driver assistant systems but is based on a unified model and algorithm framework. With the development of autonomous vehicles, especially the in-depth research on the control of the autonomous vehicle, it is essential to make a unified framework design for the longitudinal control of autonomous vehicles.

The main advantage of EACC include two aspects. Firstly, it can be applied to a variety of driving scenes while meeting the driving requirements for different driving situations and, therefore, the vehicle longitudinal control can be more intelligent. Secondly, the computational efficiency of the algorithm. For autonomous vehicles, the computer needs to calculate and process a large number of data, including environmental perception data, positioning data and vehicle driving data. The unified framework design of the longitudinal control algorithm will reduce the complexity of the code and improve the efficiency of operation.

The authors of [69] claim that earlier papers for AEB systems focus only on safety; however, in this paper, the authors want to optimize safety and vehicle handling comfort. A non-linear model predictive algorithm is used to satisfy the comfort requirements. This algorithm takes a multi-performance evaluation function as the cost function to optimize the vehicle states according to surroundings information and calculates the optimized brake force for the braking subsystem. A limit on the vehicle deceleration is set to achieve more longitudinal comfort.

Formal methods

Optimization methods determine the optimal avoidance trajectory if and only if a collision is avoidable. Therefore, it would be useful to have full information about what points on the road can be reached by the evading car. In [28], [18] set-based approaches are used that use reachability analysis to describe the complete set of future trajectories. These formal methods predict all the future trajectories considering driver and vehicle constraints. If there exists no future path where the driver can avoid a collision, the AEB system will be used.

In [6], combined braking and steering maneuvers are considered and, therefore, non-linear vehicle dynamics need to be included. The problem is formulated as a constraint satisfaction problem. For systems with non-linear dynamics and possibly non-linear, non-convex constraints, reachable sets are more challenging to compute. The authors of [6] use interval techniques and, therefore, the solution sets are represented by one or several intervals or boxes. By restricting the sets to

this limited structure, the interval-based methods can be used to obtain approximate solutions to non-convex constraint satisfaction problems, enabling the possibility to utilize non-linear models and constraints.

Probabilistic methods

Generally speaking, a probabilistic threat-assessment method assigns probabilities to different events, e.g., how likely it is to collide with another object in a near future given some assumptions on uncertainties. In automotive applications, some of the significant sources of uncertainty include dynamical modelling errors, measurement noise, and the misinterpretation of the drivers' intention. In [60], the question of how uncertainties affect the timely activation of a brake intervention is addressed and how this varies among different scenarios. In [61], a new methodology for the robust design of an AEB system considering sensor measurement errors is proposed, which is capable of determining the optimal parameters of both the sensor and the threat-assessment function by solving an optimization problem based on a stochastic model. The authors of [42] aims to develop a systematic collision-avoidance reliability analysis framework for AVs equipped with adaptive cruise control (ACC) and autonomous emergency braking (AEB) systems. The developed framework consists of two main elements, namely, uncertainty modeling and reliability analysis. In the uncertainty modeling module, a recently developed Gaussian mixture copula is employed to model the uncertain traffic conditions such as vehicle speed and relative distance based on the naturalistic driving data. A Gaussian mixture copula is a generalization of the usual Gaussian mixture model. A Gaussian mixture copula model consists of a weighted sum of a finite number of joint distributions, each of which contains a Gaussian copula. This copula model can be used to study marginal distributions and their dependence structure separately. Furthermore copulas can be calibrated to data sets that are sparse and unevenly distributed. The Gaussian mixture copula allows for not only accurate modeling of the marginal distributions of various traffic conditions but also gives a precise representation of the complicated dependence between different variables. In the reliability analysis element, the adaptive surrogate modeling-based reliability analysis method with active learning function is employed to perform collision-avoidance reliability analysis efficiently. The synthesis of these two elements enables us to accurately and efficiently evaluate the collision-avoidance reliability of an AV control system.

2.1.1.1 Conclusions upper-level controller

System performance SBTMs usually only consider the most likely state estimates, discarding in many cases the associated distribution of the states. Instead, robustness concerning uncertainties are gained by putting margins in the decision-making stage, that are typically tuned by empirically testing to maximize the system performance [48]. Probabilistic methods, on the other hand, tend to make use of the entire uncertainty model to estimate the probability of a collision. Nevertheless, it is generally not obvious how to derive the uncertainty model, especially in cases of time-varying uncertainties [36]. This is, e.g., the case for uncertainties related to driver's intentions. From [17], it follows that probabilistic methods are preferred in scenarios where the uncertainties can be modeled by a few random variables, or in cases where the prediction horizon is sufficiently short. Regarding formal methods, the underlying objective is usually to verify and formally guarantee whether a situation can evolve into an unavoidable dangerous situation. These methods are best suited for applications where formal guarantees of performance are required, or when the system is subject to complex combinations of safety, comfort, or logic requirements, for example [17].

Implementation Generally speaking, SBTMs are computationally cheap by design. For set-based approaches, the authors of [39] have proposed a toolbox that is able to compute set based predictions in time frames smaller than 20 ms. Regarding optimization-based methods, their computational complexity usually scales poorly with the size of the problem, which means that only small problems can be efficiently solved in real-time. Unfortunately, constrained MPC-problems

tend to be non-convex, which, together with long prediction horizons, usually yields prohibitive complex problems [63]. Probabilistic methods may also lead to computational efficient solutions in some exceptional cases where the noise is strictly Gaussian and the dynamics linear, for example, in [61]. However, that is rarely the case in practice. Furthermore, the solution often needs to be numerically approximated by Monte-Carlo simulations or particle filtering, which are known to be accurate but computationally expensive.

Robustness Another essential aspect for any safety system is robustness, here defined as the measure of the system's ability to handle uncertainties due to, e.g., measurement noise and variation in road conditions. Formal methods have an intrinsic ability to guarantee robustness, where the level of robustness can be adjusted by over- or underestimating the uncertainties in the set definitions. SBTM and optimization-based methods, on the other hand, fall short in terms of robustness, as a result of over-simplifications made on the system modelling and problem statement [29], [68]. To handle such issues, it is common practice to measure the state after some period and to solve the dynamic optimization problem again starting from the new measured state. By using feedback on the measurement information, this provides the whole procedure with a robustness that is typical for closed-loop systems.

2.1.2 Lower-level controller

The lower-level controller controls the vehicle dynamics system to achieve the desired acceleration based on the output of the upper-level controller. In other words, the lower-level controller is used to calculate the throttle actuation (pedal position) and the brake pressure to generate an actual acceleration to ensure that the desired acceleration is tracked. Usually, a lower-level controller consists of two layers: a controller to track the desired acceleration with the desired and actual acceleration as inputs and an inverse vehicle model with switching logic between the brake and throttle controller. However, in some AEB systems, only the brake is controlled. In this section, different lower-level controllers will be discussed. In the earlier mentioned paper [20], the lower-level controller is modelled as a first-order system $a_{\text{con}} = \frac{K}{\tau s+1} a_{\text{des}}$, where K is the system gain, and τ is the time constant. The pedal position and brake pressure are calculated with an unknown inverse vehicle model.

In [5], the upper-level and lower-level controllers are modelled as one system. Therefore, it can be compared with the earlier mentioned EACC system. A first-order system is used to represent the deceleration exerted by the brakes; this system can be tuned to integrate factors such as driver attention and braking efficiency. The parameters are estimated based on vehicle measurements. Together with a one-dimensional constant acceleration model, the deceleration behavior can be estimated. A fuzzy controller is used to calculate the brake input based on the vehicle speed and the predicted stopping distance. The fuzzy controller adapts the braking force dynamically during the AEB maneuver and, therefore, it is more comfortable in comparison with systems that always use maximum braking.

The authors of [38] claim that the variation of road conditions must be considered in a robust AEB system. The maximum deceleration depends on the road friction and slope. The real-time information of the road slope angle and friction coefficient cannot be easily obtained from the onboard sensors in passenger cars. Instead, the road slope angle and friction coefficient are estimated with a Kalman filter. In this paper, only the deceleration is controlled. Since there is a time delay and disturbance such as engine braking, drag force, and rolling resistance, the deceleration controller is designed using a PI controller with a feedforward term. The PI controller is added to compensate for the acceleration error. The feedforward term is included to consider the characteristics of the brake actuator and contains the relationship between the master cylinder pressure and the deceleration of the vehicle. The control gains are tuned for various road conditions.

The PID controller is a widely used technique in AEB systems because of its advantages of simple

structure and strong robustness properties. However, the authors of [67] pointed out that due to the complicated non-linear characteristics of control systems, and the time-varying features of the real-world driving process, the conventional PID controller cannot control the AEB systems effectively. In this paper, a back-propagation neural network is used to tune the PID parameters in real-time and, therefore, the system is robust to external disturbance and model uncertainty. Furthermore, an inverse vehicle model that considers air and rolling resistance is used. Similarly, in paper [31], a single neuron adaptive intelligent PID controller is used for the lower-level controller. However, they incorporated an ACC system in the upper-level controller to control the relative distance and velocity. A sliding mode control methodology is used, which has the capacity to reject the effect of bounded uncertainty acting in the input channels, the so-called matched uncertainty. Besides, the sliding mode control methodology has the advantage of producing low complexity control laws, which appear particularly suitable to be implemented in an electronic control unit (ECU) of a controlled vehicle. In order to enhance the robustness against unmatched perturbations, a combination of the sliding mode technique with other robust strategies, such as H-infinity control may be beneficial. Moreover, the controller in operation can compensate for several physical effects that are neglected by the simple model of the vehicle to make the design of the controller feasible. The same holds for disturbances of different types, as well as for parameter variations.

An AEB control system requests the brake system to have the capacity of high-performance active brake control. This new requirement is difficult for the conventional vehicular braking system. Therefore, the authors of [34] are introducing a collision avoidance system with an integrated-electro-hydraulic brake system which compared to an electro-hydraulic brake system can not only achieve more accurate pressure control but also avoid the risk of leakage. This paper distinguishes itself in the lower-level controller since it has an additional control layer. This control layer is designed to track the optimal slip ratio, which enabled the controlled vehicle to generate the highest possible deceleration. A neural network is used to control this tire slip ratio, and a pulse width modulation control method is used to convert this information into a torque.

The authors of paper [69] implement a method to estimate the tyre friction and control the optimal slip ratios to generate the highest possible deceleration with a non-singular, and fast Terminal Sliding Mode algorithm (TSM) and therefore the brake controller is robust to variations in the road surface parameters. Sliding mode control has been widely applied in non-linear systems. TSM control has the advantage of convergence in a finite time. However, when the system is far from the equilibrium point, TSM tends to converge quite slowly. Non-singularity fast TSM control can increase the absolute value of the state derivative and effectively boost the convergence speed.

In [59] a wheel slip control system based on a Youla parameterization approach is proposed, since they concluded from their literature study that a single PID controller could not provide stability and performance at all operational conditions. The paper includes actuator dynamics and therefore concluded that they designed a new wheel slip control method that was able to stabilize the wheel slip in all working conditions. However later in this research is concluded that the actuator dynamics as modelled in this paper were not modelled realistically enough, since the dynamics were described without the use of a delay. The addition of a delay in the brake dynamics leads to stability problems, however this is discussed later in this research.

2.1.3 Vehicle dynamics

Vehicle models can be classified as kinematic models and dynamic models. Kinematic models simplify the vehicle to a single point in space, and therefore, forces and torques do not play a role. Therefore, it is suitable to design the upper-level controller but not to design or assess the lower-level controller. The kinematic model describes a vehicle's motion based on the mathematical relationship between the parameters of the movement (e.g., position, velocity, acceleration), without considering the forces that affect the motion. Such simple models are relevant for trajectory prediction; however, for control-oriented applications, more complex models are needed.

Dynamic models describe motion as a consequence of forces and torques acting on the vehicle, such as the longitudinal and lateral tire forces, or effects due to the road angle. Cars are governed by complex physics (effects of driver actions on the engine, transmission, wheels, etc.). Therefore, dynamic models can become extremely large and involve many internal parameters of the vehicle.

In papers [61], [47], [60] kinematic models are used to describe the vehicle dynamics. These papers focus on deriving closed-form expressions for robust avoidance scenarios, which are scenarios where unnecessary interventions and collisions are guaranteed not to occur. These papers do not focus on controlling the vehicle dynamics. The goal of [47] is to design an upper-level controller with BTN as the threat-assessment, which is robust for sensor uncertainties in worst-case scenarios. The authors of [61] investigate the probability of a collision varying two parameters: namely, the standard deviation σ of the measurement error and the threshold τ in a TTC function at which the emergency brake intervention is triggered. Future work includes the extension to a more dynamic model with added sources of measurement errors, where, in general, computations in the closed-form will not be possible.

Road variations such as different road conditions and road angles can influence the tire-road friction and therefore adversely affect the function of AEB [43]. Dynamics models are most popular when designing AEB systems since an emergency brake often has highly non-linear dynamics. To research this phenomenon dynamic tyre models have to be used, which can simulate the tyre road friction behavior. Different mathematical tyre models have been developed in the literature, the most widely used model is the semi-emperical tyre model introduced by Pacejka [49], this tyre model is well known as the Magic Formula. This model is often used since it is reasonable accurate, easy to program and it solves quickly. Furthermore, there are a lot of Magic Formula versions. The first version was developed in 1987, over the years improvements were made with the addition of the overturning moment and improved combined slip equations [19]. A second well know model is Dugoff's tyre model, this model was developed in 1969 in [24]. Finally, another widespread model is the Brush model [49] which can be analytically derived, however they tend to be less accurate than the MF models.

2.1.3.1 Sensors

The most commonly used sensors for ADAS are camera, LIDAR, RADAR, and GPS. Several of the sensors found in the current generation of production vehicles are typically of low cost and, as a consequence, prone to time-varying offset and scale errors and may have a relatively low signal-to-noise ratio. The sensors are known to have drift and noise in the sensor measurements. Assuming that the dynamic parameters such as velocities or accelerations do not change during the prediction interval a small noise power disturbs the prediction marginally, whereas a large noise power can lead to a completely wrong prediction of how a scenario will develop in the future [9]. Systematic sensor errors are regarded as compensable and, therefore, not taken into account. Most of the papers that consider sensor uncertainty(velocity, vehicle distance) model those with a Gaussian random distribution with a standard deviation σ and a mean μ [16]. The authors of [21] used a distance-dependent standard deviation.

2.1.4 Discussion lower-level controller and vehicle dynamics

Many researchers are using a nonlinear vehicle model with tyre slip dynamics to validate their AEB and ACC controllers; however, their controllers are based on a simplified vehicle model without non-linear tyre slip dynamics. Moreover the robustness for road condition disturbances is not addressed [50], [56]. Furthermore the actuator dynamics of the brakes should be modelled, since many proposed methods concluded that they designed a wheel slip controller with good performance and stability, however they ommitted the actuator dynamics which will lead to stability problems. In order to achieve the higher-level goal the controller the following requirements are set. The lower-level controller should

- be easily implementable on an ECU of a vehicle,
- be robust to parameter and sensor uncertainties,
- guarantee stability for different road conditions,
- Consider actuator dynamics with delay.

Furthermore, in order to not over-complicate the design of an AEB system, only longitudinal dynamics are used. A dynamic model must be used for the longitudinal vehicle dynamics. If all is going well during this research steering dynamics are added to the system, therefore the used vehicle dynamic model must be easily extendable. It is concluded that the Magic Formula from [49] is used to model the non-linear tyre dynamics, since this model can simulate the tyre dynamics on different road conditions the most accurately.

2.2 ACC

Adaptive Cruise Control (ACC) originates from Cruise Control (CC), which today is a widespread functionality in modern vehicles. CC regulates the vehicle speed actuating the throttle only, via tracking of speed v that is set by the driver. ACC automatically adapts the vehicle's speed depending on a predecessor's behavior, actuating the throttle as well as the brake system.[45] The goal of ACC is partial automation of the longitudinal vehicle control and the reduction of the workload of the driver with the aim to support and relieve the driver in a convenient manner. The ACC system not only provides the drivers with comfort and safety during driving as the fundamental requirements but can also improve traffic capacity and reduce fuel consumption. The control objective for ACC is to control a desired relative distance and velocity. ACC uses information about: the distance from the ACC equipped vehicle to the preceding vehicle in the same lane, the motion of the ACC equipped vehicle and the preceding vehicle and lastly the driver commands.

In Figure 2.3, a schematic block diagram of an example of an ACC system, including the lower-level controller, the upper-level controller, and the switching logic is shown. u_t and u_b are the inputs for the throttle and brake actuators. From the figure, it can be seen that this ACC system controls the velocity; however it is also possible to control the acceleration instead of the velocity. The ACC upper-level controller focuses on comfort, which is different from the upper-level controller for AEB, since primarily, the AEB upper-level controller focuses on safety.

2.2.1 Upper-level controller

Model Predictive Control (MPC) is extensively used in the design of ACC systems since it can explicitly handle constraints. The literature shows how MPC allows managing fuel consumption, safety, and comfort even for vehicle platooning. However, many solutions are not trivial to be ported on an embedded microprocessor and are not practical. In [45] and [10], two ACC systems based on the classical formulation of MPC are presented that optimizes the vehicle behavior focusing on safety and riding comfort limiting the computed accelerations. However, in these papers non-linear vehicle dynamics are not included. The main disadvantage of MPC is that the calculation load becomes large since it needs to solve the optimization problem considering future predictions in every sampling period. In [62], they successfully implemented an MPC-based ACC running on an embedded microprocessor. They focused on decreasing the computational load for the practical use of MPC by using a low-order prediction model. The paper includes disturbances such as air drag, rolling resistance, road slope, and an acceleration resistance; these disturbances are modelled linearly and, therefore, they can be built into the prediction model.

In [56] and [8], a cascade control strategy is used. An upper level control loop is used to determine the desired velocity and the lower level controller is used to track this desired velocity. For the

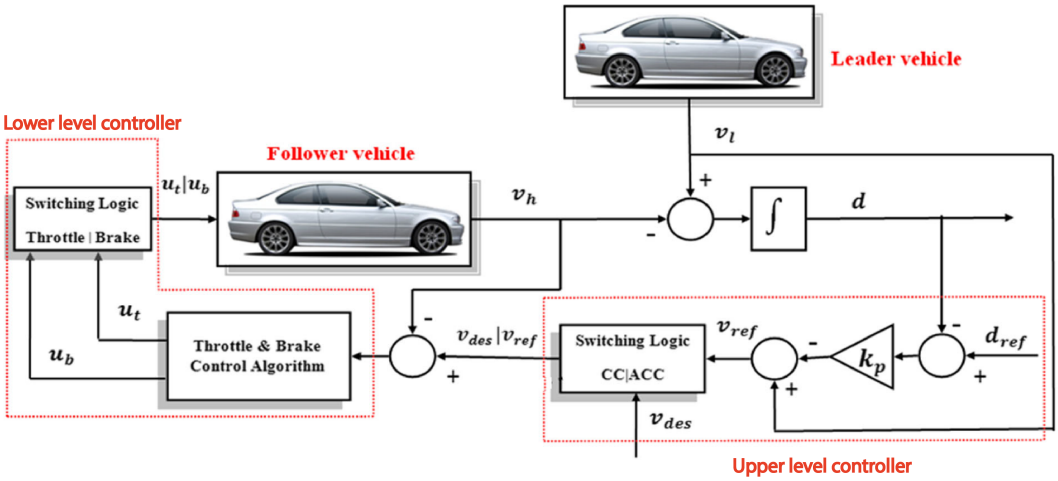

Figure 2.3: A schematic block diagram of an ACC system including the upper-level controller, the lower-level controller and the switching logic [56].

upper level controller a simple control logic is used to determine the desired velocity to track the desired relative distance to a preceding vehicle.

2.2.2 Lower-level controller

Earlier research on ACC systems varies in the types of lower-level controllers that are used; examples are classic PID control, LQR optimal synthesis approach, state feedback control, H-infinity control, fuzzy logic and neural networks. However, most of the approaches have been limited to analysis and simulations with good results, but generally, some practical issues like control saturation, sensing error, and plant parameter variation were not considered. In this section, some of the most recently used control techniques for ACC systems are discussed.

In [46], a robust H-infinity cruise control based on a feedforward and a feedback control design is designed, which guarantees a precise velocity tracking in the presence of longitudinal disturbance effects, such as road slopes, aerodynamic forces, rolling resistance, and mass parameter variations of the vehicle. However, non-linear vehicle dynamics are not modelled. A considerable amount of work has been carried out in the design of an advanced feedback controller to deal with non-linear vehicle dynamics. In [13], they used a neural network. However, the author of [8] claimed that stability in closed loop could never be guaranteed for neural network based controllers. In [44], fuzzy logic and intelligent PI control are compared. The rationale behind the design of the fuzzy controller is to select two errors (distance and speed) as inputs so that the controller can emulate the behavior of a human driver who, in this situation, would control these two parameters. Intelligent PI controllers are used in this work because they combine the well-known PI structure with an "intelligent" term that compensates the effects of non-linear dynamics, disturbances, or uncertainties in the parameters. As a consequence, the non-linear dynamics of the car at low speeds become controllable. Since no parameters appear explicitly in the closed-form controller, classical robust control tools cannot here be exploited to analyze the closed-loop system's sensitivity to disturbances or parameter uncertainty.

The authors of [50] aim to control the vehicle's speed with the target of minimizing the amount of required knowledge about the vehicle's parameters while respecting comfort requirements and achieving robustness to environmental variations. The application of Model Reference Adaptive Control (MRAC) is investigated. MRAC is usually employed in aerospace rather than automotive applications. This strategy employs a reference model to generate the desired output trajectory and relies on one or many adjustable controller parameters and an adaptation mechanism. The

MRAC approach is capable of making the controlled system stable while tracking the outputs of the reference model system. Besides, it is very effective to handle the unknown parameter variations and environmental changes.

2.2.3 Discussion on existing work on AEB and ACC

Although many research results on ACC and AEB systems have been published, little has been published on the integrated design of an ACC system with an AEB. The authors of [20] claim that a unified ACC and AEB system can be highly beneficial. Imagine a situation in which a host car is following a preceding car with a desired spacing, and another vehicle is cutting in from another lane. An ACC system can not avoid a collision in this situation, and therefore, an AEB system needs to be incorporated. These two systems can be combined. However, it is better to design a unified controller that can realize conventional ACC and AEB. The main advantages of this unified strategy include two aspects: The first advantage is that multiple driving modes can be introduced based on the level of danger. Each driving mode has its maximum acceleration and, therefore, the vehicle longitudinal control can be more intelligent and lead to a more comfortable experience.

The second potential advantage is the computational efficiency of the algorithm. For autonomous vehicles, the computer needs to calculate and process a large number of data, including environmental perception data, positioning data and vehicle driving data, etc. The unified framework design of the longitudinal control algorithm should reduce the complexity of the code and improve the efficiency of operation.

In order to achieve the higher level goal a cascade control system consisting an upper level controller and a lower level controller is developed. For the upper level controller it is concluded that a simple control rule with a good control logic could satisfy the higher level goal. The upper level controller is used to determine an acceleration setpoint. For the lower level controller a slip controller is developed to track the desired acceleration. Furthermore, an algorithm is developed to determine what slip setpoint should be used based on an inversed non-linear Pacejka tyre model.

2.3 Maximum road friction estimator

In order to ensure safety of the AEB system on all road conditions, it is concluded that the threat assessment algorithm should include information about the road conditions. In literature many approaches for identifying the maximum road friction coefficient μ_{max} are proposed, the different approaches are shown in Figure 2.4.

Past European research projects such as $FRICTI@N$ [27] have worked on cause-based methods to design a sensor, which is able to detect the friction potential based on the presence of water, snow and ice, the water depth, the road roughness and texture and lastly the precipitation density. Among other methods, artificial neural networks (ANN) are used to relate sensor information and friction potentials. The project concluded that they were not able to design a single cause based sensor that can estimate the friction potential continuously in a moving vehicle. In contrast to cause-based approaches, effect-based approaches observe parameters that are affected by the friction potential. As can be seen from Figure 2.4, effect-based approaches can be tyre related methods and vehicle-dynamics-based methods. In [64], in-tyre sensors are used to determine the friction potential based on sensors that can estimate changes in the tyre thread. In [12], they tried to relate the rolling sound of the tyre to the friction potential, it is concluded that tyre rolling sound is too sensitive to factors other than from the friction potential.

Since vehicle-dynamics-based approaches has shown to give good results, many different approaches have already been studied. Since many methods have been published, some exemplary methods are mentioned that are relevant for the method proposed in this work. In [32], is shown

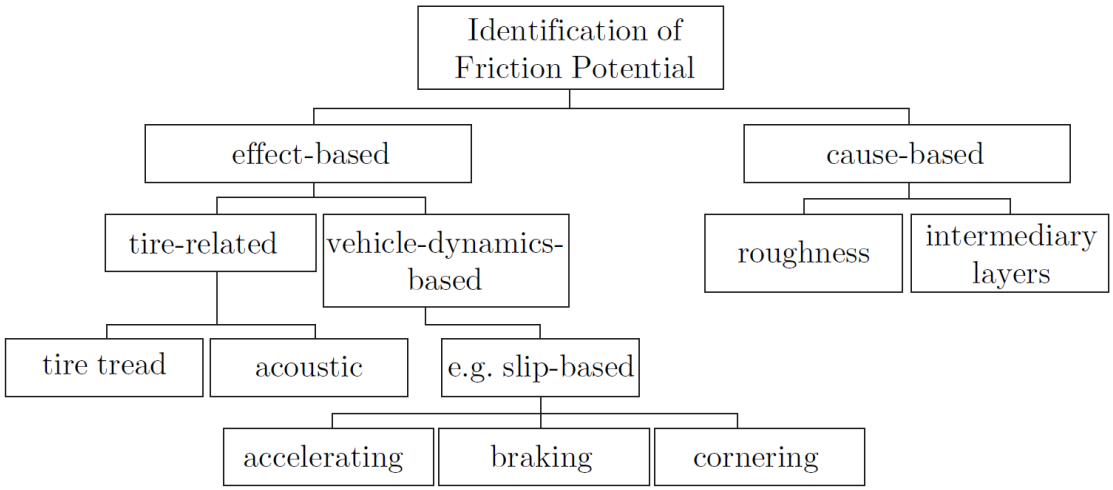

Figure 2.4: Classification of the vehicle-fixed methods for determining the maximum road friction coefficient μ_{max} (friction potential) [66].

that for small values of the wheel slip κ, the slip needed in order to transmit the same longitudinal tyre force F_x is higher on roads with with lower μ_{max}. Therefore it concluded that there is a correlation between the initial slope $\frac{dF_x}{d\kappa}$ and the friction potential, which can be used to estimate μ_{max} for small values of the longitudinal slip κ. The paper also proposed a Kalman filter to estimate the vehicle velocity from the wheel speed sensors. A look up table is used to estimate μ_{max} for different initial slopes. In [66], is shown that the variance between different initial slip slopes and the corresponding maximum road friction coefficient μ_{max} is very high. Therefore [66] estimated μ_{max} during hard braking manoeuvres. During hard braking manoeuvres it is difficult to calculate the vehicle velocity; therefore, the authors designed a so-called optimal FIR derivative to estimate the vehicle velocity during hard braking maneuvers. In [51], another method is proposed to estimate the maximum road friction coefficient. This paper used a tyre model to calculate the expected longitudinal F_x and F_y for different hypotheses of μ_{max}. Also a Kalman filter is used to estimate the longitudinal tyre forces F_x based on vehicle's state measurements. A state observer model is than used to compare the results of the Kalman filter and the expected longitudinal force F_x from the tyre model. It is concluded that a good knowledge about the vehicle and tyre parameters is needed to obtain the necessary vehicle states (longitudinal slip κ) with sufficient accuracy.

In [41], is concluded that the high amount of required knowledge of the vehicle and tyre parameters can be partially circumvented by using an ANN. The ANN identify the patterns between the input and output structures, therefore it is required to train the network before application. The neural network in this paper is trained with data from the on-board vehicle sensors which recorded the wheel speeds, the steering wheel angle, the vehicle's velocity, the engine's rotational speed, the engine torque, the accelerator pedal position, the vehicle's yaw rate and the environment temperature. In [41] is shown that the friction estimation using Recurrent Neural Networks (RNN) was accurate enough to use this information in the interventions strategy of an AEB system. However, only a few scenarios were used to train the neural network. It concluded that the neural network that was designed could not extrapolate to conditions where the neural network was not trained for. In [53] a Time Delayed Neural Network (TDNN) is trained to estimate μ_{max} based on the side slip angle α, vertical force F_z and lateral force F_y. The simulation data is generated with a Pacejka tyre model. This paper showed good results, however a limitation is that a steering input is needed to estimate μ_{max}

2.3.1 Discussion

It is concluded that there is a dependency between the longitudinal tyre force F_x, the longitudinal tyre slip κ and the maximum road friction coefficient μ_{max}. Furthermore it is shown that neural networks have the ability to predict the friction potential. The longitudinal tyre force F_x has a direct relationship with the vehicle's acceleration $\dot{u}$ which can be measured by vehicle sensors. Therefore the hypothesis is that we are able to train a neural network which can predict the maximum road coefficient μ_{max} based on simulation data which is obtained from a Pacejka tyre model. The inputs which are feed to the neural network are the acceleration $\dot{u}$ and the longitudinal front and rear wheel slip κ_f and κ_r which are estimated by a kinematic model with the vehicle's velocity u and the front and rear rotational wheel velocity ω_f and ω_r as its inputs.

2.4 Envisioned scientific contribution

As shown in the literature study the practical goal can lead to a lot of research directions. The literature review results in the conclusion that the field of estimating the maximum road friction coefficient by training a neural network with longitudinal vehicle states is undiscovered. Since an accurate road condition sensor is still an open challenge, the topic of including information about the road conditions in ABS systems and threat assessment algorithms is also fairly undiscovered. This research paper aims to fill these gaps.

The main contributions of this study can be summarized in the four following points:

1. A method to encompass information about the road conditions in threat assessment algorithms.
2. The insights obtained, when developing and analyzing a neural network which is trained to estimate the maximum road friction coefficient μ_{max} based on data obtained from a Pacejka tyre model.
3. The insights obtained, when encompassing information about the road conditions (μ_{max}) in the upper level controller which is designed to determine the desired acceleration.
4. The insights obtained, when developing and analyzing a method to control the vehicle's acceleration with a slip controller (ABS) by encompassing information about the road conditions (μ_{max}) in the slip control algorithm.
5. A vehicle model which is able capture the vehicle behavior on different surfaces for all velocities. The roll axis vehicle model from [23] is combined with a reset integrator friction model to enable accurate behavior especially at low velocities.

3. Vehicle modelling

To test and validate the ADAS systems, which will be explained later, a vehicle model is needed. As discussed in the literature review, a dynamic non-linear tyre model is needed to capture the behavior of the car on different road conditions. In this chapter, three different vehicle models are described. First, a model considering only longitudinal dynamics is described based on the vehicle models from [40] and [54], known as a double-corner model. This model is used to validate the lower level controller, which is discussed in Chapter 4. Thereafter the longitudinal model is extended to a model considering longitudinal, lateral, roll and yaw dynamics based on the roll axis vehicle model from [49] and [23]. This model is used to validate the proposed ADAS systems and to obtain measurements, which are used to train the neural network. Finally, the single-corner vehicle model from [54] is presented, which is a simplified version of the double-corner vehicle model. This model is used to design a slip controller. To validate the vehicle behavior, the double-corner model and roll-axis vehicle model are validated with a vehicle model from Simcenter Amesim, which is a high-quality model to validate against since that model is validated with real vehicle measurements [2].

3.1 Longitudinal vehicle model

A double-corner model is used to describe the longitudinal vehicle dynamics. In Figure 3.1, a schematic view of the vehicle model is given. The double-corner model can be regarded as a side view of the vehicle, where one front and one rear wheel are modelled. It is similar in principle to a half car model, which is commonly used to describe the heave dynamics for suspensions control.

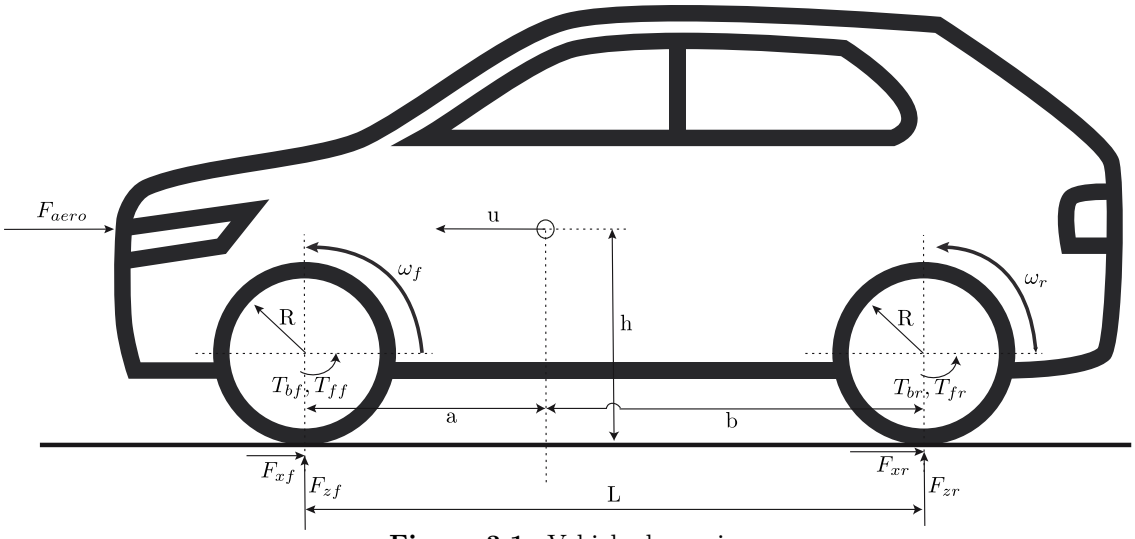

Figure 3.1: Vehicle dynamics

3.1.1 Vehicle and wheel dynamics

The vehicle dynamics can be described with the following set of equations:

$$\begin{cases} J_{wf}\dot{\omega}_f = T_{ff} - T_{bf} - T_{roll_f} - RF_{xf}, \\ J_{wr}\dot{\omega}_r = T_{fr} - T_{br} - T_{roll_r} - RF_{xr}, \\ M\dot{u} = F_{x_f} + F_{x_r} - F_{aero} - Mg\sin\theta, \end{cases} \tag{3.1}$$

where u is the longitudinal speed of the vehicle centre of mass. ω_f and ω_r are, respectively, the angular speed of the front and rear wheels. T_{bf} and T_{br} are the front and rear braking torques

and T_{ff} and T_{fr} are the engine torques. T_{rollf} and T_{rollr} are the front and rear rolling resistance torques. F_{aero} is the aerodynamic force and θ is the road inclination angle. F_{xf} and F_{xr} are the front and rear longitudinal tyre-road contact forces. The parameters J, M, g and R are, respectively, the moment of inertia of the wheel, the vehicle's mass, the gravitational acceleration and the wheel radius.

3.1.2 Longitudinal tyre model

The tires behaviour is highly characterized by non-linearity in complicated road conditions as stated in [49]. In this paper, the Magic Formula is used to reflect the transient characteristics of the tire. The Pacejka friction model is highly detailed, and it is the tyre–road friction description most commonly used in commercial vehicle simulators. The longitudinal force model is a curve characterization of the longitudinal force towards the longitudinal slip κ as shown in Figure 3.2.

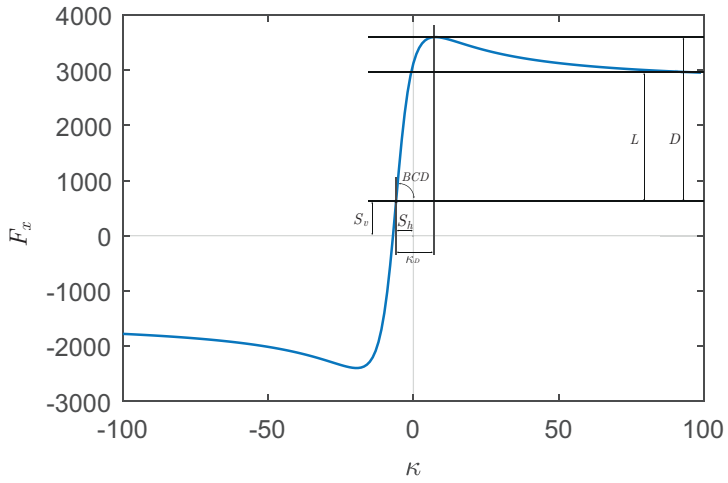

Figure 3.2: Pacejka curve characteristics.

The main curve characteristics from Pacejka 1989 tyre model are:

D	The peak factor which is the maximum longitudinal force.
BCD	The stiffness factor which is longitudinal slip stiffness (slope of Fx vs. κ curve at the origin).
E	The curvature factor which enables to fix the longitudinal slip where the longitudinal force is maximum.
L	The asymptotic factor which is the longitudinal force asymptote at high longitudinal slip.
S_h	The horizontal shift which fix the anti-symmetry center of the curve.
S_v	The vertical shift which fix the anti-symmetry center of the curve.
κ_D	The longitudinal slip peak antecedent which is the longitudinal slip related to the maximum longitudinal force.

Table 3.1: Pacejka 1989 model parameters.

The Pacejka 1989 parameters are calculated through the following equations:

$$\begin{aligned} C &= b_0 \cdot \lambda_{cx} \\ D &= (b_1 \cdot F_z + b_2) \cdot F_z \cdot \lambda_{\mu x} \cdot \\ BCD &= (b_3 \cdot F_z + b_4) \cdot F_z \cdot e^{-b_5 F_z} \cdot \lambda_{kx} \\ E &= ((b_6 \cdot F_z + b_7) \cdot F_z + b_8) \cdot \lambda_{ex} \\ Sh &= (b_9 \cdot F_z + b_{10}) \cdot \lambda_{hx} \\ Sv &= (b_{11} \cdot F_z + b_{12}) \cdot \lambda_{vx} \cdot \lambda_{\mu x} \end{aligned} \tag{3.2}$$

where $b_{i,(i=1,\ldots,12)}$, are constant parameters which are related to specific tyre properties, F_z is the normal force, $\lambda_{i,(i=\mu_x,\ldots,vx)}$, are scaling factors where $\lambda_{\mu x}$ is the the scaling factor for the maximum tyre-road friction coefficient μ_{max}.

The longitudinal force can now be calculated with

$$\begin{aligned} &B = \tfrac{BCD}{C \cdot D} \\ &\varphi = B \cdot (\kappa + Sh) - E(B \cdot (\kappa + Sh) - \arctan(B \cdot (\kappa + Sh))) \\ &F_x = D \cdot \sin(C \cdot \arctan(\varphi)) + Sv. \end{aligned} \tag{3.3}$$

Summarizing, the longitudinal force relationship can be simplified to

$$F_x = F_z \mu(\kappa, \mu_{max}). \tag{3.4}$$

The longitudinal wheel slip κ is expressed in percent and defined between plus and minus hundred. This longitudinal wheel slip is defined during braking as follows

$$\begin{aligned} \kappa &= 100 \cdot \left(\tfrac{R\omega - V_x}{V_x}\right) \quad \text{with} \quad |V_x| > V_{\text{cmin}} \\ \kappa &= 100 \cdot \left(\tfrac{R\omega - V_x}{V_{\text{cmin}}}\right) \quad \text{with} \quad |V_x| < V_{\text{cmin}} \end{aligned}, \tag{3.5}$$

and during accelerating as follows

$$\begin{aligned} \kappa &= 100 \cdot \left(\tfrac{R\omega - V_x}{R\omega}\right) \quad \text{with} \quad |V_x| > V_{\text{cmin}} \\ \kappa &= 100 \cdot \left(\tfrac{R\omega - V_x}{V_{\text{cmin}}}\right) \quad \text{with} \quad |V_x| < V_{\text{cmin}}. \end{aligned} \tag{3.6}$$

where V_x is the vehicle velocity and ωR is the linear speed of the tyre at the road-tyre contact point. V_{cmin} is the minimum velocity where the standard slip equation is valid. If the vehicle's velocity falls below V_{cmin}, the current vehicle velocity or the linear speed of the tyre is replaced with V_{cmin}. This constraint is needed to deal with discontinuities handling at low speed.

3.1.3 Rolling resistance and aerodynamic forces

The rolling resistance torque can be computed by

$$T_{roll_i} = RF_{zi}R_c, \tag{3.7}$$

where R is the tyre rolling radius [m], F_z is the normal force on tyre [N] and R_c is the rolling resistance coefficient [-].

The aerodynamic drage force is modelled as

$$F_{\text{aero}} = \frac{1}{2}\rho A C_d v^2, \tag{3.8}$$

where ρ is the air density $[kg/m^2]$, C_d is the drag coefficient depending on the body shape [-], A is the maximum vehicle cross area $[m^2]$ and v is the vehicle velocity.

3.1.4 Normal load force

To complete the model, only the expression for the vertical load has to be specified. To describe the load transfer phenomena between front and rear axles, the force and torque balance is taken at the projection of the centre of mass to the ground, which gives

$$
\begin{aligned}
F_{zf} &= \frac{-F_{\text{aero}}h - mh\dot{u} - mgh\sin(\theta) + mgb\cos(\theta)}{b+a} \\
F_{zr} &= \frac{F_{\text{aero}}h + mh\dot{u} + mgh\sin(\theta) + mga\cos(\theta)}{b+a}
\end{aligned}
\quad , \tag{3.9}
$$

where a is the distance from the center of gravity to the front wheel center, b is the distance from the center of gravity to the rear wheel center and θ is the road inclination angle.

3.1.5 Reset integrator friction model

A reset integrator friction model computes the friction force between the tyre and the ground. This friction model is used since this model was developed to reduce the computational time while retaining its capacity to accurately represent the slip-stick friction phenomenon. Furthermore the simulation results are validated with a Simcenter Amesim model which is also using a reset integrator friction model. The reset friction integrator is modelled following the paper from [33]. The reset integrator friction model takes the stiction (T_s) and the Coulomb (dynamic) friction (T_c) into account, see Figure 3.3. The input is the relative velocity between the contacting surfaces, which is defined as the rotational wheel velocity and R times the tyre radius. Starting from a position where there is no frictional torque, if the stick displacement p changes, a friction torque T_{frict} appears. This frictions torque consists of a torque which varies linearly with the stick displacement until the full user specified stiction torque (T_s).

When the displacement exceeds a specified threshold p_0, the friction torque is constant and equals the Coulomb friction torque T_c. Figure 3.3 shows the friction torque as a function of relative velocity for the reset integrator model.

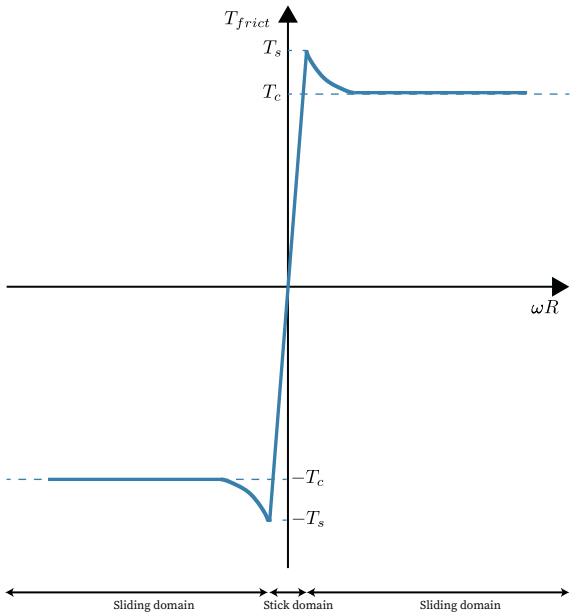

Figure 3.3: Friction torque as a function of the angular displacement for the reset integrator model.

The model name comes from the fact that the model uses an internal state variable (the displacement during stiction p) that implies the introduction of an integrator. The integrator input is forced to zero ("reset" action) when sliding; when sticking it is set at the relative velocity ("integrator" action). When the stick displacement threshold p_0 is reached, macroscopic sliding starts and the model changes from the sticking mode to the slipping mode. The stick displacement time derivative is given by

$$\frac{dp}{\mathrm{d}t} = \begin{cases} 0 & \text{if } (\omega R < 0 \text{ and } p \leq -p_0) \\ 0 & \text{if } (\omega R > 0 \text{ and } p \geq p_0) \\ \omega R & \text{otherwise} \end{cases} . \tag{3.10}$$

The stiction domain is defined using a stick stiffness k_{rel}, the switch between the stiction and the sliding is defined by a displacement threshold that is computed as

$$p_0 = \frac{T_s}{k_{rel}}, \tag{3.11}$$

where T_s is the stiction torque, which is computed from the braking input signal T_b.

The friction torque T_{frict} can now be computed with

$$T_{\text{frict}} = \begin{cases} k_{rel}p + \sigma_1 \omega R & \text{if } |p| < p_0 \\ Tc \cdot \text{sgn}(\omega R) & \text{if } |p| \geq p_0 \end{cases} \tag{3.12}$$

where k_{rel} is the stick stiffness, ωR is the relative velocity between the surfaces, T_c is the Coulomb friction torque and σ_1 is the damping coefficient, tuned to avoid vibrations when the solids stick together.

To illustrate this model a use-case is given: A vehicle is driving with a certain velocity and starts to brake with a braking torque T_b as shown in Figures 3.4 and 3.5. In Figure 3.4, the brake input signal T_b and the friction torque T_{frict} of the front wheel is shown. In Figure 3.5, the front wheel rotational velocity is shown and in Figure 3.6, the stick displacement is shown, together with its displacement threshold. As can be seen from these figures, the friction torque will increase to T_s until the stick displacement p is almost equal to p_0, at that moment $T_{frict} = k_{rel}\frac{T_s}{krel} + \sigma_1 \omega R$. The stick displacement p is further increasing until its value is higher than p_0. At this moment T_{frict} will switch to $T_c \cdot sgn(\omega R)$ and $\frac{dp}{dt}$ is reset to zero. The car will decrease its speed and wheel velocity until the wheel velocity is negative and, therefore, $\frac{dp}{dt}$ is set to its integrator action. However, $\frac{dp}{dt}$ is now negative, since ωR is negative. This process is repeated a few times and, therefore, ωR will damp out to zero angular velocity.

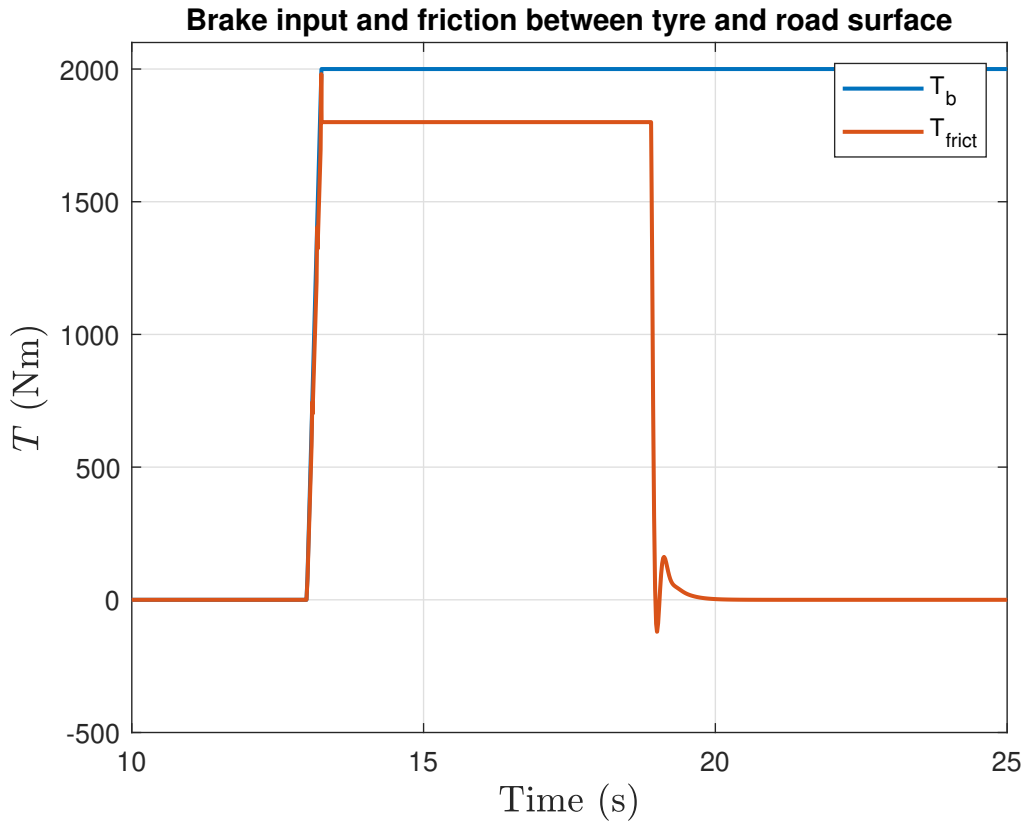

Figure 3.4: The brake input signal T_b and the friction torque T_{frict} of the front wheel.

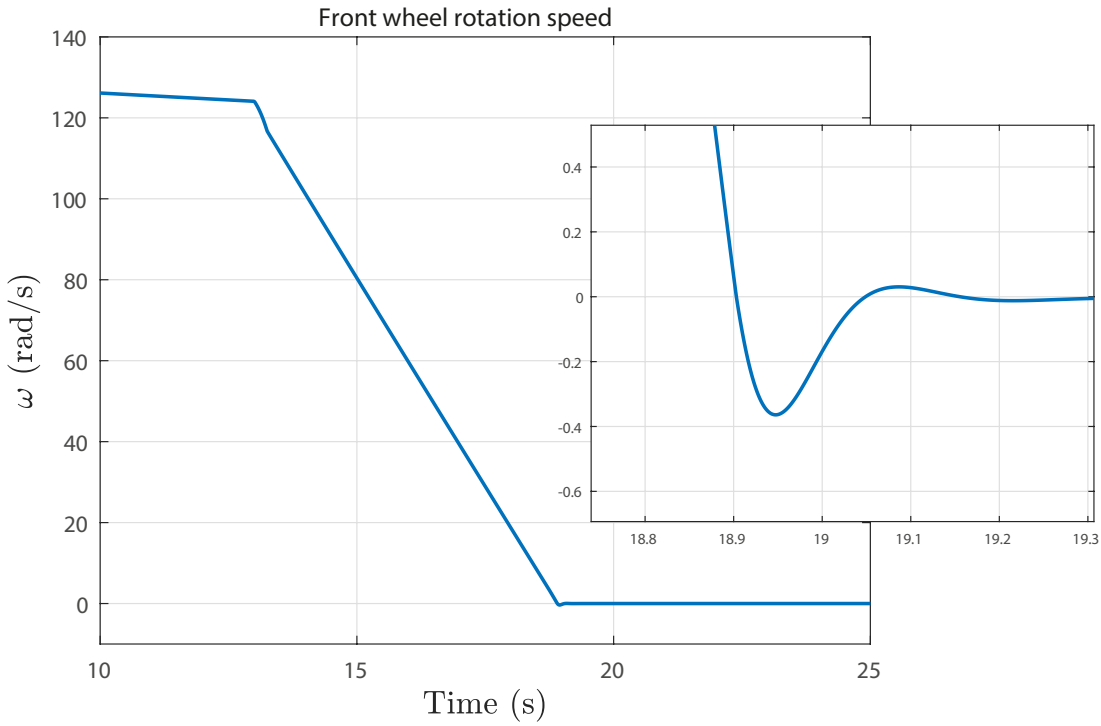

Figure 3.5: The front wheel rotational velocity .

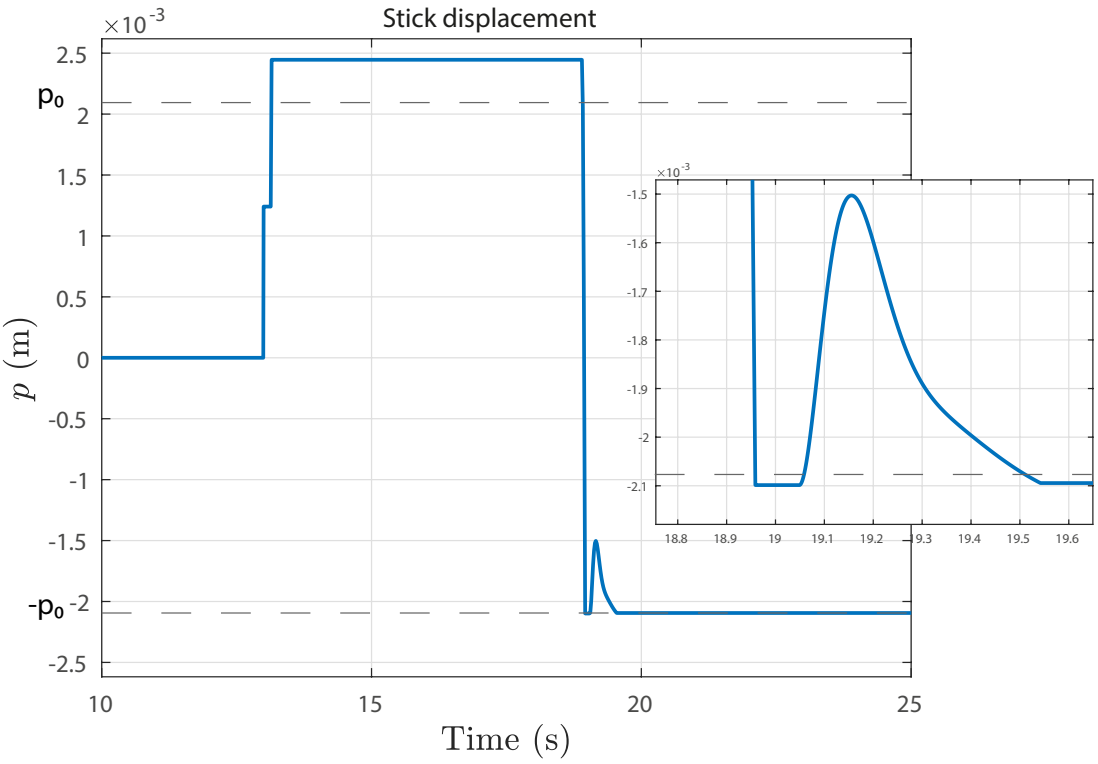

Figure 3.6: The stick displacement together with its displacement threshold.

3.2 Roll axis vehicle model

The roll axis vehicle model from [49] and [23] is used in this project to validate the ADAS systems in PreScan and to obtain data which is used to train a neural network based estimator to estimate the maximum road friction coefficient. There are multiple reasons to use this model. The most important reason originates from the requirement that Siemens wants a vehicle model which is able to simulate the steering behavior of a car. The second reason is that this model is also using the Magic Formula to calculate the tyre forces, only now the tyre forces are modelled in multiple directions, since the tyre has now more degrees of freedom. Another benefit for using this model is that the animation in PreScan looks more realistic, since the vehicle's body has four degrees of freedom: longitudinal, lateral, yaw and roll (u, v, r, φ).

A brief description of the equation of motion is presented in this section. For a thorough derivation of these equations the reader is advised to read [55]. In Figure 3.7 the vehicle model with four degrees of freedom is shown with the longitudinal velocity u, lateral velocity v, the yaw velocity r and the roll angle φ as motion variables. Point A is located in the ground plane, where point B is located on the roll axis. When the center of mass (CM) is above point A the roll angle φ is zero. The distance from the center of mass to point B is given by h'. In the roll centers $rc1$ and $rc2$ torsional springs and dampers are modelled with roll stiffness $c_{\varphi i}$ and damping coefficient $k_{\varphi i}$.

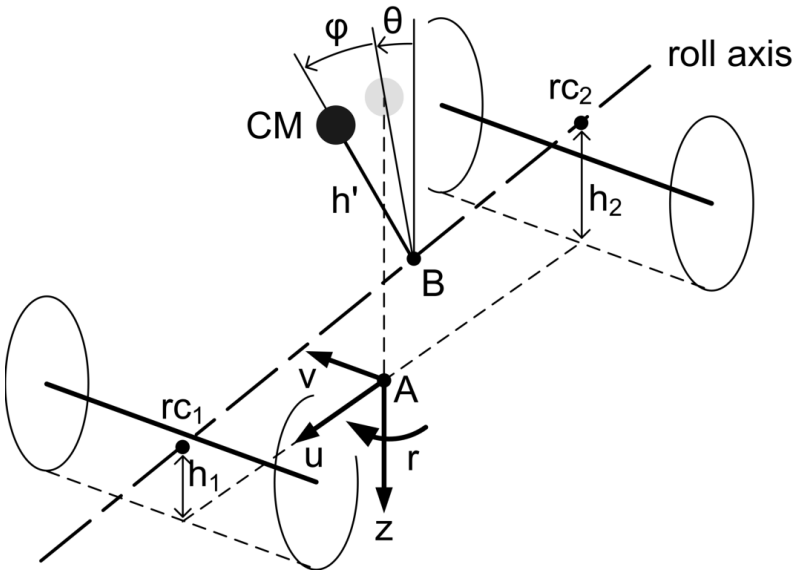

Figure 3.7: Roll axis vehicle model [55].

3.2.1 Vehicle body dynamics

The equations of motion of the system are presented in Equations (3.13), (3.14), (3.15) and (3.16).

$$m\dot{u} - mrv - mh'\varphi\dot{r} - 2mh'r\dot{\varphi} = \sum F_x \tag{3.13}$$

$$m\dot{v} + mru + mh'\ddot{\varphi} - mh'r^2\varphi = \sum F_y \tag{3.14}$$

$$I_{zz}\dot{r} + (I_{zz}\theta_r - I_{xz})\,\ddot{\varphi} - mh'(\dot{u} - rv)\varphi = \sum M_Z \tag{3.15}$$

$$\begin{aligned}\left(I_{xx}+mh'^2\right)\ddot{\varphi}+mh'(\dot{v}+ru)+(I_{zz}\theta_r-I_{xz})\,\dot{r}\\ -\left(mh'^2+I_{yy}-I_{zz}\right)r^2\varphi+(k_{\varphi1}+k_{\varphi2})\,\dot{\varphi}=0\\ +(c_{\varphi1}+c_{\varphi2}-mgh')\,\varphi\end{aligned}\tag{3.16}$$

in which I_{ii} are the vehicle's moments of inertia. The sum of the longitudinal and lateral forces and moments can be found with respectively

$$\sum F_x = F_{x1}+F_{x2}-(F_{y1}+F_{y2})\,\delta+F_{x3}+F_{x4},\tag{3.17}$$

$$\sum F_y = (F_{x1}+F_{x2})\delta+F_{y1}+F_{y2}+F_{y3}+F_{y4},\tag{3.18}$$

and

$$\begin{aligned}\textstyle\sum M_z &= a\,(F_{x1}+F_{x2})\,\delta\\ &+a\,(F_{y1}+F_{y2})+M_{z1}+M_{z2}-b\,(F_{y3}+F_{y4})+M_{z3}+M_{z4}\\ &+F_{x3}s_2-F_{x4}s_2+(F_{x1}-F_{y1}\delta)\,s_1-(F_{x2}-F_{y2}\delta)\,s_1,\end{aligned}\tag{3.19}$$

where a is the distance from the center of gravity to the front wheel center, b is the distance from the center of gravity to the rear wheel center, s_1 and s_2 are the vehicle half track widths and δ is the steering angle. The dimensions of the vehicle are illustrated in Figure 3.8 together with the longitudinal and lateral tyre forces and moments.

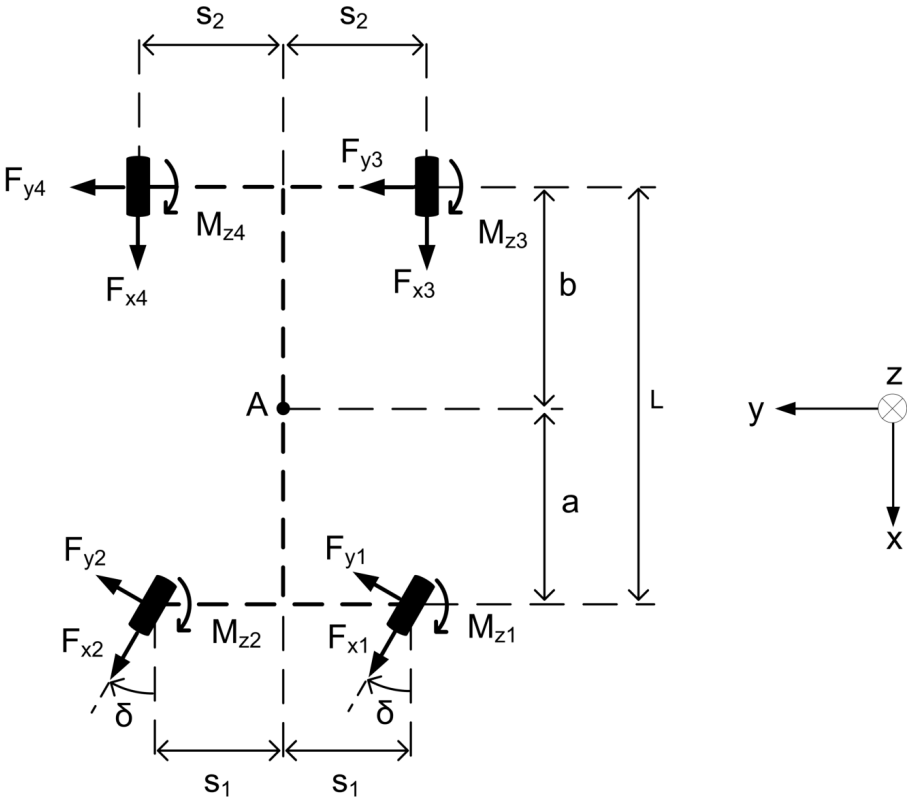

Figure 3.8: View from above of the roll axis vehicle model with dimensions [55].

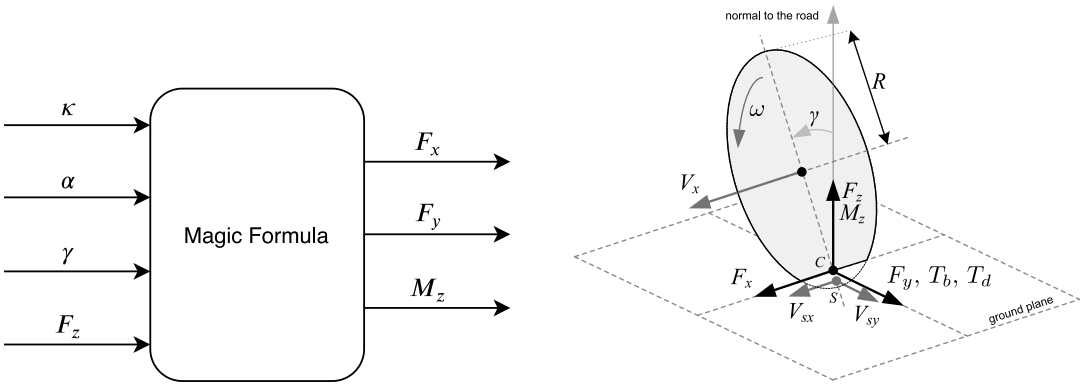

Figure 3.9: Magic Formula version 5.1: Inputs and Outputs.

3.2.2 Combined longitudinal and lateral dynamics tyre model

The Magic Formula model (Pacejka 1989) from Section 3.1.2 calculates the longitudinal tyres forces depending on the vertical load F_z and longitudinal slip κ. This tyre model is now extended to a combined slip model from Pacejka 1996 (MF 5.2) [49], which is able to calculate the longitudinal force F_x, lateral force F_y and the the self aligning moment M_z as illustrated in Figure 3.9.

For steady-state rolling conditions the input variables are the inclination angle γ, the longitudinal slip κ which can be calculated with Equations (3.5) and (3.6), the side slip angle which is calculated with

$$\alpha = \arctan\left(\frac{V_{sy}}{|V_x|}\right), \tag{3.20}$$

where V_{sy} is the lateral slip velocity and V_x is the forward velocity. Furthermore the vertical force F_z on each wheel which is calculated with the following equations:

$$\begin{aligned} F_{z1} &= \frac{a_2}{2l} mg + \Delta F_{z1,roll} - \Delta F_{z,brake} \\ F_{z2} &= \frac{a_2}{2l} mg - \Delta F_{z1,roll} - \Delta F_{z,brake} \\ F_{z3} &= \frac{a_1}{2l} mg + \Delta F_{z2,roll} + \Delta F_{z,brake} \\ F_{z4} &= \frac{a_1}{2l} mg - \Delta F_{z2,roll} + \Delta F_{z,brake}, \end{aligned} \tag{3.21}$$

where the load transfer due to the vehicle body roll can be calculated with

$$\begin{aligned} \Delta F_{z1,roll} &= \frac{(F_{y1} + F_{y2})\, h_1 - c_{\varphi 1}\varphi - k_{\varphi 1}\dot{\varphi}}{2s_1} \\ \Delta F_{z2,roll} &= \frac{(F_{y3,\text{chassis}} + F_{y4})\, h_2 - c_{\varphi 2}\varphi - k_{\varphi 2}\dot{\varphi}}{2s_2} \end{aligned} \tag{3.22}$$

and the load transfer due to braking is calculated with

$$\Delta F_{z,\text{brake}} = \frac{h}{2l} m\dot{u}. \tag{3.23}$$

The Magic Formula equations and parameters are stated in Appendix B.2. In Figure 3.10 the

influence of the inclination angle γ, the longitudinal slip κ and the side slip angle α on the Pacejka curve characteristics is shown.

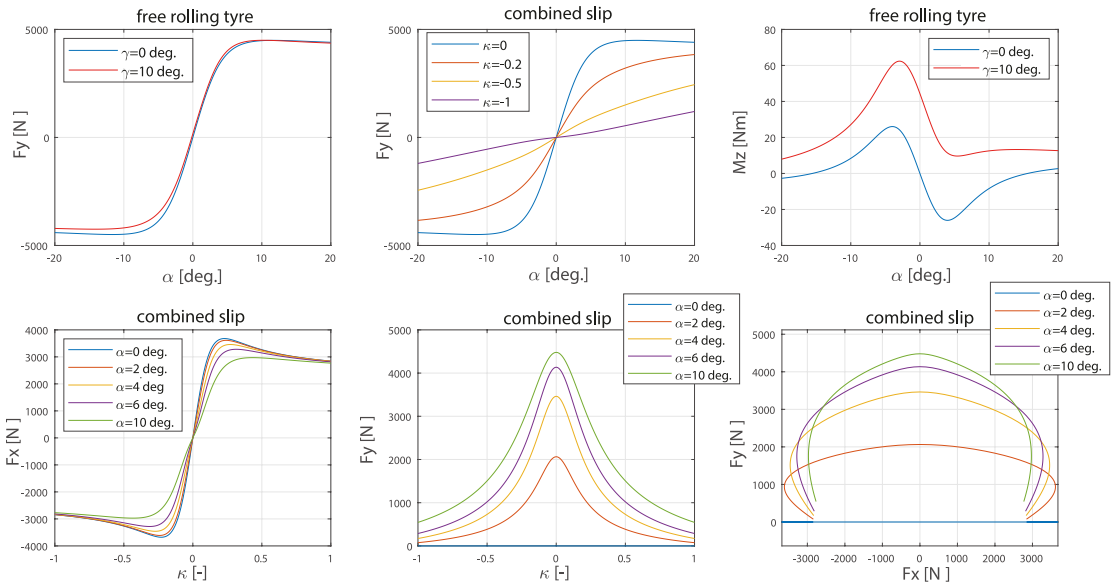

Figure 3.10: Influence of the inclination angle γ, the longitudinal slip κ and the side slip angle α on the Pacejka curve characteristics.

3.3 Control-oriented vehicle model

For the preliminary design and testing of braking control algorithms, the model which is described in Section 3.1 is simplified. This model is known as the single-corner model:

$$\begin{cases} J\dot{\omega} = RF_z\mu\left(\frac{v-\omega R}{v}\right) - T_b \\ m\dot{u} = -F_z\mu\left(\frac{v-\omega R}{v}\right) \end{cases}, \tag{3.24}$$

where

ω [rad/s] is the angular speed of the wheel; u [m/s] is the longitudinal speed of the vehicle centre of mass T_b [Nm] is the braking torque, F_z [N] is the vertical force; and J [kgm^2], m [kg] and R [m] are the moment of inertia single-corner mass and the wheel radius, respectively.

In system (3.24), the state variables are u and ω. As κ, u and ω are linked by the algebraic relationship $\kappa = \frac{u-\omega R}{u}$ it is possible to replace the state variable ω with the state variable κ. Substituting

$$\dot{\kappa} = -\frac{R}{u}\dot{\omega} + \frac{R\omega}{u^2}\dot{u} \tag{3.25}$$

and

$$\omega = \frac{u}{R}(1-\kappa) \tag{3.26}$$

into Equation (3.24), the following equation is obtained

$$\begin{cases} \dot{\kappa} = -\frac{1}{u}\left(\frac{(1-\kappa)}{m} + \frac{R^2}{J}\right)F_z\mu(\kappa) + \frac{R}{Ju}T_b \\ m\dot{u} = -F_z\mu(\kappa) \end{cases}. \tag{3.27}$$

The single-corner model relies on the following simplifications:

- The four wheels are treated as dynamically decoupled, which means that the dynamic load transfer phenomena induced by pitch motion are neglected.
- The suspension dynamics are neglected.
- The wheel radius is assumed to be constant. As a matter of fact – during braking– as consequence of the pitch motion is a dynamic change in the wheel radius, which is a function of the instantaneous vertical load.
- There are no tyre relaxation dynamics considered.
- Straight-line braking is considered.

Since the velocity u can be considered as a slowly-varying parameter compared to the state variable κ due to the large differences in inertia, the second equation of Equation (3.24) can be neglected, so that the model reduces to a first-order model of the wheel slip dynamics:

$$J\dot{\omega} = RF_z\mu\left(\frac{v-\omega R}{v}\right) - T_b \tag{3.28}$$

3.3.1 Model analysis

In this section, the single-corner model is analysed, its equilibrium points are computed and lastly the model is linearized. Further, the transfer function from braking torque to wheel slip will be determined and analysed to illustrate the dynamic dependency of the model on vehicle speed and vertical load.

3.3.1.1 Equilibrium points

To compute the equilibrium points note that by setting $\dot{u} = 0$ and $\dot{\omega} = 0$ in system (3.24), the corresponding equilibrium is given by $\kappa = 0$ and $T_b = 0$. This corresponds to a constant-speed condition without braking; this equilibrium condition is trivial and meaningless for the design of a braking controller. For the design of a braking controller the interesting equilibrium points are characterised by $\dot{\kappa} = 0$, which gives a constant longitudinal slip $\kappa = \bar{\kappa}$. The first-order model of the wheel slip dynamics is

$$\dot{\kappa} = -\frac{1}{u}\left(\frac{(1-\kappa)}{m} + \frac{R^2}{J}\right)F_z\mu(\kappa) + \frac{R}{Ju}T_b \tag{3.29}$$

.

Note that for any control input $T_b \geq 0$, the wheel slip is non-negative since $\kappa \in [0, 1]$. The vehicle is either braking or at constant speed. With $u = \frac{\omega R}{1-\kappa}$ and assuming that $\kappa \in [0, 1)$, Equation (3.29) can be rewritten as

$$\dot{\kappa} = -\frac{1-\kappa}{J\omega}\left(\left(R + \frac{J}{Rm}(1-\kappa)\right)F_z\mu(\kappa) - T_b\right). \tag{3.30}$$

From Equation (3.30), it can be seen that the equilibrium points are characterised by:

$$\bar{T}_b = \left(R + \frac{J}{Rm}(1-\bar{\kappa})\right)F_z\mu(\bar{\kappa}). \tag{3.31}$$

In Figure 3.11 the equilibrium points are shown. It can be seen that the number of equilibrium points is dependent on the value of the braking torque $\bar{T}_b$. The possible solutions are given below:

- If $\bar{T}_b > max(\left(R + \frac{J}{Rm}(1-\bar{\kappa})\right) F_z \mu(\bar{\kappa}))$, the system has no equilibrium points.
- If $\bar{T}_b \leq max(\left(R + \frac{J}{Rm}(1-\bar{\kappa})\right) F_z \mu(\bar{\kappa}))$, the system has at most two equilibria, namely $\bar{\kappa_1}$ and $\bar{\kappa_2}$, where $\bar{\kappa_1}$ and $\bar{\kappa_2}$ coincide only if $\bar{T}_b = max(\left(R + \frac{J}{Rm}(1-\bar{\kappa})\right) F_z \mu(\bar{\kappa}))$.

Since the nonlinear system is a first-order system, the stability properties of the equilibrium points can be easily investigated. Figure 3.12 shows $\dot{\kappa}$ as a function of κ for $T_b = \bar{T}_b = 1000$ Nm. As can be seen from Figure 3.12, $\bar{\kappa_1}$ is a locally asymptotically stable equilibrium, while $\bar{\kappa_2}$ is unstable. From this analysis it can be concluded that, for constant values of the braking torque, the equilibria corresponding with slip values beyond the peak friction of the tyre-road friction curve are unstable. A remark about model is due. If we remove the assumption that $\kappa \in [0, 1)$, and consider also the value $\kappa = 1$, which is a state where the wheels are completely locked, as an equilibrium point. The stability properties cannot be directly investigated with the standard analysis tools used in Lyapunov stability theory, as the concept of neighbourhood of the equilibrium point cannot be properly defined. Moreover, for this model to hold one needs $\omega > 0$, which in turn implies that κ cannot be equal to 1, but can only approach 1 from the left.

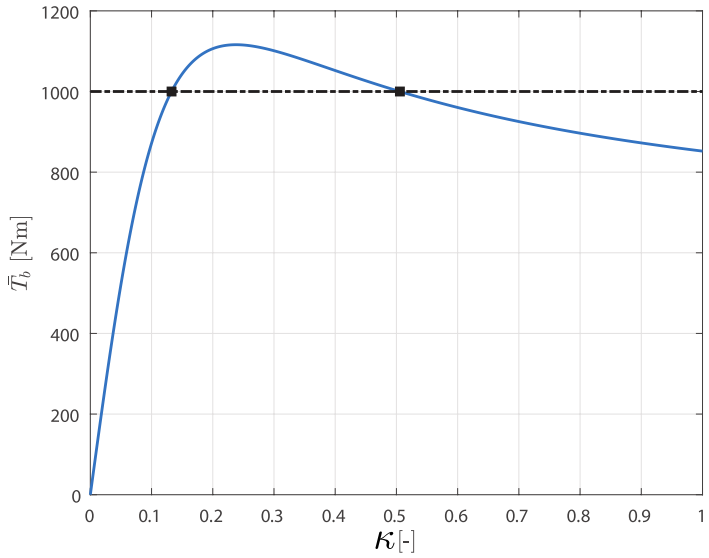

Figure 3.11: Equilibrium points for the single-corner model in the (κ,T_b) plane (example with $F_z = mg$ and dry asphalt).

3.3.2 Model linearisation

Let us consider now the following variables, defined around an equilibrium point (characterised by T_b and κ):

$$\delta T_b = T_b - \bar{T}_b; \quad \delta\kappa = \kappa - \bar{\kappa};$$

To carry out the linearisation of the system, a crucial issue is how to consider and manage the dynamic dependency on the variable u. Since it is assumed that the rotational dynamics of the wheel are much faster than the longitudinal dynamics of the vehicle, u is considered to be an slowly varying parameter. Therefore u can be considered to be quasi constant, i.e., $u = \bar{u}$. To linearise

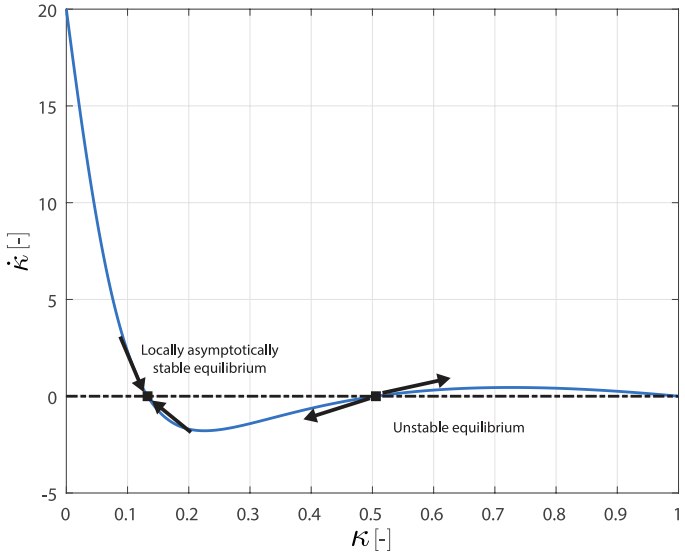

Figure 3.12: $\bar{\kappa}$ as a function of κ for $\bar{T}_b = 1000$.

the first-order model of the wheel dynamics (Equation (3.29)) first the slope of the friction curve $\mu(\kappa)$ around an equilibrium point is defined as

$$\mu_1(\bar{\kappa}) := \left.\frac{\partial \mu}{\partial \kappa}\right|_{\kappa=\bar{\kappa}}. \tag{3.32}$$

which leads to the first-order Taylor expansion of the friction curve $\mu(\kappa)$:

$$\mu(\kappa) \approx \mu(\bar{\kappa}) + \mu_1(\bar{\kappa})\delta\kappa. \tag{3.33}$$

Linearising system (3.29) with the assumption that the speed is constant ($u = \bar{u}$), the following linearization is obtained

$$\delta\dot{\kappa} = \frac{F_z}{\bar{u}}\left[\frac{\mu(\bar{\kappa})}{m} - \mu_1(\bar{\kappa})\left(\frac{(1-\bar{\kappa})}{m} + \frac{R^2}{J}\right)\right]\delta\kappa + \frac{R}{J\bar{u}}\delta T_b. \tag{3.34}$$

The transfer function $G_\kappa(s, \bar{u})$ from δT_b to $\delta\kappa$ is than given by

$$G_\kappa(s) = \frac{\frac{R}{J\bar{u}}}{s + \frac{F_z}{m\bar{u}}\left[\mu_1(\bar{\kappa})\left((1-\bar{\kappa}) + \frac{mR^2}{J}\right) - \mu(\bar{\kappa})\right]}. \tag{3.35}$$

having its single pole located at

$$s_p = -\frac{F_z}{m\bar{u}}\left[\mu_1(\bar{\kappa})\left((1-\bar{\kappa}) + \frac{mR^2}{J}\right) - \mu(\bar{\kappa})\right] \tag{3.36}$$

3.3.2.1 Stability analysis

The linearised single-corner model with transfer function $G_\kappa(s)$ is asymptotically stable if and only if

$$\mu_1(\bar{\kappa})\left[(1-\bar{\kappa})+\frac{mR^2}{J}\right] > \mu(\bar{\kappa}).$$

Since $\mu(\bar{\kappa}) \in [0,1]$ and $\frac{mR^2}{J} >> \mu(\bar{\kappa})$ it can be seen that the open-loop (locally) asymptotically stable equilibrium points are found just before the peak of the friction curve and the unstable ones are found at the peak of the friction curve where $\mu_1(\bar{\kappa}) = 0$ and beyond.

3.3.2.2 Sensitivity analysis

In this section the effects that some specific system parameters have on the linearised single-corner dynamics are analysed. First the vehicle speed is varied, thenn the vertical load, and lastly the road condition. The analysis carried out in the previous section has shown that the vehicle speed and vertical load does not affect the stability properties of the linearised braking dynamics.

In Figure 3.13 the magnitude and phase Bode plots of the frequency response associated with $G_\kappa(s)$ are displayed for four different values of $\bar{u}$, with $F_z = mg$, $\bar{\kappa}$ around the peak friction on a dry asphalt.

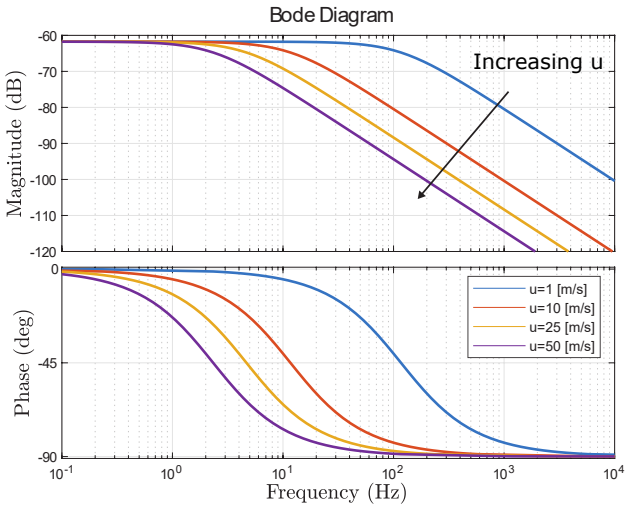

Figure 3.13: Magnitude and phase Bode plots of the frequency response associated with $G_\kappa(s)$ are displayed for four different values of $\bar{u}$, with $F_z = mg$, $\bar{\kappa}$ around the peak friction on a dry asphalt.

From Figure 3.13 it can be seen that the angular frequency of the pole of the linearised wheel dynamics for lower velocities is larger than that for higher velocities. This scaling effect could be taken into account in the design of a braking controller.

During braking a load transfer occurs. The effects of vertical load variations should therefore be investigated. In Figure 3.14 the magnitude and phase Bode plots of the frequency response associated with $G_\kappa(s)$ are displayed for three different values of F_z, with $u = 25$, $\bar{\kappa}$ around the peak friction on a dry asphalt. As can be seen the vertical load mainly effects the low frequency behaviour of $G_\kappa(s)$.

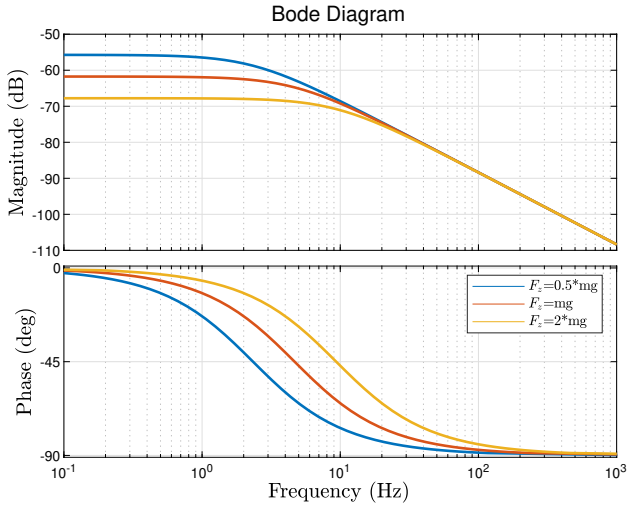

Figure 3.14: Magnitude and phase Bode plots of the frequency response associated with $G_\kappa(s)$ are displayed for three different values of F_z, with $u = 25[m/s]$, $\bar{\kappa}$ around the peak friction on a dry asphalt.

3.4 Conclusion

In Appendix A the simulation results of the double corner model are compared with the simulation results of the Simcenter Amesim vehicle model. From this Appendix is concluded that the double corner model accurately simulates the vehicle behavior. Therefore, this model can be used to validate the proposed control and ADAS systems.

The roll-axis vehicle model is also validated against the Amesim model, however a different tyre model was used. In the double corner model, the tyre model from Pacejka 1989 is used, where the roll-axis vehicle model uses a tyre model based on Pacejka 1996 (MF 5.2). The longitudinal behavior from the older model is fitted into the longitudinal behavior from the new model by a parameter estimation by hand. The results are shown in Figure 3.15, where the longitudinal force F_x is shown for different κ. At first it was concluded that the longitudinal behavior is estimated accurately enough; however the small differences lead to large velocity errors as can be seen in Figure 3.16.

In the rest of this research project the roll-axis vehicle model with these poorly estimated parameters is used to validate the proposed control and ADAS systems. The poor tyre parameter estimation is not a problem, since the tyre parameters are based on a fictional tyre. The roll-axis vehicle model is therefore simulating the tyre dynamics properly, but the tyre parameters do not correspond with the particular tyre which has been used in Simcenter Amesim.

Summarizing, the single corner model is used to develop a wheel slip controller to control the vehicle and the double corner model is used to validate this controller, which is discussed in Chapter 4. Finally, the roll-axis vehicle model is used to validate the proposed ADAS systems and to obtain the simulation data which is used to train a neural network to estimate the maximum road friction coefficient.

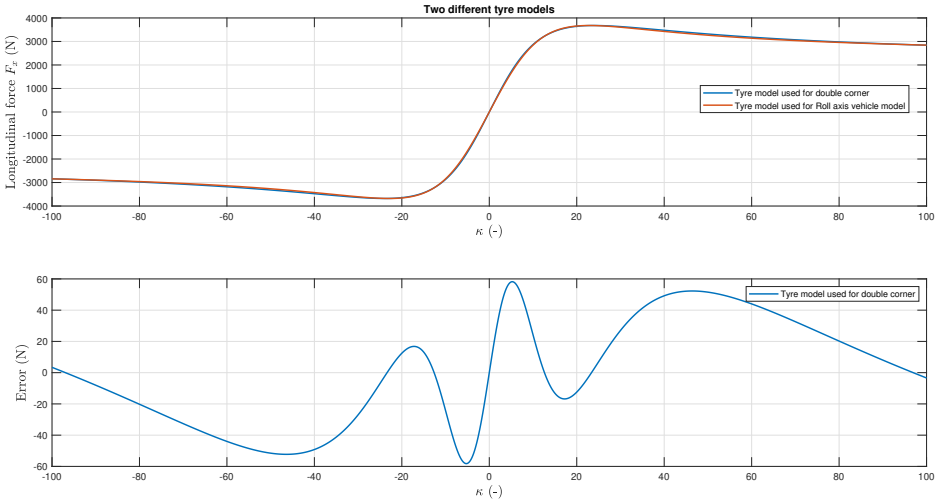

Figure 3.15: Longitudinal force F_x as function of κ for $F_z = mg$ on a a dry asphalt for two different tyre models.

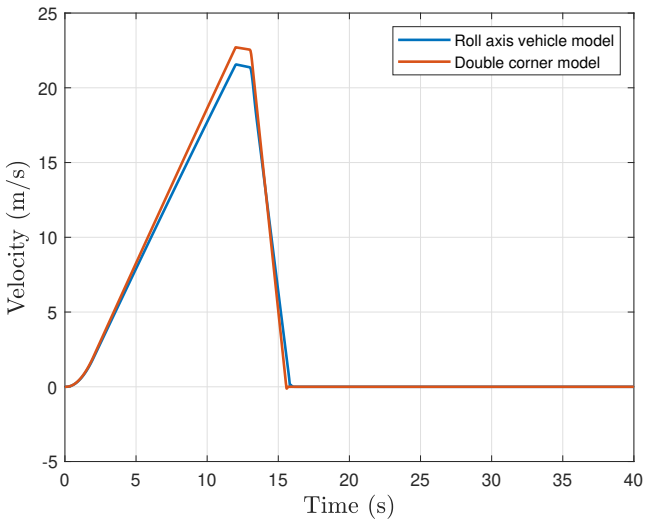

Figure 3.16: Velocity response from time simulation of double corner model and the roll axis vehicle model with poorly estimated tyre parameters.

4. Control system design

In Figure 4.1 the block diagram of the proposed unified AEB and ACC system is presented. In this chapter multiple blocks of this diagram are explained in detail. A slip controller is used to control the acceleration and deceleration of the vehicle. The control system should meet the following requirements:

- The controller should be easily implementable on an ECU of a vehicle,
- The controller should guarantee stability for different road conditions and all admissible speed values,
- The controller should have robust performance for different road conditions and all admissible speed values,
- The controller should ensure asymptotic tracking of a constant wheel slip setpoint with a maximum settling time of 1.5 seconds.

Therefore, the aim is to design a controller with a bandwidth between 1 to 10 Hz, with a maximum overshoot of 15%. Furthermore the nominal robustness margins are used, which are a modulus margin lower than 6 dB, a phase margin higher than 30 degrees and a gain margin higher than 6 dB. The motivation and implementation of the slip controller is discussed in Section 4.1. From this section, it is concluded that a road condition estimator is needed to ensure robust performance. The road condition estimator block is explained in Chapter 5. Furthermore the slip control algorithm is presented in Section 4.2, the ACC system is discussed in Section 4.3.2 and the AEB controller is explained in Section 4.3.1.

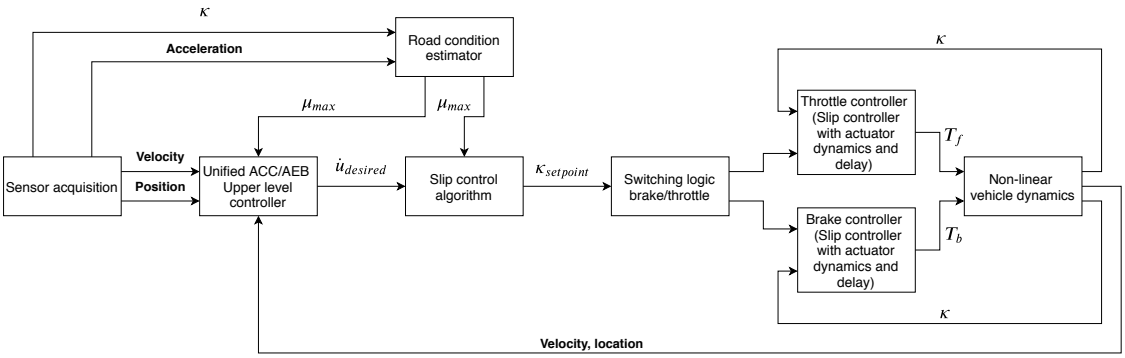

Figure 4.1: The block diagram of full system.

4.1 Slip controller

In this section the slip controller is discussed. First the motivation for a slip controller is given in Section 4.1.1. Multiple iterations of designing, testing and improving were needed to find the final controller. In Section 4.1.2 a stability and uncertainty analysis is presented.

In Appendix A.2.2, a PI-controller is designed for an ideal situation, where no actuator dynamics and delay are considered. To move to a more realistic situation the actuator dynamics with delay is added to the control loop. It is concluded that a PI-controller can not ensure closed-loop stability for all velocities in such a realistic situation. Therefore a new literature review was conducted to find a solution. In [59] a new wheel slip control system based on a Youla parameterization approach is proposed. The paper concluded that the proposed controller was able to stabilize the system in all working conditions. The single Youla parameterized controller was based on a stable nominal plant with actuator dynamics, however they did not add a delay to the system. In this

research it is investigated if a Youla parameterized controller could stabilize the nomimal plant dynamics with actuator dynamics and delay for all admissible speeds. The Youla parameterized controller is introduced in Section 4.1.3. Finally, this controller is validated and compared with an PID-controller in Section 4.1.4.

4.1.1 Motivation

In Appendix A.2.1 the results of an open-loop simulation are presented. It is concluded that a brake controller is needed to prevent the wheels from slipping.

Figure 4.2 shows the longitudinal friction coefficient $\mu_(\kappa)$ plotted against the longitudinal slip κ for different road conditions. It can be seen that for a dry road the optimal longitudinal friction coefficient is achieved with a longitudinal slip ratio of around 0.22. A high friction coefficient will lead to a shorter stopping distance. For an AEB system it is important to decelerate the car with its highest deceleration. The highest achievable deceleration occur at the peaks of the diagrams which are plotted in Figure 4.2, therefore it would be beneficial to control the brake input.

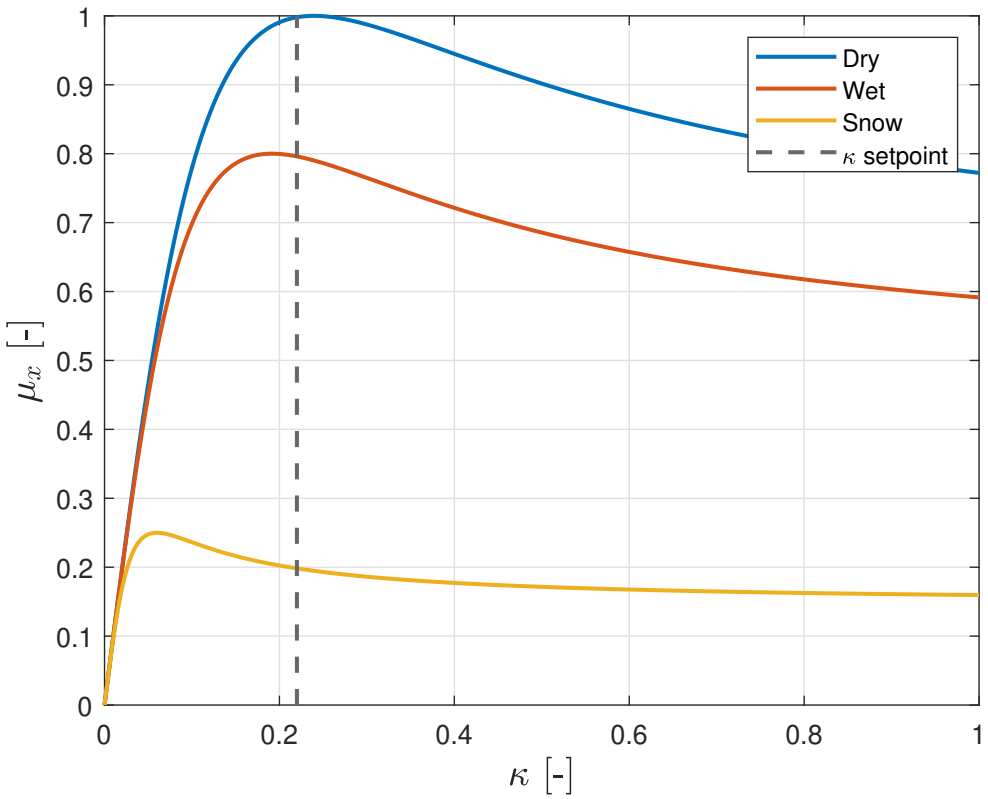

Figure 4.2: The friction coefficient $\mu_x(\kappa)$ plotted against the longitudinal slip κ for different road conditions. The horizontal dashed line represents the setpoint κ.

In braking control systems, two output variables are normally considered for regulation purposes: wheel slip and wheel deceleration. Traditionally the controlled variable is the wheel deceleration, since the wheel deceleration can be easily measured with a simple wheel encoder. However, it can be dynamically critical if the surface of the road is changing rapidly, which can be seen from Figure 4.3, which shows a diagram where the normalised wheel deceleration as function of κ is plotted against κ for different road conditions. The normalised wheel deceleration is expressed as $\eta = \frac{\dot{\omega} r}{g}$, where η is the linear deceleration of the contact point of the tyre, normalised with respect

to the gravitational acceleration g. From this figure it can be seen that it is impossible to find a unique value of the setpoint-η that provides good performance in every road condition.

On the other hand, the control of the wheel slip is very robust from the dynamical point of view, but then the slip measurement is critical, since it requires the estimation of the speed of the vehicle. Noise sensitivity of slip control hence is a critical issue, especially at low speed. One of the requirements for this project is that the control system should be robust for changes in road condition and therefore wheel slip control is further investigated.

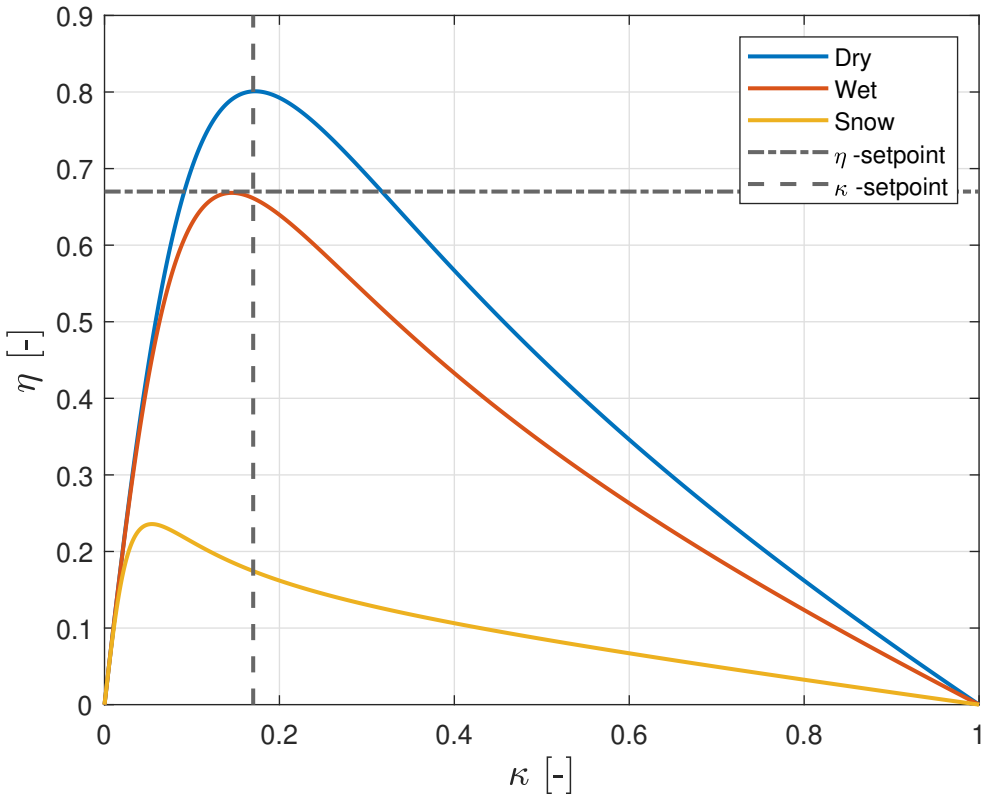

Figure 4.3: The normalised wheel deceleration as function of κ for different road conditions. The horizontal dashed line represents the setpoint η and the vertical dashed line represents the setpoint κ.

4.1.2 Single-corner model stability and uncertainty analysis

In Figure 4.4 the wheel slip closed-loop system with actuator dynamics and sensor noise is shown.

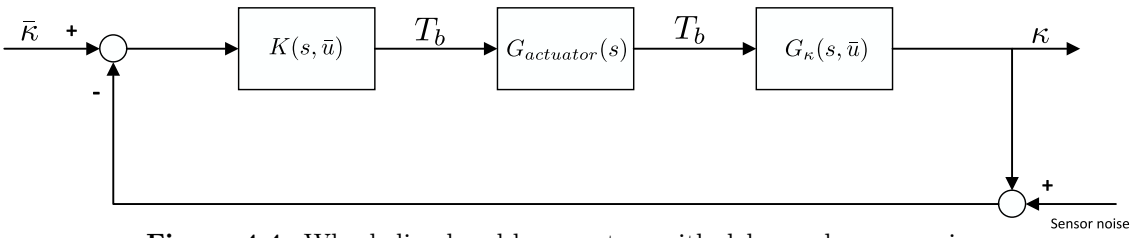

Figure 4.4: Wheel slip closed-loop system with delay and sensor noise.

4.1.2.1 Stability analysis plant without actuator dynamics

To analyse the dynamic properties of

$$G_\kappa(s,\bar{u}) = \frac{\frac{R}{J\bar{u}}}{s + \frac{F_z}{m\bar{u}}\left[\mu_1(\bar{\kappa})\left((1-\bar{\kappa}) + \frac{mR^2}{J}\right) - \mu(\bar{\kappa})\right]}, \tag{4.1}$$

the system is first analysed without actuator dynamics and sensor noise. The characteristic polynomial $\chi_\kappa(s)$ of the closed-loop system $\frac{KG_\kappa(s)}{1+KG_\kappa(s)}$ is given by:

$$\chi_\kappa(s) = s + \frac{1}{\bar{u}}\left[\frac{F_z}{m}\left(\mu_1(\bar{\kappa})\left((1-\bar{\kappa}) + \frac{mR^2}{J}\right) - \mu(\bar{\kappa})\right) + K\frac{R}{J}\right], \tag{4.2}$$

where $K(s,u) = K$ is a simple gain. From this equation a closed-loop stability condition can be obtained and is given by

$$K > -\frac{F_z J}{mR}\left[\mu_1(\bar{\kappa})\left((1-\bar{\kappa}) + \frac{mR^2}{J}\right) - \mu(\bar{\kappa})\right]. \tag{4.3}$$

It can be seen that the stability does not depend on $\bar{u}$ and that a simple proportional controller K can stabilize the plant for all κ. So the closed-loop system is asymptotically stable in every working condition, namely for all values of $\bar{\kappa}$ and for every road, the closed-loop stability can be guaranteed. From Figure 4.2 it can be seen that it is easy to find a setpoint κ that provides good results for every road condition. However to always brake with an optimal friction coefficient the road conditions should be identified online, see chapter 5.

4.1.2.2 Stability analysis plant with actuator dynamics

Now the system is analysed with the delayed actuator dynamics. The transfer function of the brake actuator dynamics which is a first-order linear time-invariant system is given by

$$G_{\text{actuator}}(s) = G_{act}(s)G_d(s) = \frac{\omega_{\text{act}}}{s + \omega_{\text{act}}}e^{-s\tau} \tag{4.4}$$

with a pole at ω_{act} and a pure delay of τ. Nominal values for these kind of brake actuators are ω_{act}=70 rad/s with a delay of τ=20 ms.

The transfer function of the system with actuator dynamics linearized around and unstable setpoint $\kappa = 0.5$ and quasi constant u with actuator dynamics and delay is now given by

$$G_{delay}(s,\bar{u}) = G_\kappa(s)G_{act}(s)G_d(s) = \frac{\frac{0.6}{\bar{u}}}{(s - \frac{259}{\bar{u}})}\frac{70}{(s+70)}\frac{-s+200}{s+200} \tag{4.5}$$

where $G_d(s)$ is a first-order Pade approximation for the delay.

The characteristic polynomial $\chi_\kappa(s,\bar{u})$ of the closed-loop system $\frac{KG_{delay}(s,\bar{u},K)}{1+KG_{delay}(s,\bar{u})}$ is given by:

$$\chi_\kappa(s,\bar{u},K) = (\frac{\frac{-42Ks}{\bar{u}} + \frac{8400K}{\bar{u}}}{(s - \frac{259}{\bar{u}})(s+70)(s+200) + \frac{-42Ks}{\bar{u}} + \frac{8400K}{\bar{u}}} \tag{4.6}$$

where K is a simple proportional gain. The closed-loop poles are now calculated for different gain and velocity. The stability analysis of the closed-loop system is shown in Figure 4.5, where the blue surface represents the unstable region and the white surface the stable region.

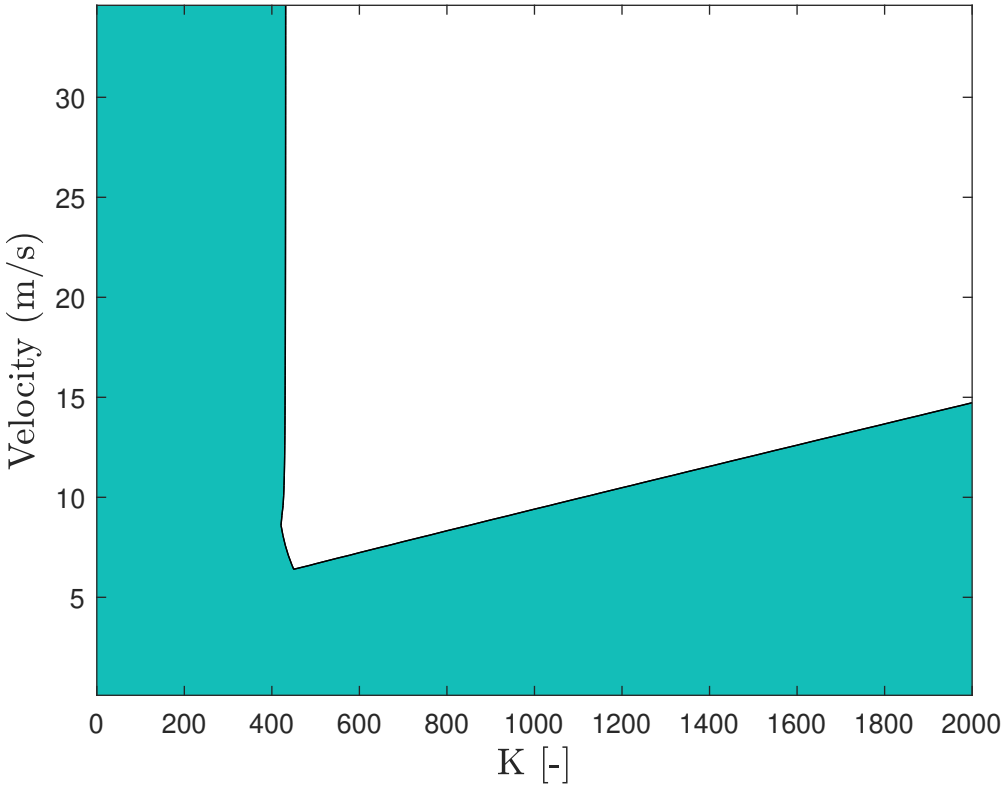

Figure 4.5: Stability analysis of closed loop system for different gain and velocities. Blue surface is unstable region and white surface is stable region.

Figure 4.5 shows that single classical controller could not stabilize the plant for velocities lower than 5 $ms^{-}1$. Therefore, a single classical controller could not guarantee stability for all velocities.

4.1.2.3 Uncertainty analysis

The control-oriented linear plant model that is derived in Section 3.3.2 depends on the tyre normal F_z, the vehicle velocity $\bar{u}$ and the road conditions (which is reflected on $\mu_1(\kappa)$ and $\mu(\kappa)$) during braking. To investigate the variation of plant dynamics, the maximum and minimum values of these variables are derived.

The normal force range limit is:

$$0 \leq F_{z,i} \leq \frac{1500g}{4} kN \tag{4.7}$$

with the i the index for front wheels and rear wheels. The velocity range is

$$1 \leq V_x \leq 35\text{m/s}. \tag{4.8}$$

By investigating different road surfaces at different slips, the maximum and minimum values of $u_1(\kappa)$ occur on dry asphalt. Therefore the slip slope limit is:

$$-0.4 \leq \mu_1(\kappa) \leq 10.1. \tag{4.9}$$

And finally the slip κ is bounded between 0 and 1. The maximum and minimum values of gain and pole of the plant can now be obtained. With this information an uncertainty model can be obtained. Consider the family of plant transfer functions for the stable region as follows

$$P(s) = \frac{b}{s+a}, \tag{4.10}$$

where $0.017 \leq a \leq 0.6$ and a is expressed as $\frac{F_z}{m\bar{u}}\left[\mu_1(\bar{\kappa})\left((1-\bar{\kappa}) + \frac{mR^2}{J}\right) - \mu(\bar{\kappa})\right]$. Moreover $1 \leq b \leq 6720$ and b is expressed as $\frac{R}{J\bar{u}}$. The family can be expressed as

$$\frac{P(s)(1+\Delta W_1)}{1+\Delta W_2 P(s)}, \quad -1 \leq \Delta \leq 1, \tag{4.11}$$

where

$$P(s) := \frac{0.3085}{s+3360}, \quad W_1 := 0.95, \quad W_2 := 3350. \tag{4.12}$$

It is concluded that the plant dynamics are highly sensitive to its operating points. A proper selection of nominal operating points is very important for the design of the control system.

4.1.3 Youla parameterization

In this subsection the idea of a Youla parameterization controller is first explained thereafter this idea is implemented. Let us consider a unity-feedback system with block diagram as shown in Figure 4.6.

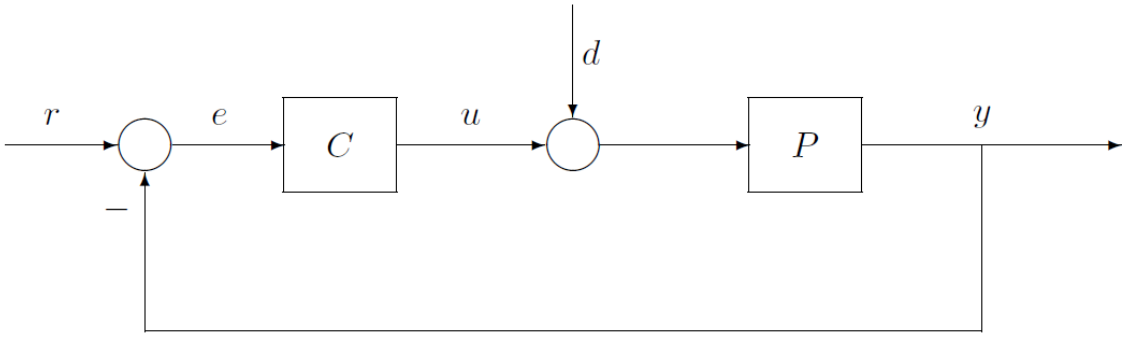

Figure 4.6: Unity-feedback system.

Here the plant P is assumed strictly proper and the controller is assumed C proper. A proper transfer function is a transfer function in which the degree of the numerator does not exceed the degree of the denominator. A strictly proper transfer function is a transfer function where the degree of the numerator is less than the degree of the denominator.

A Youla parameterization is a method to parametrize all C(s) for which the feedback system is internally stable, and then see if there exists a parameter for which an additional desired property can be acquired. For example, the output y asymptotically tracks a step input r. According to [22] the feedback system is internally stable iff the nine transfer functions

$$\frac{1}{1+PC}\begin{bmatrix} 1 & -P & -1 \\ C & 1 & -C \\ PC & P & 1 \end{bmatrix} \tag{4.13}$$

are all proper and stable. The theorem from [22] is as follows .

Theorem 1 Assume that P is stable and $P \in \mathcal{S}$. Then the set of all C for which the feedback system is internally stable equals

$$\left\{ \frac{Q}{1-PQ} : Q \in \mathcal{S} \right\}. \tag{4.14}$$

where $\mathcal{S}$ is a symbol to introduce the family of all stable, proper, real rational functions.

Equation (4.14) can be substituted in Equation (4.13) which leads to

$$\begin{bmatrix} 1-PQ & -P(1-PQ) & -(1-PQ) \\ Q & 1-PQ & -Q \\ PQ & P(1-PQ) & 1-PQ \end{bmatrix}.$$

As can be seen these nine entries belong to $\mathcal{S}$, since all nine transfer functions above are affine fuctions of the free parameter Q; each is of the form $A_1 + A_2Q$ for some A_1, A_2 in $\mathcal{S}$.

4.1.3.1 Implementation

The plant dynamics consists of two first-order transfer functions and a first-order Pade approximation of the delay. As explained before, the stability and dynamics of the plant are highly dependent on the nominal linearization parameters. To obtain an appropriate plant, the nominal operating points are chosen such that $\mu(\kappa)$ is near to its peak value but still in its stable region. Therefore $\mu_1(\kappa) > 0$. The nominal operating points are chosen to be $u = 15\ m/s$ and $\kappa = 0.2$ and the car is driven on dry asphalt. The plant is linearized around these operating points which leads to the stable plant

$$G_{delay}(s) = G_\kappa(s)G_{act}(s)G_d(s) = \frac{0.04}{(s+24.86)}\frac{70}{(s+70)}\frac{-s+200}{s+200}. \tag{4.15}$$

The Youla parameter Q is chosen to be:

$$Q = \frac{1}{G_d(s)}\left[\frac{(-s+200)}{(\tau_1 s+1)(\tau_2 s+1)(s+200)}\right], \tau_1, \tau_2 > 0 \tag{4.16}$$

where τ_1 and τ_2 are tunable parameters to tune the sensitivity and complementary sensitivity transfer functions S and T. τ_1 and τ_2 are tuned to ensure robust performance considering plant dynamics uncertainties at low frequencies and attenuate sensor noise at high frequencies. Therefore a modulus margin lower than 6 dB, a phase margin higher than 30 degrees and a gain margin higher than 6 dB must be guaranteed.

Since $G_{delay}(s)$ is a stable plant the proposed Youla transfer function is stable (and minimum phase), therefore, internal stability of the feedback system is guaranteed.

The complementary sensitivity T and sensitivity S transfer functions are:

$$T = QG_{delay}(s) = \frac{-s+200}{(\tau_1 s+1)(\tau_2 s+1)(s+200)} \tag{4.17}$$

$$S = 1 - T = \frac{(s-200)+(\tau_1 s+1)(\tau_2 s+1)(s+200)}{(\tau_1 s+1)(\tau_2 s+1)(s+200)} \tag{4.18}$$

The controller transfer function K, can be derived as:

$$K = \frac{Q}{S} = \frac{(-s+200)}{G_{delay}(s)\left[(s-200)+(\tau_1 s+1)(\tau_2 s+1)(s+200)\right]} \tag{4.19}$$

and the open loop transfer function L is:

$$L = KG_{delay}(s) = \frac{(-s+200)}{\left[(s-200)+(\tau_1 s+1)(\tau_2 s+1)(s+200)\right]}. \tag{4.20}$$

the closed loop transfer function $\frac{L}{1+L}$ for $\tau_1 = \frac{1}{35}$ and $\tau_2 = \frac{1}{500}$ becomes

$$\frac{L}{1+L} = \frac{-17500(s-200)}{(s+500)(s+200)(s+35)}, \tag{4.21}$$

which is stable.

The magnitude Bode plots of T and S are shown in Figure 4.7. Figure 4.7 shows that the peak values of S and T are less than 2 dB so a gain margin higher than 6 dB is guaranteed. The Bode plots of transfer function G_{delay} and open loop transfer function L are shown in Figure 4.8 which shows that the bandwidth is 4 Hz and that a minimum of 30 degrees phase margin is also guaranteed, which means that a good control performance is met. In Section 4.1.4 the behaviour of the control system in time domain is investigated.

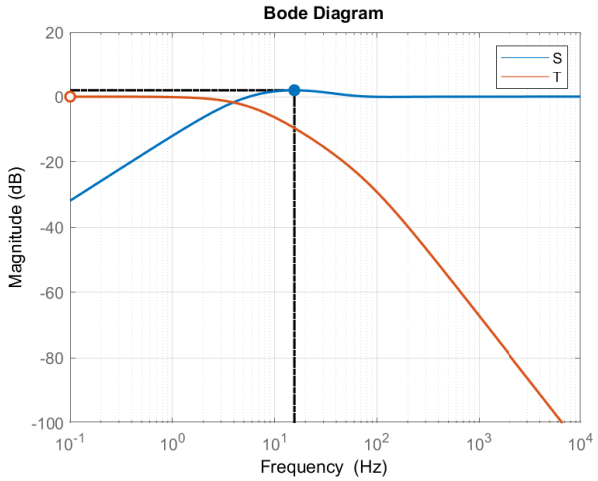

Figure 4.7: Magnitude Bode plots of complementary sensitivity T and sensitivity S.

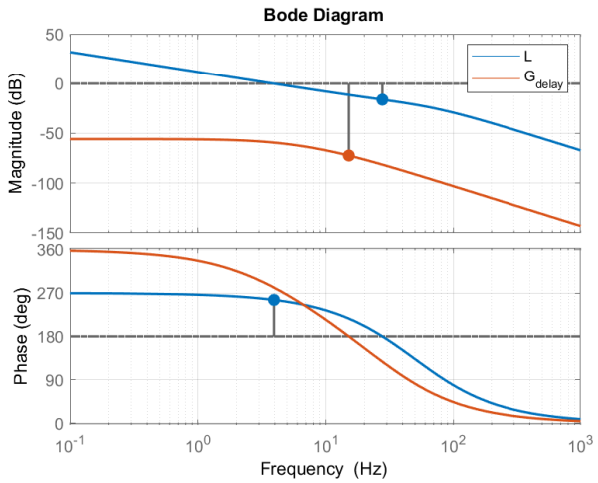

Figure 4.8: Bode plots of transfer function G_{delay} and open loop transfer function L.

4.1.4 Validation

In this section the designed controllers are validated. To investigate the behaviour of the control system in time domain, the response of the closed-loop control system subject to unit step input at different operating points is simulated. In Figure 4.9 the block diagram of the wheel slip closed-loop system with delay is shown.

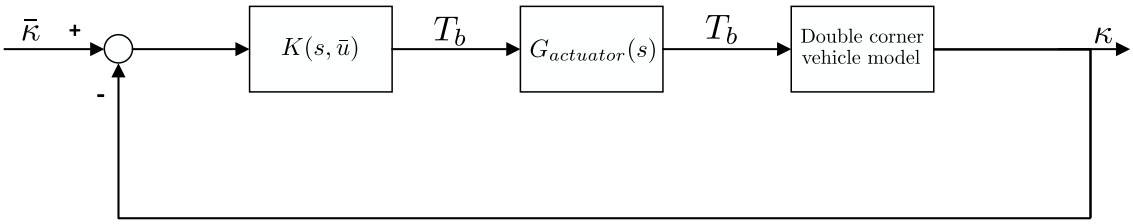

Figure 4.9: Wheel slip closed-loop system with delay.

As can be seen the linearized plant G_κ is now replaced with the non linear double corner vehicle model. The proposed Youla controller is based on the linearized plant transfer function with nominal operating points as discussed before. However, the plant is highly sensitive to variation of parameters as shown in Equation (4.12), where the uncertainty model of the stable region of the plant is shown. The varying parameters are the vehicle velocity, the tyre normal forces, the tyre slip and the road condition. Moreover if the tyre slip κ is increased the plant can even become unstable. As discussed before the goal of the Youla parameterized controller is to stabilize the plant with delay on a broader range of operating points compared to the PI-controller.

To investigate the robustness and stability of the control system at the entire range of operating points, the response of closed loop brake control system subject to slip step input at different operational conditions and surfaces are simulated. Figure 4.10 shows the friction coefficient μ as function of κ for different road conditions. A dry surface corresponds to $\mu_{max} = 1$, a wet surface corresponds to $\mu_{max} = 0.8$ and a snow surface corresponds to $\mu_{max} = 0.2$.

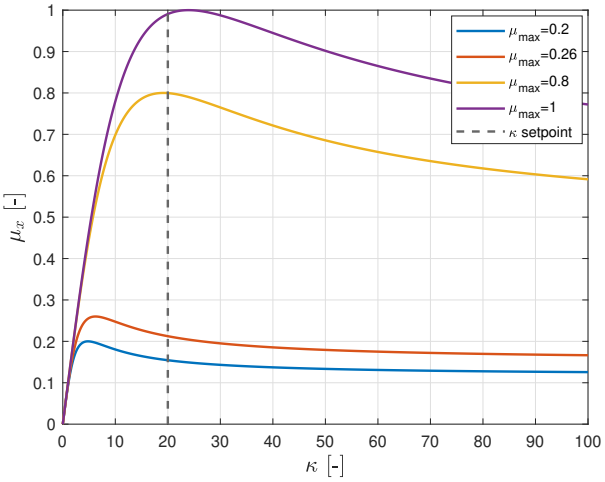

Figure 4.10: The friction coefficient μ as function of κ for different road conditions.

In all simulations the wheel slip setpoint κ is set to 20 after 5 seconds, since this will cover multiple stability regions. On a dry surface the plant dynamics are stable. A wet surface leads to unstable dynamics, however these dynamics are near to its stability boundary and lastly the snow surface leads to unstable plant dynamics. Furthermore, the the performance and robustness of the controllers is tested on a dry surface for different initial velocities. Four different controllers are developed and based on the analysis the best controller is chosen. The first controller K_1 is a PID controller which is optimized for a stable linearized plant with actuator dynamics and delay. The plant is linearized around $\bar{u} = 15$ and $\bar{\kappa} = 20$ on a dry surface. The second controller K_2 is also a PID controller optimized for an unstable linearized plant with actuator dynamics and delay. The plant is linearized around $\bar{u} = 5$ and $\bar{\kappa} = 20$ on a snow surface. Thereafter, a Youla controller K_3 is designed based on a stable plant with actuator dynamics and delay as discussed in the previous section. τ_1 and τ_2 are optimized for robustness. Lastly, a second Youla controller K_4 is designed with τ_1 and τ_2 optimized for performance. In this section the simulation results of controller K_1 and K_4 are analysed. If the reader is interested in controller K_2 and K_3, the reader is referred to Appendix A.2.3.

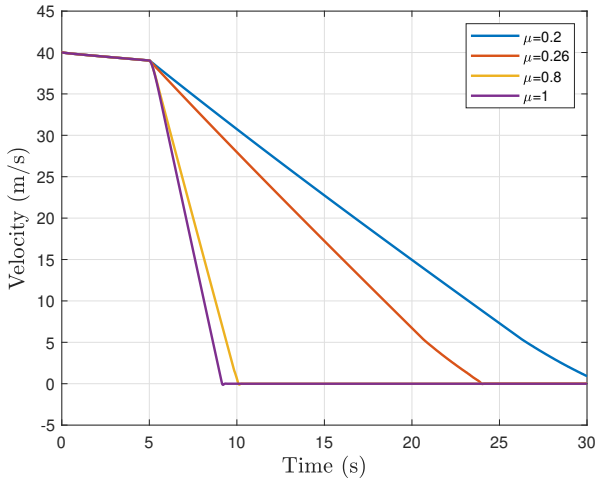

Figure 4.11: The velocity for different road conditions with initial velocity $u_{init} = 40$. Controller: K_1. Slip setpoint $\kappa = 20$.

In Figure 4.11, the velocity simulation results for K_1 on different road surfaces (different μ_{max}) are shown. As can be seen from Figure 4.11, the maximum achievable deceleration is higher on high friction roads, which will lead to a shorter braking distance. The difference in maximum achievable deceleration is caused by a lower road friction coefficient. The velocity simulation results are only shown for controller K_1, since the velocity simulation results for K_4 do not deviate much from it.

In Figure 4.12, the wheel slip simulation results for K_1 on different road surfaces (different μ_{max}) are shown, in Figure 4.13 a zoomed version of Figure 4.12 is shown.

As can be seen from Figure 4.12 the controller is able to stabilize the unstable dynamics for velocities higher than a certain value. However, undesirable oscillations can be seen at low velocities. The undesirable oscillations occur at different moments in time for different road conditions, since the maximum vehicle's deceleration is different for different road conditions as shown earlier in Figure 4.11. From Figure 4.13, it can be seen that settling time is around 0.4 seconds and the overshoot varies from 15% to 30%. The best control performance can be seen on a road with $\mu_{max} = 1$. In Figure 4.14, the initial velocity is varied for a simulation on a dry surface ($\mu_{max} = 1$). The purple line from Figure 4.12 corresponds to the green line in Figure 4.14. Again undesired oscillations can be seen at low velocities.

It is concluded that the controller K_1 is not stable for all admissible velocities, and therefore, K_4 is designed.

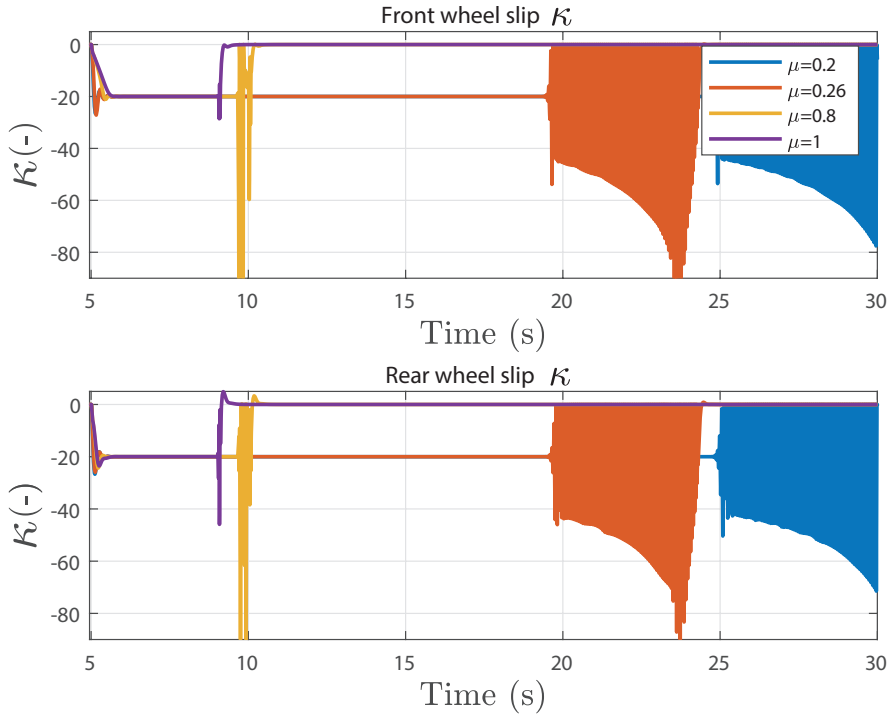

Figure 4.12: The controlled front and rear wheel slip κ_f and κ_r for different road conditions with initial velocity $u_{init} = 40$. Controller: K_1. Slip setpoint $\kappa = 20$.

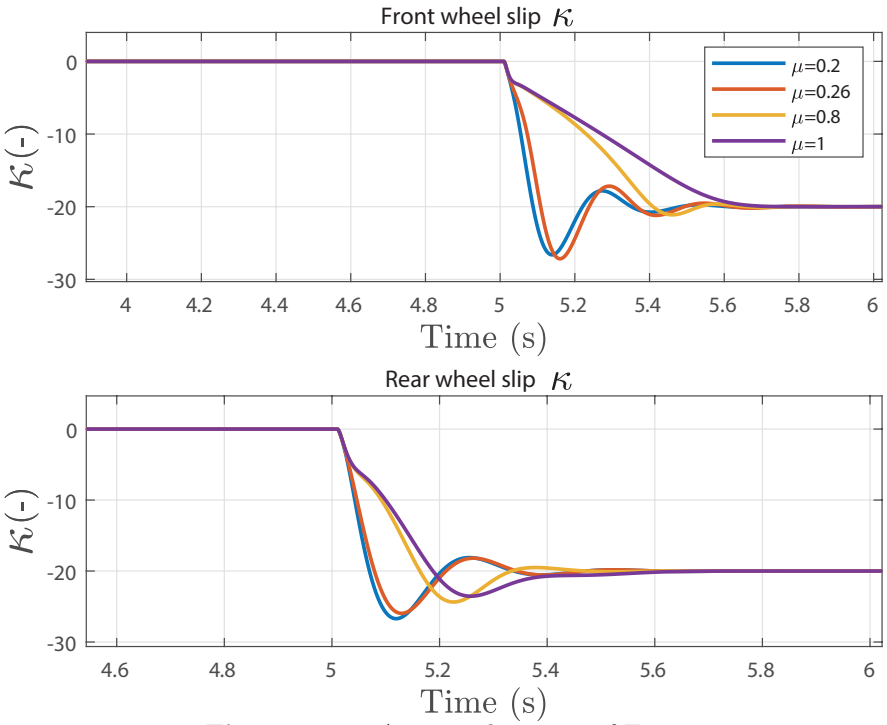

Figure 4.13: A zoomed version of Figure 4.12.

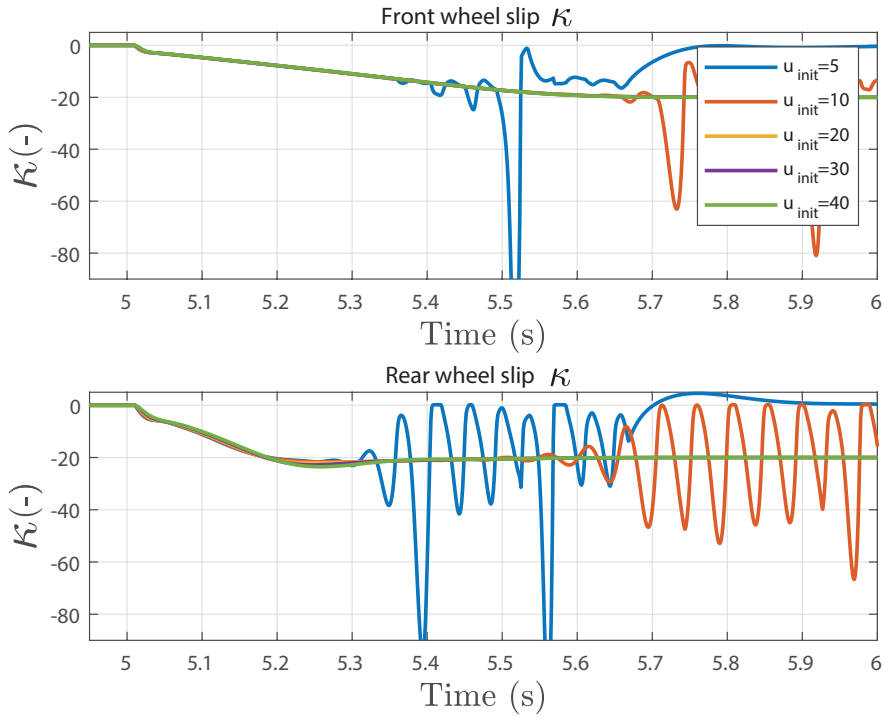

Figure 4.14: The controlled front and rear wheel slip κ_f and κ_r for different initial velocities on dry surface $\mu_{max} = 1$. Controller: K_1. Slip setpoint $\kappa = 20$.

In Figure 4.15 and 4.16 the simulation results for K_4 are shown. The purple line in Figure 4.15

corresponds to the green line in Figure 4.15. It can be seen that K_4 is not able to stabilize κ for unstable setpoints ($\mu_{max} < 0.8$). However, the purple line shows that K_4 is able to stabilize κ. To clarify, for a road with maximum road friction coefficient $\mu_{max} = 1$ the stable slip setpoint is bounded between 0 and 20 and for a road with maximum road friction coefficient $\mu_{max} = 0.2$ the stable slip setpoint is bounded between 0 and 6. From Figure 4.15, can be concluded that controller K_4 is able to stabilize the plant with delayed actuator dynamics at low velocities.

To show that K_4 is also able to stabilize the plant at different initial velocities. A simulation is performed on a road with maximum road friction $\mu_{max} = 1$, where the initial velocity is varied. The results are shown in Figure 4.16. The results confirms the hypothesis that a Youla controller is able to stabilize the plant with actuator dynamics and delay for all velocities. The mean settling time is 0.6 seconds and the overshoot is between zero and 15%, therefore it is concluded that the requirements are met.

4.1.5 Conclusion

It is concluded that a controller that is able to stabilize the plant for all working conditions could not be designed. However, the Youla controller made it possible to control the slip for all velocities for stable setpoints.

To ensure stability a stable setpoint must be selected anytime. In current ABS systems the brake input is increased until unstable dynamics are detected, thereafter the brake input is limited to go back to the stable region. However, if the stability boundary is known before the brakes are actuated, there is no need to go into the unstable region. Therefore it is highly beneficial to know the stability boundary, which is only possible if the tyre dynamics and road conditions are known. Part of this research will study if it is possible to estimate the road conditions by estimating the maximum road friction coefficient μ_{max}. For now it is assumed that the maximum road friction coefficient μ_{max} is known and therefore a stable setpoint could always be selected. Therefore, it is concluded that the controller could guarantee stability.

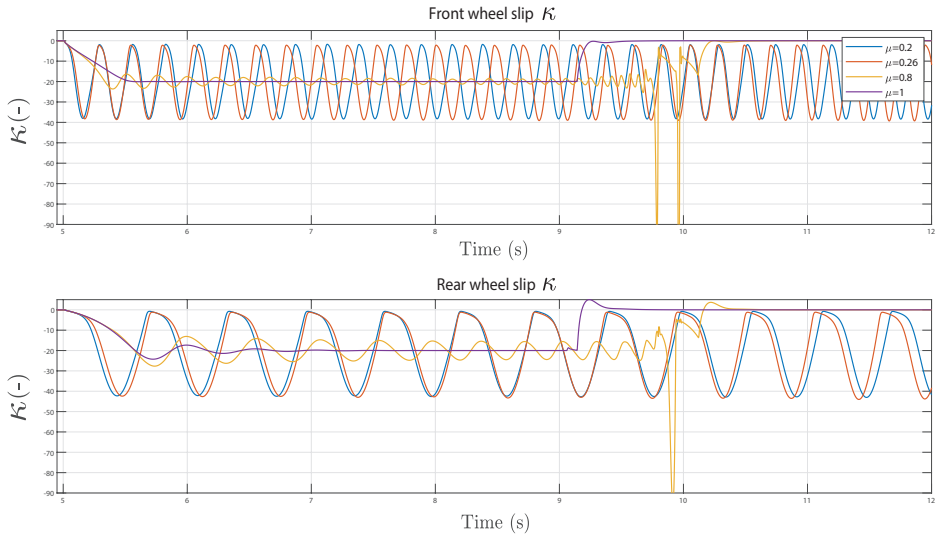

Figure 4.15: The controlled front and rear wheel slip κ_f and κ_r for different road conditions with initial velocity $u_{init} = 40$. Controller: K_4. Slip setpoint $\kappa = 20$.

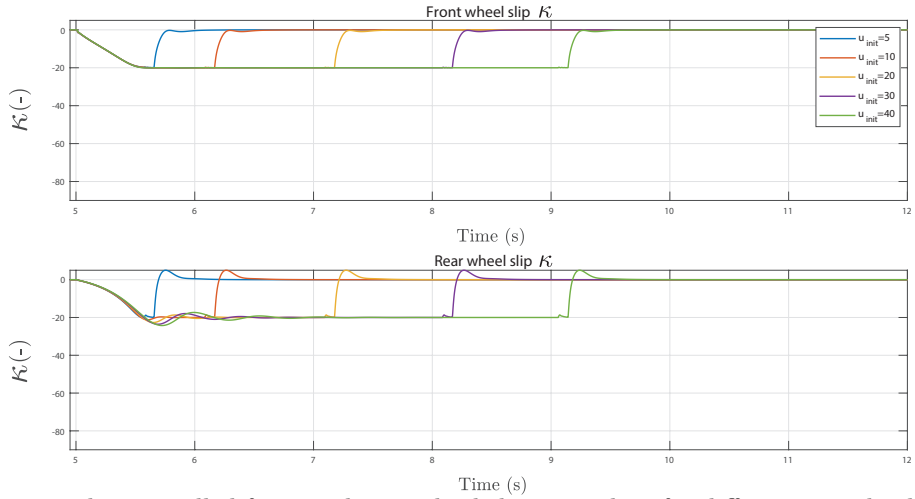

Figure 4.16: The controlled front and rear wheel slip κ_f and κ_r for different initial velocities on dry surface $\mu_{max} = 1$. Controller: K_4. Slip setpoint $\kappa = 20$.

4.2 Slip control algorithm

In this section the slip control algorithm is presented. The goal of this algorithm is to determine a stable wheel-slip setpoint corresponding to the desired acceleration. In Figure 4.17 the slip control algorithm architecture is shown.

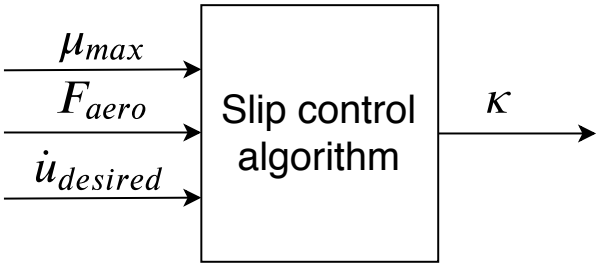

Figure 4.17: A slip control algorithm to determine a stable wheel-slip setpoint corresponding to the desired acceleration.

As discussed in Section 3.1, the longitudinal acceleration is calculated with

$$M\dot{u} = F_{x_f} + F_{x_r} - F_{aero} - Mg\sin\theta. \tag{4.22}$$

The longitudinal tyre force is calculated with a Pacejka model as shown in Equations (3.2) and (3.3).

As shown before the longitudinal force can be calculated with

$$\begin{aligned} B &= \tfrac{BCD}{C \cdot D} \\ \varphi &= B \cdot (\kappa + Sh) - E(B \cdot (\kappa + Sh) - \arctan(B \cdot (\kappa + Sh))) \\ F_x &= D \cdot \sin(C \cdot \arctan(\varphi)) + Sv. \end{aligned} \tag{4.23}$$

If the tyre parameters are well known, this relationship could be inversed to determine what wheel-slip setpoint κ is needed for a certain acceleration. It is assumed that the vehicle is driving on a straight road. Therefore, the road inclination angle is assumed to be zero. For the tyre parameters as expressed in Appendix B.1, the inverse of Equation 3.3 is given as

$$\kappa = 16\mu_{max} \tan(\frac{5}{8} sin^{-1}(\frac{M\dot{u}_{desired} + F_{aero}}{14715\mu_{max}})) \tag{4.24}$$

As can be seen the desired wheel-slip setpoint depends on the desired acceleration $\dot{u}$, the drag force F_{aero} and the maximum road friction coefficient μ_max. A maximum road friction estimator is proposed in Chapter 5. If the estimated maximum road friction coefficient can be estimated with a good accuracy, a stable wheel-slip setpoint can be selected. However, if the accuracy is not good enough a robustness margin needs to be added to this design. This can be done by scaling the desired acceleration to a lower value.

4.3 Upper level controller

In this section the upper level controller for the AEB system is explained in subsection 4.3.1 and the upper level controller for the ACC system is explained in subsection 4.3.2. The upper level controller is an algorithm which controls the desired acceleration based on information from the sensors. Autonomous Emergency Braking (AEB) is braking that is applied automatically by the vehicle in response to the detection of a likely collision. From the literature study it is concluded that current AEB may fail in avoiding rear-end collision on low frictions surfaces. The AEB system is able to reduce the speed on impact, but cannot always avoid accidents under these conditions. In current vehicles with automated driving functions below SAE level 3, the driver can adapt certain ADAS settings. For example the distance to other vehicles can be chosen in case of the ACC or the driver can set the intervention settings corresponding to the current road conditions. To improve the current AEB and ACC systems the road condition information is included in the upper level controller for these systems. Therefore a maximum road friction estimator is needed, which is designed in Chapter 5.

The AEB and ACC systems are designed based on the Euro NCAP [25] requirements which are stated in Appendix C together with some extra requirements to improve the current systems that are used in vehicles.

One of these requirements is to include road condition information in the threat assessment algorithm. Another requirement from the literature analysis is to unify the AEB and ACC system, which can lead to a more comfortable experience. In Figure 4.18 the states and transitions of the unified AEB and ACC system are shown. It can be seen that the ACC system can be activated manually, however the AEB threat assessment algorithm is always running simultaneously with the ACC. Furthermore the AEB system will always overrule the ACC system.

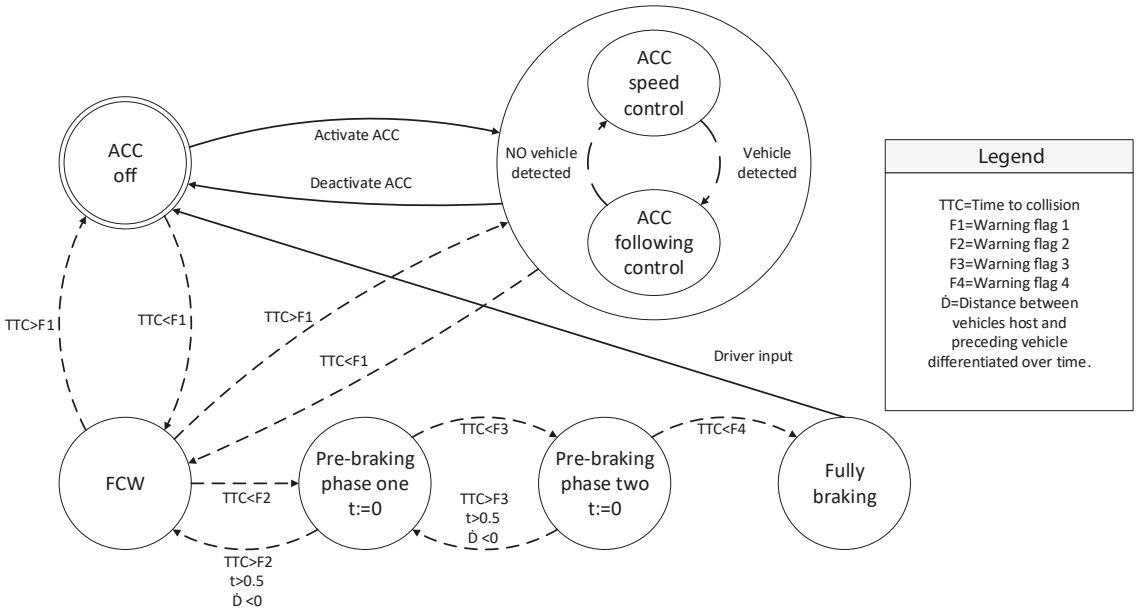

Figure 4.18: The states and transitions of the unified AEB and ACC. Solid line: controllable event Dashed line: uncontrollable. event

The evaluation of the performance of the AEB and ACC controller is done in Chapter 6. In this chapter the AEB and ACC system which considers road information is compared to these same sytems without road information.

4.3.1 Autonomous emergency braking

As shown in Figure 4.1 the proposed AEB system includes an environment perception system, an upper-level controller and a slip controller. The environment perception system consists of different sensor systems including a wheel speed encoders to measure the wheel speeds ω and a radar system to measure the distance D to a preceding vehicle and the velocity v_p of that preceding vehicle. Furthermore a GPS and accelerometer can be used to measure the host vehicle speed v_h and acceleration.

The upper-level controller controls the desired acceleration based on a threat assessment algorithm. The literature analysis shows that many threat assessment algorithms could be used to asses the threat with each their arguments. The most commonly used algorithm is time-to-collision [17], which is described by

$$TTC = \frac{D}{(v_h - v_p)}. \tag{4.25}$$

Based on the TTC the upper level controller decides what action to perform. In Figure 4.19 the different control actions for the proposed AEB system can be seen.

Threat stage	Desired deceleration ($\frac{m}{s^2}$)
Pre-braking phase one	$-\mu_{max}$
Pre-braking phase two	-5μ_{max}
Fully braking	-10μ_{max}

Table 4.1: The desired deceleration for the different threat stages.

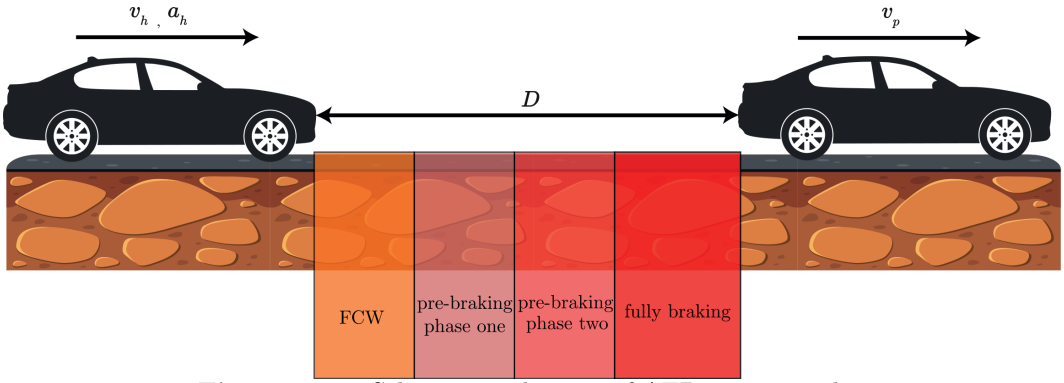

Figure 4.19: Schematic side view of AEB system with inputs.

Different phases of the AEB system are activated after certain flags, which can be seen in Figure 4.18. First a Forward Collision Warning (FCW) is given to the driver to give the driver a possibility to correct its velocity and distance to the preceding vehicle. Thereafter two partial braking phases are activated with each their own deceleration profile to avoid a collision without the need to decelerate with its maximum deceleration, which leads to a more comfortable experience. Under certain conditions the control system is switching fast between FCW and pre-braking phase one or between pre-braking phase one and phase two which leads to chattering in the desired acceleration profile, therefore an extra requirement is added to prevent this behavior which can be seen in Figure 4.18. The requirement is that the control system will only switch back to a lower threat stage if the host vehicle is not closing in on the preceding vehicle for half a second.

If the TTC is still decreasing to a point where the TTC is lower than the last warning flag $F4$, the car will exert its brake with its maximum deceleration until standstill.

The values of these warning flags must be optimized to prevent false interventions or accidents with the notion that both variables which are measured to calculate the TTC are subject to measurement uncertainties.

As discussed before these warning flags are optimized by the supplier based on their measurements and sometimes they can be adjusted by the driver to compensate for their driving style and weather conditions. Therefore the current AEB sytems will decrease the speed on impact on low friction roads but not always avoid a collision. To improve the robustness of the AEB system for different road conditions the activation times $F1$ to $F4$ can be described as a function of the maximum friction coefficient μ_{max} which is given by

$$F_i(\mu_{max}) = \frac{F_i}{\mu_{max}}, \tag{4.26}$$

where i is the index 1 to 4 corresponding to the different threat stages. The desired deceleration for the different threat stages are given in Table 4.1. The maximum road friction estimator is designed in Chapter 5 and the AEB performance is evaluated in Chapter 6.

4.3.2 Adaptive cruise control

In contrast to an autonomous emergency braking system, a adaptive cruise control system aims on comfort. As can be seen in Figure 4.18 an adaptive cruise control system can switch between speed control and following control. Adaptive Cruise Control originates from Cruise Control, which today is a widespread functionality in modern vehicles. CC regulates the vehicle speed actuating the throttle only, via tracking of speed v that is set by the driver. ACC automatically adapts the vehicle's speed depending on a predecessor's behavior, actuating the throttle as well as the brake system. The aim of the proposed ACC system is to maintain a certain relative distance D_{ref} with the preceding vehicle and track its speed v_p taken into account certain comfort requirements. All the ACC requirements are stated in Appendix C. However the most important comfort requirements are that when the ACC is active the acceleration is limited by [-2, 2] $\frac{m}{s^2}$ and the jerk is limited by [-2, 2] $\frac{m}{s^3}$. The control rule which is used to control the vehicle speed and relative distance is described by

$$a_{desired} = k_1(v_p - v_h) - k_2(D_{ref} - D), \tag{4.27}$$

where v_p, v_h and D are the measured host vehicle's speed, the preceding vehicle's speed and relative distance respectively. Furthermore k_1 and k_2 are proportional gains to tune the performance. In current similar ACC systems the desired relative distance is defined with the Constant-Time Headway policy [56]:

$$D_{ref} = d_s + T_h v_h, \tag{4.28}$$

where d_s is a distance buffer between two vehicles in order to avoid a collision, T_h is the constant-time headway that approximates the human reaction time. To unify the AEB and ACC system the constant-time headway is chosen to be the same value as F_1 corresponding to the TTC flag of the forward collision warning system. Therefore the ACC system is autonomously adapting its desired distance for different road conditions. Moreover, the distance buffer d_s ensures that the host vehicle is following the preceding vehicle just before the boundary of switching to FCW.

The unified AEB and ACC system as shown in Figure 4.18 can be seen as two independent systems running simultaneously. However the system is optimized to work fluently by setting the constant-time headway to $f1$ the TTC flag of the forward collision warning system. Both systems have a positive influence on each other. The ACC system is maintaining the desired relative distance D_{ref} and tracks the preceding vehicle's speed v_p, therefore the ACC system can be seen as another pre-braking stage in some situations, which can lead to more comfort and less interventions from the AEB system. On the other hand the AEB system leads to a safer experience.

4.4 Conclusions

In this chapter, the lower-level controller and upper-level controller are described. For the lower-level controller it is concluded that a PID-controller was not able to stabilize the plant with actuator dynamics at low velocities. Therefore this chapter focused on finding a method to stabilize the plant. It is concluded that a Youla parameterized controller is able to stabilize the plant at low velocities, however as shown in the results the controller is not able to stabilize the unstable dynamics which occur after the maximum peak friction. One solution could be to design a control logic which lowers the setpoint κ when unstable dynamics are seen. Another solution which is further researched is to design a maximum road friction estimator. If the maximum road friction coefficient is known, the optimal slip setpoint κ could be determined.

In the second section of this chapter the upper-level controller is described. The threat assessment algorithm assesses the threat with the TTC. The activation times are scaled proportionally with

the road conditions.

Finally, it is concluded that the unified AEB and ACC system as shown in Figure 4.18 can be seen as two independent systems running simultaneously. However the system is optimized to work fluently by setting the constant-time headway to $f1$ the TTC flag of the forward collision warning system. Both systems have a positive influence on each other. The ACC system is maintaining the desired relative distance D_{ref} and tracks the preceding vehicle's speed v_p, therefore the ACC system can be seen as another pre-braking stage in some situations, which can lead to more comfort and less interventions from the AEB system. On the other hand the AEB system leads to a safer experience.

5. Road friction estimator

In Chapter 4 is concluded that a maximum road friction estimator could be used to guarantee the stability of the proposed slip controller, since the maximum road friction estimator could determine a suitable slip κ setpoint for different road conditions. Furthermore in Section 4.3 is concluded that a maximum road friction estimator can also improve the robustness of the AEB and ACC system for different road conditions. In the literature analysis which is conducted in Section 2.3 multiple ways of designing a maximum road friction estimator are discussed with each their own arguments. Some researches concluded that a well-trained Neural Network is able to estimate the road conditions. The main benefits of using a neural network is that a neural network can establish relationships between input and output instead of storing an entire complex tyre model in the controller, which can reduce the computational time significantly, avoid model errors due to model discrepancy and lastly guarantee real-time performance by accurately capture the hidden structure in the measured data [53]. In this section it is investigated how well a Neural Network trained by simulation data can estimate the maximum road friction coefficient on straight roads. The simulation data is captured from a non linear vehicle model with a Pacejka tyre model as explained in Section B.2. Paper [41] researched what the accuracy of a maximum road friction estimator must be to not exceed a certain impact speed when approaching a standstill object. The following cases can occur:

- $\hat{\mu_{max}} > \mu_{max}$ (over-estimation): Over-estimation leads to smaller activation times than required to avoid an accident.
- $\hat{\mu_{max}} < \mu_{max}$ (under-estimation): Under estimation leads to false interventions.

Current AEB systems assume dry roads. It can be assumed that the current systems over-estimate the road condition in order to minimize false interventions on dry roads. If the driver fails to react an AEB is supposed to react at the latest moment possible. Therefore the AEB system will fail in avoiding a collision on surfaces with lower friction. In Figure 5.1 the relation between the tolerable deviation $\Delta\mu_{max}$ and μ_{max} is shown in order to not exceed a certain impact speed for different initial velocities.

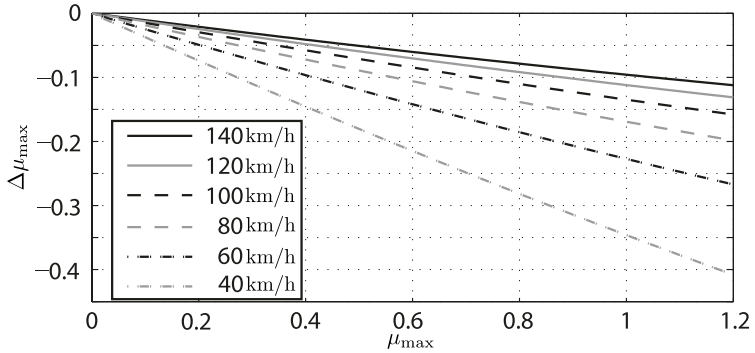

Figure 5.1: Tolerable deviation $\Delta\mu_{max}$ in dependence on the real value μ_{max} of the maximum road friction coefficient for different initial longitudinal speeds [41].

In this research the maximum road friction coefficient μ_{max} is also used to determine the set point of the wheel slip which is sent to the slip controller. The following cases can occur:

- $\hat{\mu_{max}} > \mu_{max}$ (over-estimation): Over-estimation can lead to unstable behavior.
- $\hat{\mu_{max}} < \mu_{max}$ (under-estimation): Under estimation leads to a lower maximum deceleration, since the slip control algorithm selects a lower slip setpoint.

Over-estimation is certainly not desired since that will lead to unstable behavior. However the slip control algorithm which decides on what slip setpoint must be used could be optimized based on the performance of the maximum road friction estimator. If for example the estimation is poor on low friction surfaces a robustness margin can be added to the slip control algorithm, this leads to a lower maximum deceleration for that surface.

5.1 Neural Network

A general workflow for the design of a Neural Network adapted for our use case is shown in Figure 5.2. In this section all these steps will be elaborated.

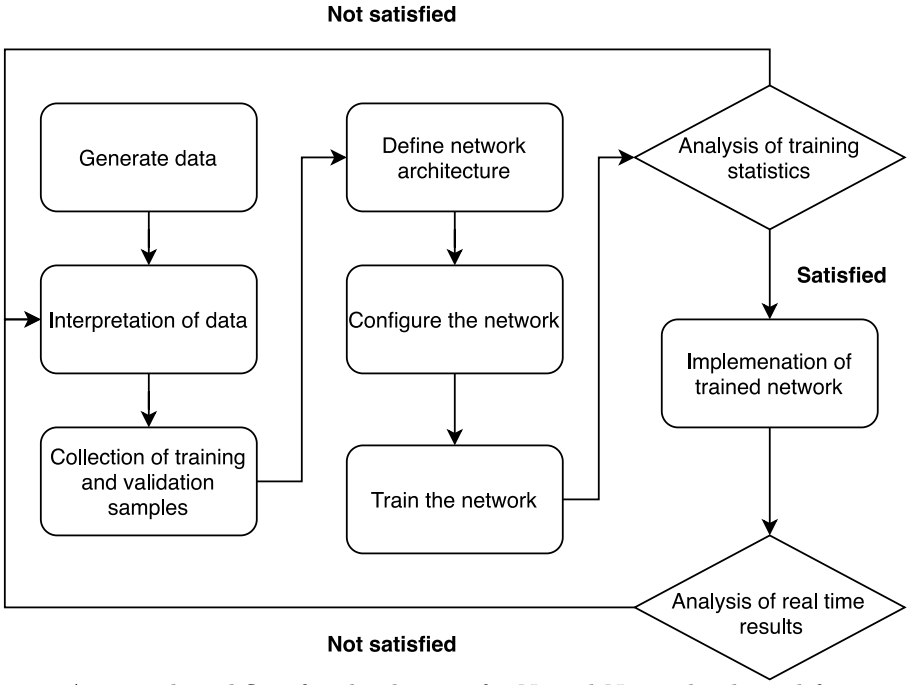

Figure 5.2: A general workflow for the design of a Neural Network adapted for our use case.

5.1.1 Data generation

As the analytical models from Chapter 3 show, the longitudinal force F_x on straight roads is dependent of the vertical force F_z, the longitudinal slip κ, the tyre parameters and the maximum road friction coefficient μ_{max}. As can be seen from Equation (3.13) the main contribution of the acceleration $\dot{u}$ is the longitudinal force F_x. The longitudinal slip κ can be estimated from the wheel velocity ω and vehicle velocity u which can be measured with sensors. Furthermore the tyre parameters and the total vertical force acting on the vehicle's center of mass stay constant. Therefore the longitudinal slip κ and the acceleration $\dot{u}$ are selected as input to feed the neural network. The overall structure to estimate μ_{max} is shown in Figure 5.3.

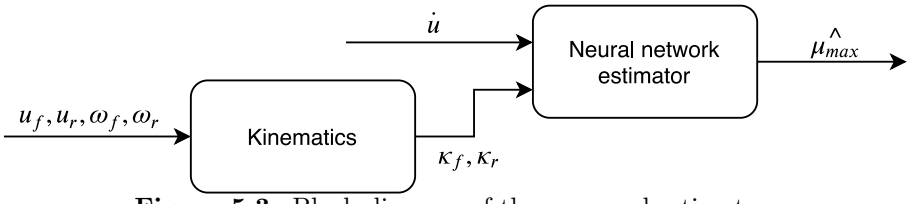

Figure 5.3: Block diagram of the proposed estimator.

Inputs parameter	Variation
Maximum friction coefficient μ_{max}	**0.1 to 1.0 at intervals of 0.1**
Simulation time	**9000 s**
Velocity	[1 35] $\frac{m}{s}$
Acceleration	[-4 4] $\frac{m}{s^2}$
κ	[-1 1]

Table 5.1: Data training parameters and space dimensions.

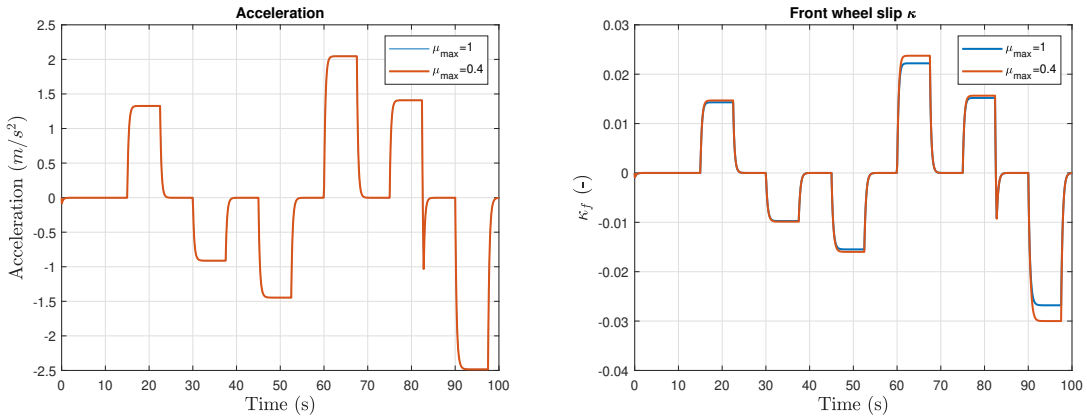

(a) Acceleration plotted against time.

(b) Front wheel slip κ plotted against time.

Figure 5.4: Simulation results of the acceleration $\dot{u}$ and the front wheel slip κ_f for two different values of μ_{max} over time.

The dataset is created from MATLAB Simulink simulations. The roll-axis vehicle model is simulated for 9000 seconds for every simulation at a 100 Hz sampling rate with a different maximum road friction coefficient. A range from 0.1 to 1.0 of the maximum friction coefficient is considered with increments of 0.1. The vehicle of the simulation is first controlled with the slip controller with random input of acceleration and deceleration on dry road surface with a maximum road friction coefficient of 1.0. These reference inputs are generated by differentiating a randomly created velocity profile with 600 data points over a certain time step. This time step is chosen such that the acceleration and deceleration stay between the desired limits. The acceleration limit is chosen to be [-4 4] $\frac{m}{s^2}$, since the estimator should be capable to estimate the maximum road friction coefficient under normal driving conditions.

The wheel and braking torque time responses are saved from the simulation and thereafter these random torques are used for the other simulations corresponding to different road conditions. The range of inputs and the simulation environment are denoted in Table 5.1. Since the simulation time is 9000 seconds and the sampling rate is 100 Hz, a dataset with 900000 data points is generated for every output (μ_{max}). To feed the data in a neural network this data must be re-sampled.

5.1.2 Data interpretation

To better understand the data which is generated, the simulation results of the acceleration $\dot{u}$ and the front wheel slip κ_f for two different values of μ_{max} over time are shown in Figure 5.4. From this figure, it can be seen that for the same constant acceleration a different wheel slip is measured, also this difference is increasing with higher accelerations. Furthermore, during a transition from one acceleration to another no difference in slip can be seen.

In Figure 5.5 a scatter plot is shown which is taken from the acceleration for different wheel slips for two different values of μ_{max}. The Pacejka curve characteristics can be recognized in this plot,

however the data has a lot of variation. Feeding this data to a neural network will certainly not lead to any good results. As discussed before the data should be re-sampled and since it is concluded that the data during a transition from one acceleration to another acceleration is not any useful, this data is filtered out.

The results are shown in Figure **??**.

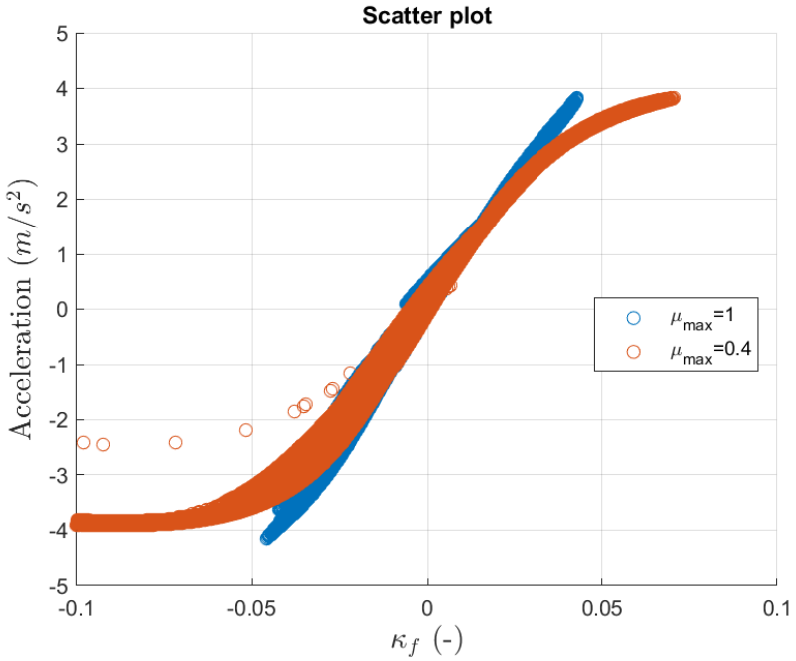

Figure 5.5: A scatter plot is shown which is taken from the acceleration for different wheel slips for two different values of μ_{max}

As discussed before there is no variation for low accelerations. Since it is impossible for the neural network to estimate the road friction coefficient at constant speed a new requirement is created, which is that the road friction estimator should only estimate the road friction if the acceleration is higher than 0.05 or lower than -0.05 $\frac{m}{s^2}$. The training data with all the unwanted data filtered out is shown in Figure 5.6. The training data is divided in 70 % training data, 15 % validation data an 15 % test data. The training data will be used to train the neural network, the simulation data is used to not over fit the neural network and the test data is used to test the neural network.

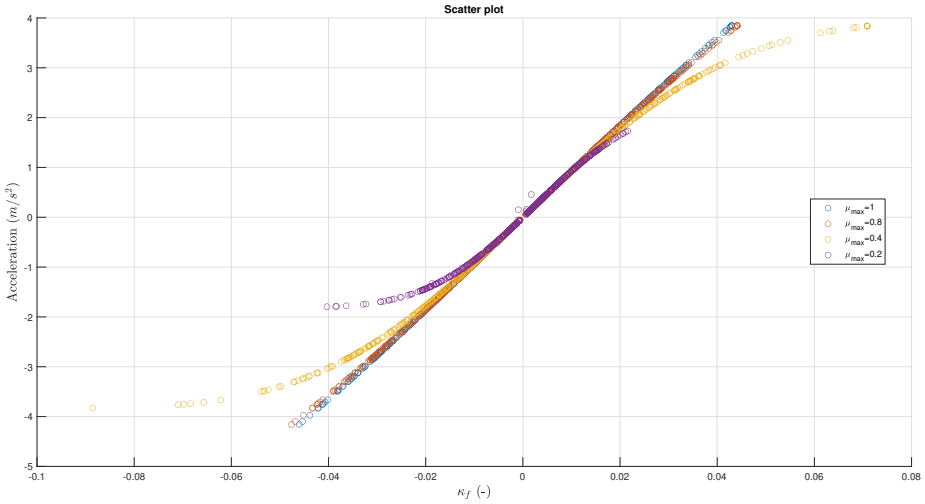

Figure 5.6: The training data with all the unwanted data filtered out.

5.1.3 Network architecture

In Figure 5.7 the neural network architecture is presented. One input layer with three inputs namely the acceleration $\dot{u}$ and the front and rear wheel slips κ_f and κ_r is used. Thereafter two hidden layers with each 15 neurons are used, where W_i is the composition of the weights associated to each neuron. Finally one output layer with the estimated maximum road friction μ_{max} as output.

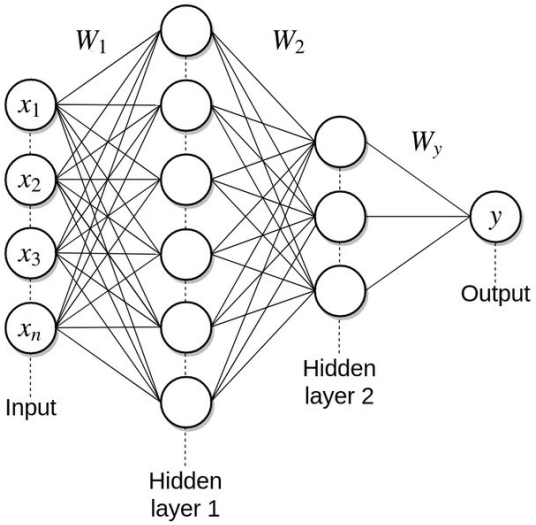

Figure 5.7: Neural network architecture [52].

The training is carried out using the Matlab Neural Network Toolbox [37]. A back-propagation *Levenberg-Marquardt* algorithm is used with 1000 epochs of training iterations. The neural network is trained to minimize the mean squared error calculated with

$$\text{MSE} = \frac{1}{n}\sum_{i=1}^{n}\left(\mu_{max_i} - \hat{\mu_{max_i}}\right)^2. \tag{5.1}$$

All the other training parameters can be found in Appendix B.

5.1.4 Analysis of training statistics

In this section the trained network is analysed. To optimize the performance of the Neural Network, multiple configurations of the network are tested. For example the number of hidden layers and the number of neurons in each layer is varied. Since training a Neural Network with the same configuration can lead to different results the training is performed multiple times and the best performance for each configuration is selected. The performance of the models is primarily measured through their root mean squared error (RMSE), which is the standard deviation of the prediction errors. This is a well-known method to validate regression prediction models [65]. Considering the ANN, the RMSE is not used as the Loss function that the *Levenberg-Marquardt* algorithm tries to minimize during training. Next to the RMSE, the mean absolute error (MAE) is computed to get a better understanding of these evaluation metrics the corresponding formulas are:

$$RMSE = \sqrt{\frac{1}{n}\sum_{t=1}^{n} e_i^2} \qquad MAE = \frac{1}{n}\sum_{t=1}^{n} |e_i| \,,$$

in which e_i is $\mu_{max_i} - \hat{\mu_{max}}$ and n is the number of samples.

Finally it is concluded that the best performance is achieved with 2 hidden layers with each 15 neurons. The results of other settings are shown in Appendix A.3. In Figure 5.8 the performance during training is shown, it can be seen that the best performance is achieved at epoch 889 with a Mean Squared Error of 0.0035. In Figure 5.9 the regression plot is shown for the training data, validation data, test data and all the data, where R is the Correlation Coefficient. A high value of R means that the Neural Network has successfully managed to model most of the variation in the input to target transformation [65]. In Figure 5.10 an error histogram is shown, from this figure it can be seen that most of the predicted values of μ_{max} have an error of 0.00951 or lower however in some cases the absolute error is almost 0.35. Another test data set is feed to the trained neural network and the estimated $\hat{\mu_{max}}$ and real values of μ_{max} can be seen in Figure 5.11. From these two figures can be concluded that the estimator is working well enough for further validation.

As discussed before the large errors that sometimes occur leads to over-estimation and under-estimation, which is not desired. Multiple causes can lead to these poor estimates. The most obvious cause is that the bad estimate occur at low accelerations, since the variation is very low at these data points. Another cause could be that the test data is still too noisy after filtering the re-sampled data. The Neural Network is implemented in real time simulations in the next section.

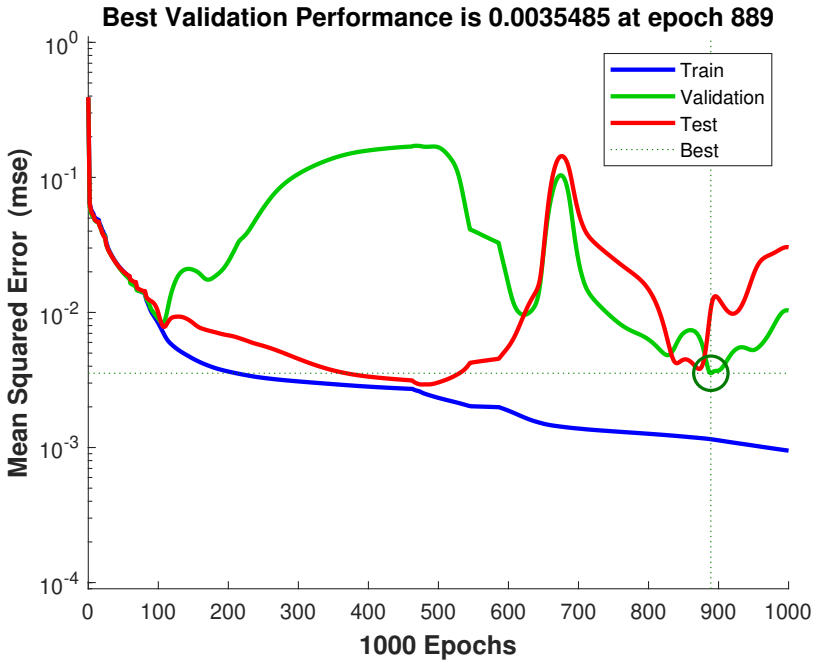

Figure 5.8: A performance plot which shows the Mean Squared Error during training for the training, validation and test data.

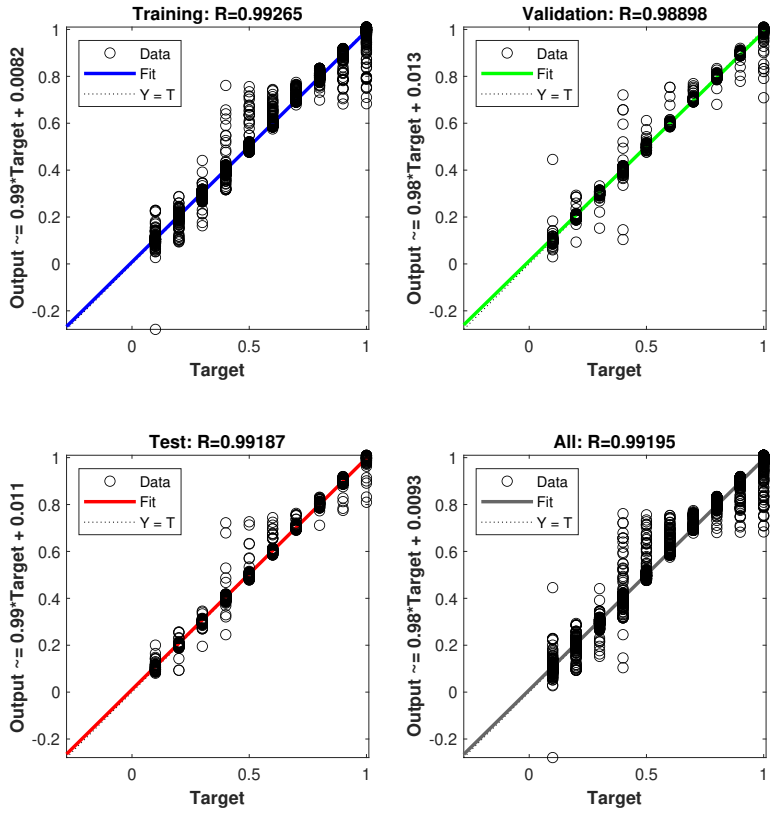

Figure 5.9: Regression plot which shows the target and output values of μ_{max} for the training, simulation and test data.

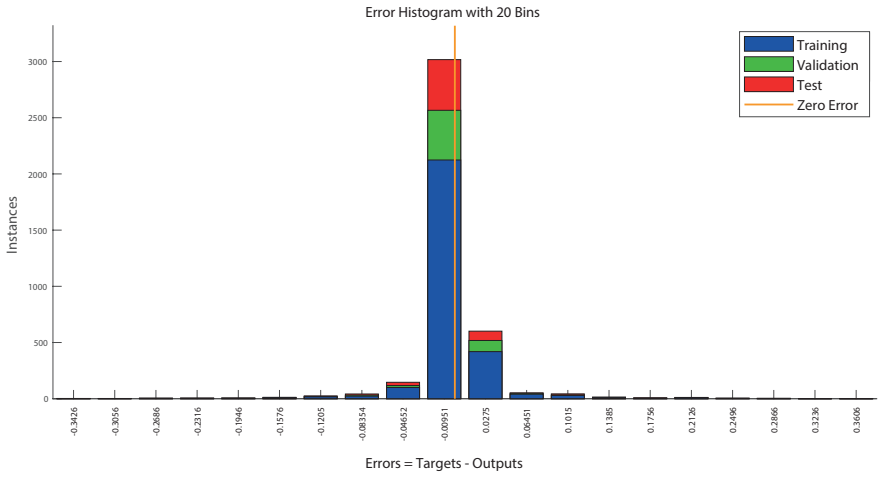

Figure 5.10: A histogram which shows the error of the estimated μ_{max} for all samples.

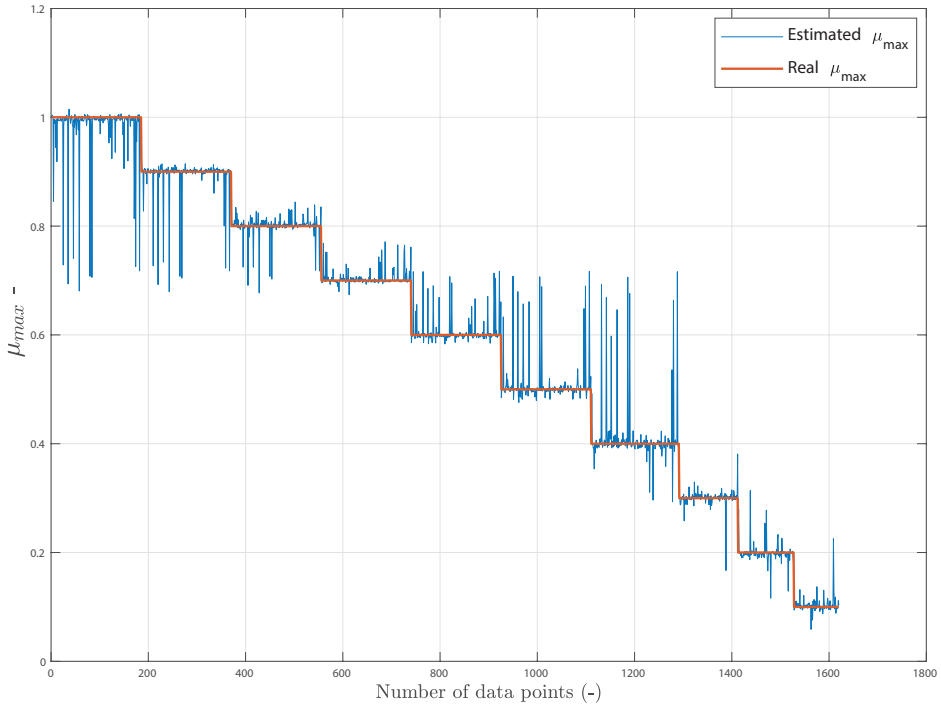

Figure 5.11: A simulation with a test data set which is not used during training of the neural network.

5.2 Analysis of real-time results

To analyse the Neural Network in real time, the input data should be supplied to the Neural Network in the same way as it was supplied to train the network. The Neural Network is trained with data from constant accelerations higher than 0.05 or lower than -0.05 $\frac{m}{s^2}$. Therefore a state machine must be designed to ensure that the estimator is only estimating the road friction coefficient under certain conditions. To illustrate the need of such a machine, first a real time estimation is performed without this algorithm. The results are presented below. In Figure 5.12 the measured acceleration is plotted and Figure 5.13 shows the estimated and real values of μ_{max}. The estimates during constant acceleration are marked with black lines. It can be seen that the estimation outputs exceed its limits [0.1 1] and the estimate is quite bad half of the time, however the estimates for constant accelerations higher and lower than a certain value are quite accurate.

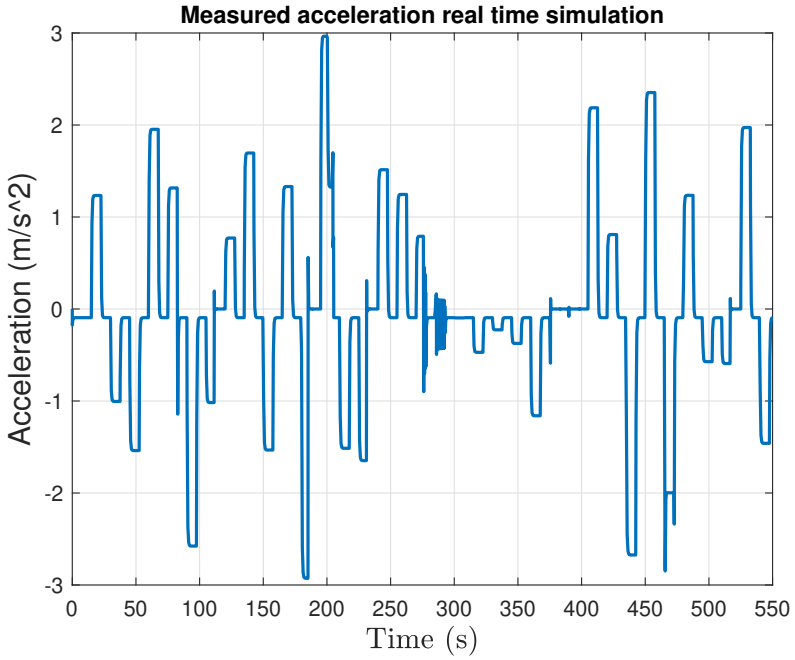

Figure 5.12: Acceleration during a scenario simulation to validate the neural network.

It is concluded that a state machine must be designed with the following requirements:

- The estimator should only estimate if the acceleration $0.05 < \dot{u} < 4$ and $-4 < \dot{u} < -0.05$.
- The estimator should only estimate if the jerk is between $-0.1 < jerk < 0.1$.
- The estimator should only estimate driving on straight road (no steering input).
- The estimator should remember its previous estimation when it is not aloud to estimate.

The state machine is designed and the new estimation results are shown in Figure 5.14.

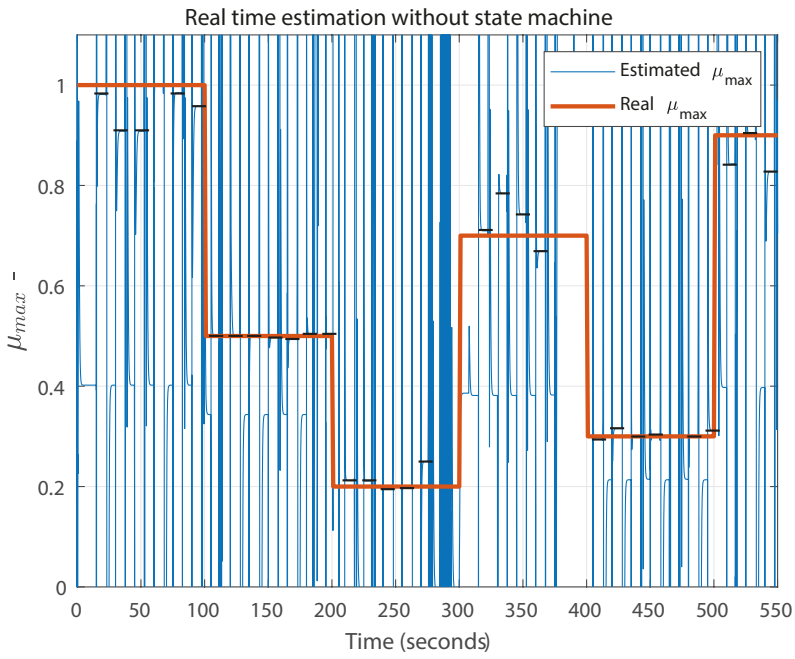

Figure 5.13: The estimated and real values of μ_{max} during a scenario as shown in Figure 5.12.

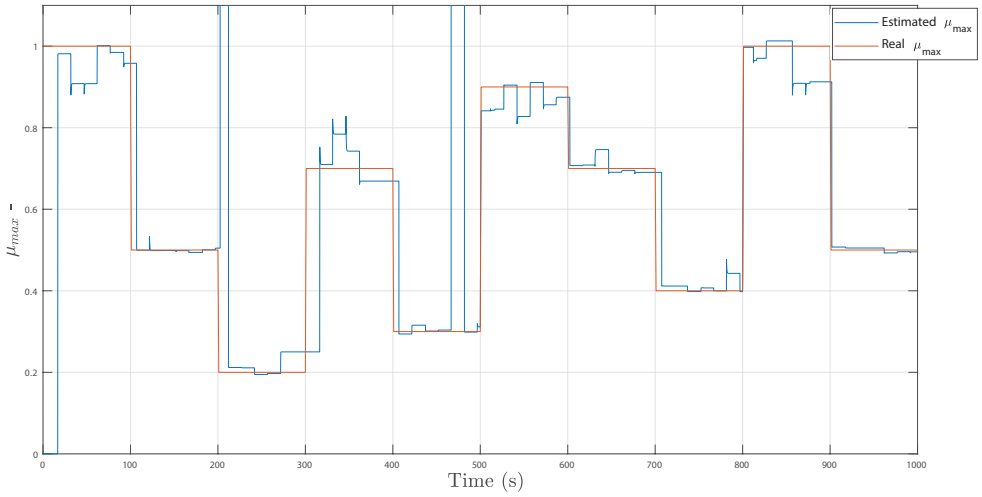

Figure 5.14: The estimated and real values of μ_{max} during a scenario as shown in Figure 5.12 with the inclusion of a state machine.

5.3 Discussion

In this chapter, a neural network is trained to estimate the maximum road friction coefficient μ_{max} The estimation algorithm is evaluated on varying road surfaces and shows a good accuracy. It is concluded that the maximum road friction estimator is able to accurately predict the maximum road friction coefficient μ_{max} if the vehicle is driving on a straight road with a nonzero constant acceleration or deceleration. The predicted μ_{max} can be used in the upper level controller of the ADAS systems to improve the performance on different road conditions. However it is not recommended to use this information in the design of a slip controller, since it is very important to always be able to have full control of the vehicle. If the estimation fails to detect μ_{max} for example during a sensor fail, the well-trained neural network may not be able to accurately estimate and therefore, which can lead to unstable control behavior. Furthermore as can be seen in Figure 5.14, the estimator sometimes still give poor estimates.

Furthermore it is concluded that a good knowledge about the tyre dynamics is needed. The trained data is now obtained from a mathematical tyre model. The proposed method is only analyzed theoretically and validated via simulation and therefore subsequent work is needed to validate the ANN with real-world tyre data.

6. Validation of ADAS systems

In this chapter the designed ADAS systems are validated. First the AEB system is validated according to the performance tests from Euro NCAP [25]. In [25] is stated that the tests are conducted in dry conditions with ambient temperature above $5°C$ and below $40°C$ and the test track shall have a so called peak braking coefficient of 0.9. This coefficient is called the maximum road friction coefficient μ_{max} in this research. To rate the AEB system for different road conditions the Euro NCAP test procedure must be adapted. In Section 6.1.1 the adapted Euro NCAP test procedure is validated for different maximum road friction coefficients. The standard AEB system without information is compared with the AEB system with road information.

6.1 Euro NCAP AEB performance

In this section the AEB system is validated according to the performance tests from Euro NCAP [25]. Euro NCAP rates AEB systems of cars based on their performance on their test scenarios. There are three scenarios namely CCRs, CCRm and CCRb:

Car-to-Car Rear Stationary (CCRs) – a collision in which a vehicle travels forwards towards another stationary vehicle and the frontal structure of the vehicle strikes the rear structure of the other.
Car-to-Car Rear Moving (CCRm) – a collision in which a vehicle travels forwards towards another vehicle that is travelling at constant speed and the frontal structure of the vehicle strikes the rear structure of the other.
Car-to-Car Rear Braking (CCRb) – a collision in which a vehicle travels forwards towards another vehicle that is travelling at constant speed and then decelerates, and the frontal structure of the vehicle strikes the rear structure of the other.

All three scenarios are illustrated in Figure 6.1. The vehicle sponsor will fund 10 verification tests per scenario, where applicable. For AEB City, 10 tests in CCRs (10-50km/h). For AEB Inter-Urban, 10 tests for AEB (CCRm). The end of a test is considered when one of the following occurs:

- Velocity subject vehicle is 0 km/h.
- Velocity subject vehicle is lower than preceding vehicle.
- A collision between subject vehicle and preceding vehicle.

When a collision occurs the relative velocity is measured which is defined as velocity at impact. Based on these measurements the performance is rated.

6.1.1 Car-to-Car Rear Stationary performance

Normally there is a distinction between AEB City and AEB Inter-Urban. The AEB City should only work in the range 10-50 km/h and the AEB Inter-Urban should work in the range 30-80 km/h. In this research only one AEB system is designed which is tested in the range 10-80 km/h with increments of 5 km/h. Another difference between the proposed test procedure and the the Euro NCAP test procedure is that the AEB is only validated with zero overlap. Normally the sensor system of the car is validated by overlapping the car from -50% to 50% with increments of 25% as can be seen in Figure 6.4. Since our sensor is an ideal sensor this test is not necessary. Multiple simulations are performed for different initial velocities and different road conditions. If the host vehicle collide with the standstill vehicle, the relative velocity at impact denoted as u_r is measured. If the AEB system accomplish to avoid a collision the relative distance at standstill is given denoted denoted as D_r.

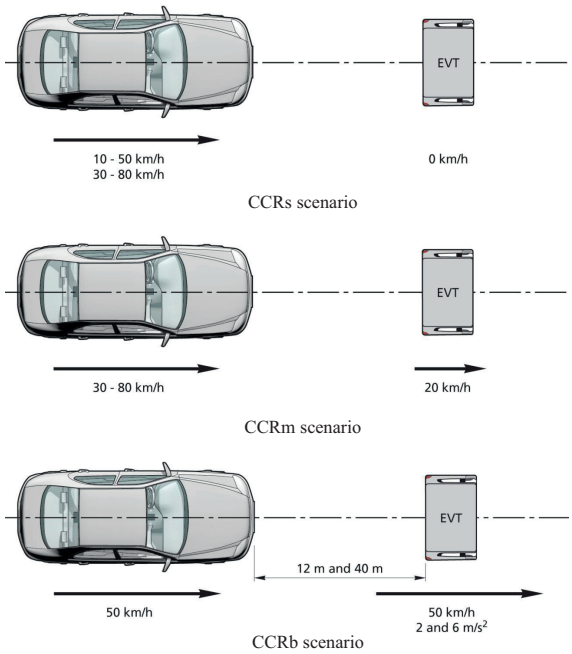

Figure 6.1: Test scenarios [26].

In Table 6.1, the results for an AEB system without road information is shown and compared to the results for an AEB system with road information which are presented in Table 6.2. In Figure 6.2, the acceptable performance for every initial velocity according to Euro NCAP for CCRs scenarios is shown.

The overall performance of the AEB system is good on dry surfaces according to Euro NCAP. The main conclusions from these results is that an AEB with road information succeeds to avoid a collision in more operational working conditions compared to the AEB without road information. The proposed AEB system seems to benefit the most on roads where the maximum road friction coefficient is low which corresponds to snow and wet roads. The collisions can be avoided since the AEB system is activated earlier, however as can be seen in the upper plot from Figure 6.3, due to the pre-braking phases the AEB system is not activated at the last possible moment. The pre-braking phases are added to improve the comfort of the AEB system, however for scenarios on low friction roads the maximum achievable deceleration is already low therefore it is decided to do the simulations on the road with a maximum road friction coefficient $\mu_{max} = 0.3$ again without the pre-braking phases.

Figure 6.3 shows two CCRs scenario on a snowy road with an initial velocity of 40 km/h. In the upper plot an AEB with pre-braking phases is used and in the lower plot an AEB system without pre-braking phases is used. It can be seen that the AEB system without pre-braking states starts to brake 5 seconds later. Furthermore the brakes are activated at nearly the last possible moment. This behavior is desired and therefore it is concluded to remove the first and second pre-braking phase for roads with a maximum road friction coefficient lower than 0.3 and remove only the second pre-braking phase for roads with maximum road friction coefficient between 0.3 and 0.6.

6.1.2 Car-to-Car Rear Braking performance

To test the Car-to-Car rear braking performance only four scenarios have to be tested according to Euro NCAP. The initial velocities for both the preceding and host vehicle is 50 km/h in all four scenarios, furthermore the simulations are performed on a road with a maximum road friction coefficient of 0.9. The initial distance and the preceding vehicle's acceleration is varied for the

AEB without road information

Initial velocity [km/h]	Friction coefficient									
	0.3		0.5		0.7		0.9		1	
	D_r [m]	u_r [km/h]	D_r [m]	u_r [km/h]	D_r [m]	u_r [km/h]	D_r [m]	u_r [km/h]	D_r [m]	u_r [km/h]
10	1.2184	-	1.0869	-	1.0555	-	1.0428	-	1.0395	-
15	1.4175	-	1.1181	-	1.0463	-	1.0177	-	1.0097	-
20	0.2432	-	2.5399	-	3.9254	-	3.9676	-	3.9724	-
25	0.4120	-	1.4468	-	0.8381	-	0.6448	-	0.5926	-
30	2.2703	-	1.9496	-	1.1776	-	0.8311	-	0.7362	-
35	0.4405	-	1.4880	-	0.7023	-	0.2205	-	0.0904	-
40	-	12.4092	0.00982	-	4.7019	-	4.5369	-	4.4840	-
45	-	19.7710	3.7513	-	3.7854	-	3.5247	-	3.4515	-
50	-	26.0301	2.2620	-	2.3706	-	2.0714	-	1.9872	-
55	-	31.8423	0.3602	-	1.0861	-	1.1310	-	1.54	-
60	-	37.4139	-	15.4772	-	4.7030	0.7090	-	1.0446	-
65	-	42.8355	-	23.9350	-	17.5206	-	9.0092	0.1710	
70	-	48.1577	-	30.9154	-	25.4595	-	19.5332	-	15.3991
75	-	53.4100	-	37.2553	-	32.2934	-	27.1598	-	23.9524
80	-	58.6082	-	43.2320	-	38.5886	-	33.8702	-	31.0599

Table 6.1: Results CCRs scenarios of AEB without road information.

AEB with road information

Initial velocity [km/h]	Friction coefficient									
	0.3		0.5		0.7		0.9		1	
	D_r [m]	u_r [km/h]	D_r [m]	u_r [km/h]	D_r [m]	u_r [km/h]	D_r [m]	u_r [km/h]	D_r [m]	u_r [km/h]
10	0.2259	-	0.9717	-	0.6946	-	1.5004	-	1.0395	-
15	1.9656	-	1.6538	-	0.9651	-	1.5466	-	1.0097	-
20	1.2971	-	1.8986	-	1.5970	-	0.2134	-	3.9724	-
25	0.1970	-	1.3835	-	1.2106	-	1.4025	-	0.5926	-
30	0.5006	-	0.9398	-	1.7037	-	1.6541	-	0.7362	-
35	0.5332	-	1.3375	-	1.4180	-	1.1172	-	0.0904	-
40	1.8270	-	1.6955	-	0.1755	-	5.0282	-	4.4840	-
45	1.5825	-	1.7616	-	0.0596	-	4.0446	-	3.4515	-
50	0.6980	-	0.2313	-	3.8043	-	2.4559	-	1.9872	-
55	0.2058	-	2.8738	-	1.2886	-	1.7360	-	1.5400	-
60	5.4821	-	3.0457	-	1.9336	-	1.2827	-	1.0446	-
65	3.7768	-	1.7379	-	0.8555	-	0.3530	-	0.1710	-
70	0.7817	-	-	5.1716	-	10.4745	-	13.9274	-	15.3991
75	-	15.1208	-	18.1515	-	20.6561	-	22.8918	-	23.9524
80	-	23.9257	-	26.2408	-	28.2638	-	30.1426	-	31.0599

Table 6.2: Results CCRs scenarios of AEB with road information.

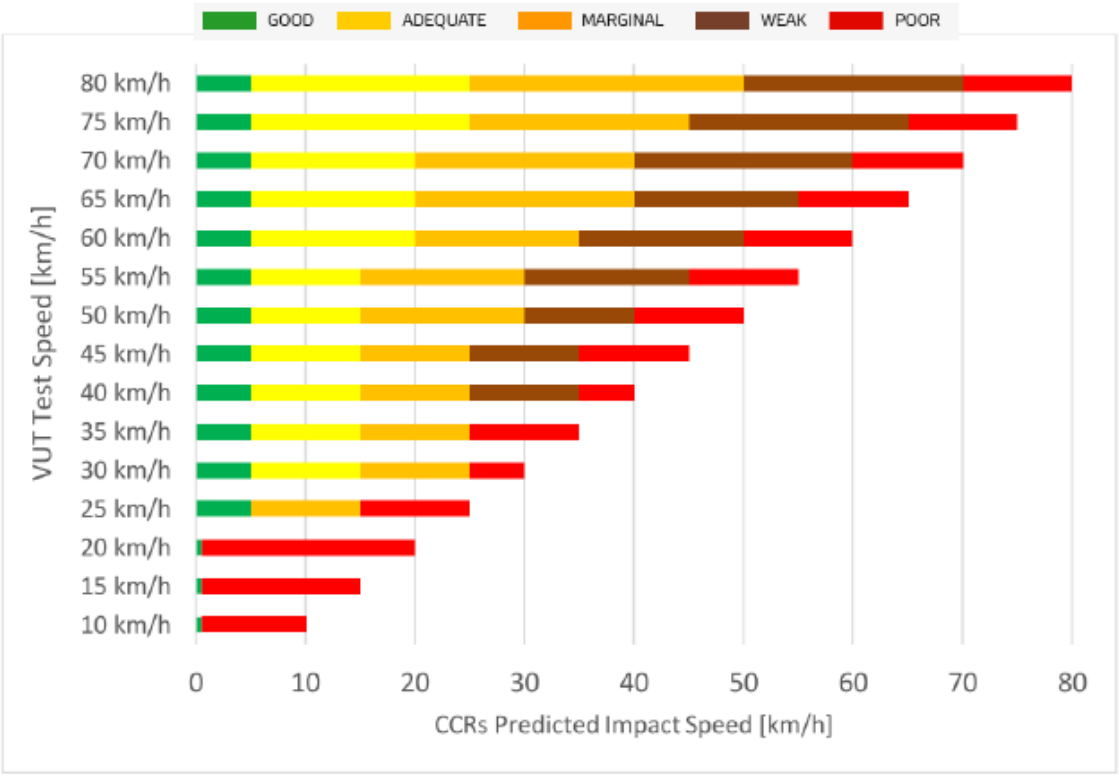

Figure 6.2: Performance rating for every initial velocity for CCRs scenarios [26].

	Initial distance D (m)	**Deceleration preceding vehicle a_p ($\frac{m}{s^2}$)**
Scenario 1	40	2
Scenario 2	40	6
Scenario 3	12	2
Scenario 4	12	6

Table 6.3: CCR Braking scenarios.

four scenarios as shown in Table 6.3.

In Figure 6.5, 6.6, 6.7 and 6.8 the results are shown. In these figures the velocity of both the preceding and host vehicle and their relative distance is shown. From Figure 6.5, it can be concluded that the AEB is working as designed, since the two pre-braking phases and the fully braking phase is clearly visible. To overcome chattering from the AEB algorithm the transition from pre-braking phase two to pre-braking phase one or the transition from pre-braking phase one to FCW is only allowed if the relative distance is increasing and the warning flag corresponding to each state is not active anymore for at least 0.5 seconds. From Figure 6.7, it can be concluded that the designed state machine is working well. Furthermore, as can be seen from Figure 6.8 the AEB system fails to avoid a collision in the fourth scenario, the speed at impact is around 20 km/h. As stated in Table 6.3, the preceding vehicle decelerates with a very high deceleration of 6 $\frac{m}{s^2}$, the maximum achievable deceleration on a road with a maximum road friction coefficient of 0.9 is theoretically around 9 $\frac{m}{s^2}$. However, the slip control algorithm limited the maximum deceleration to around 8.5 $\frac{m}{s^2}$ to ensure stable behavior.

As discussed in the literature study, TTC is not the best threat assessment algorithm, since it is only assessing the threat based on the relative distance and relative velocity. Scenario four confirms this hypothesis. As discussed before the second pre braking phase leads to a deceleration of 5 $\frac{m}{s^2}$ and since the preceding vehicle decelerates with 6 $\frac{m}{s^2}$ the change in relative velocity is quite

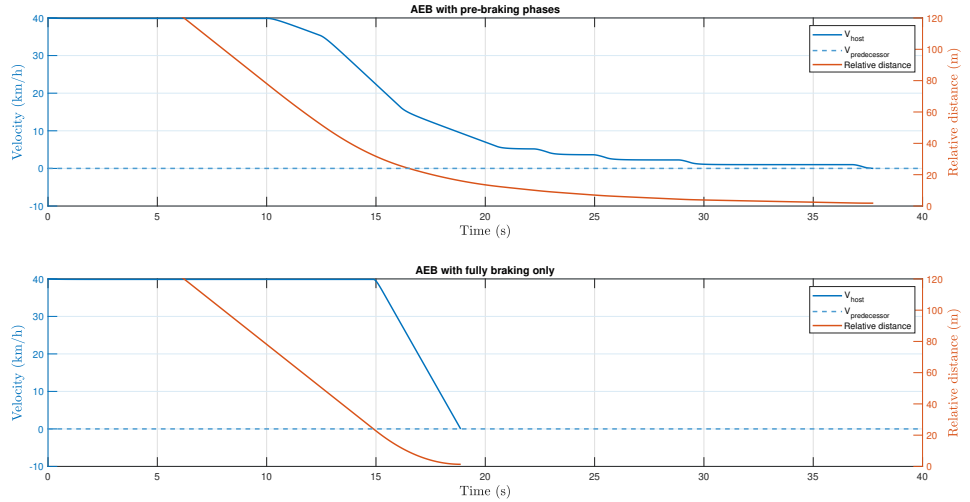

Figure 6.3: Two CCRs scenario on a snowy road with an initial velocity of 40 km/h. In the upper plot an AEB with pre-braking phases is used and in the lower plot an AEB system without pre-braking phases is used.

low and therefore TTC is not changing fast enough. As discussed in this research unifying an AEB and ACC can improve safety and comfort. Scenario four is now validated with the unified AEB and ACC system. In Figure 6.9, the results of this simulation are shown. The main goal of an ACC system is not safety, however from the comparison between Figure 6.9 and Figure 6.8, it can be concluded that an ACC system can improve the overall safety of the AEB system. In the AEB scenario the speed at impact is 20 km/h where the speed at impact is halved in case of the unified AEB and ACC scenerio.

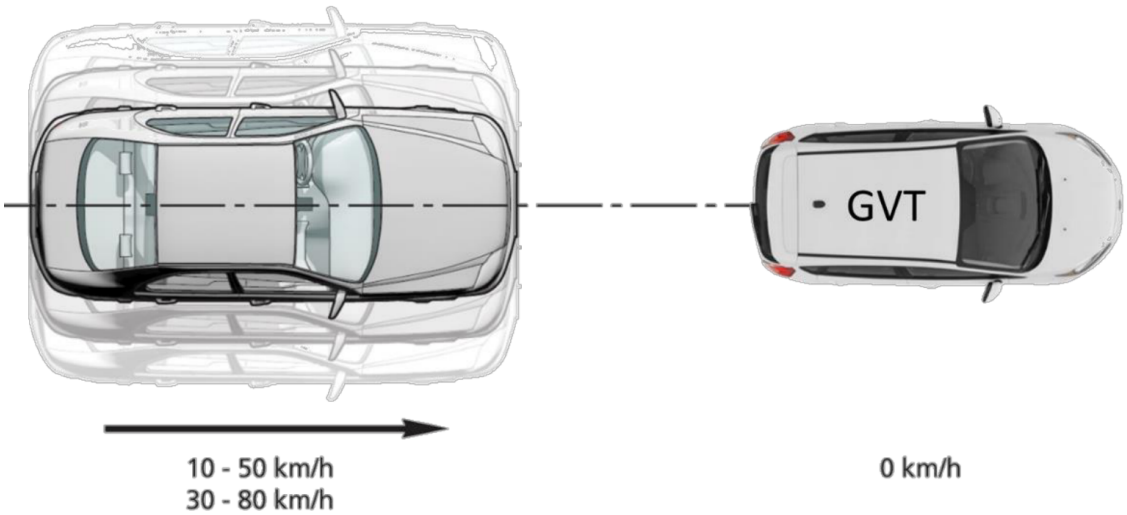

Figure 6.4: CCR test scenario according to Euro NCAP [26].

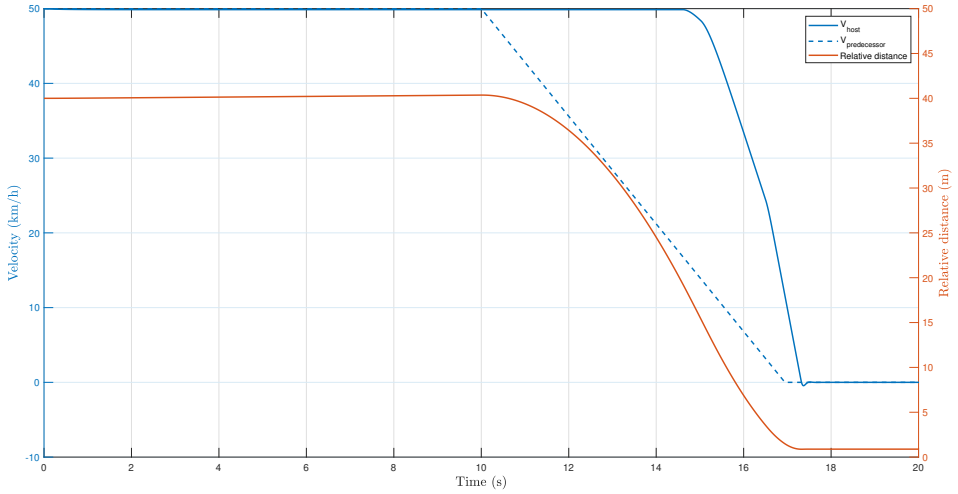

Figure 6.5: Simulation results CCR braking Scenario 1.

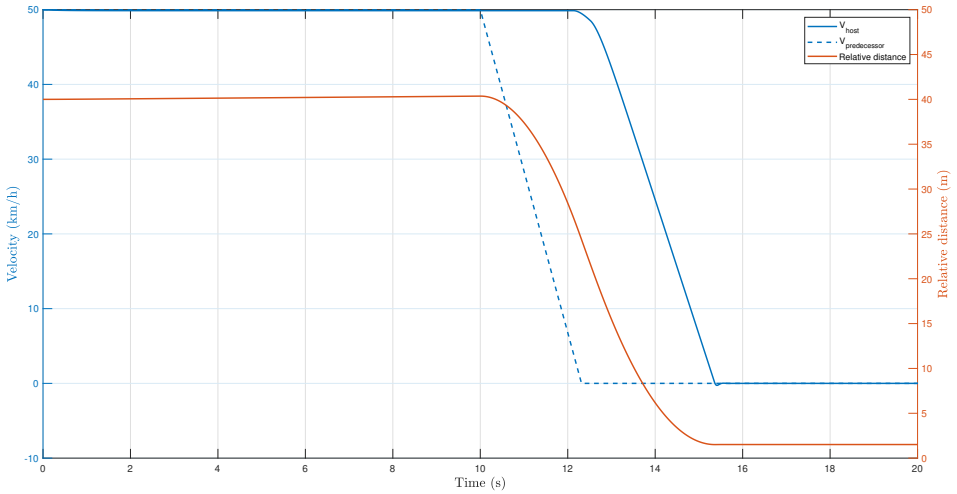

Figure 6.6: Simulation results CCR braking Scenario 2.

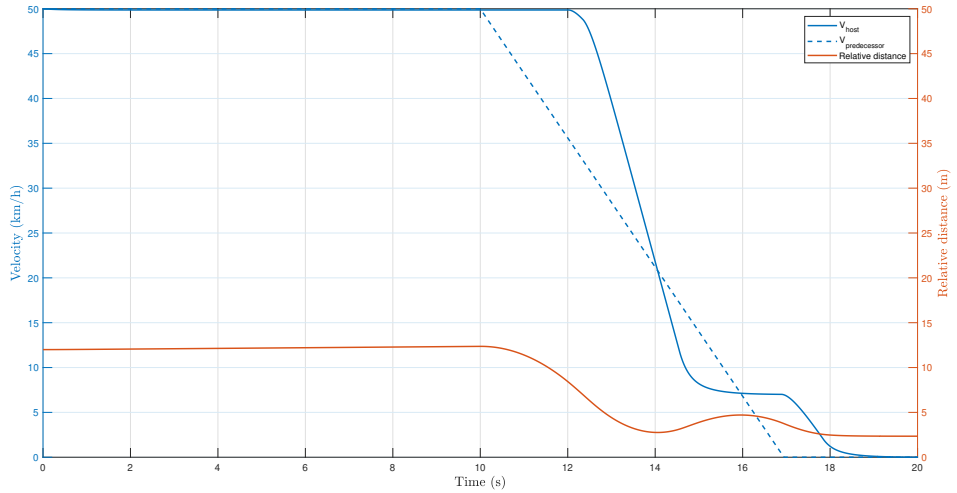

Figure 6.7: Simulation results CCR braking Scenario 3.

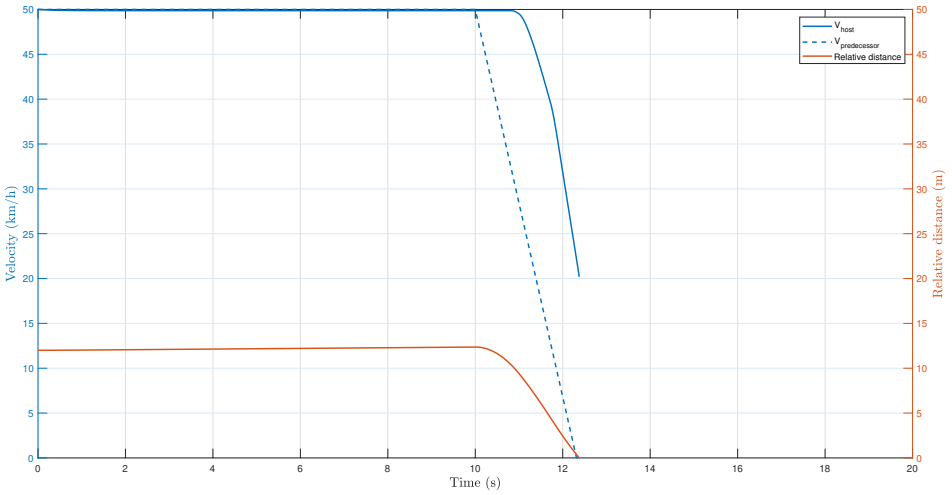

Figure 6.8: Simulation results CCR braking Scenario 4.

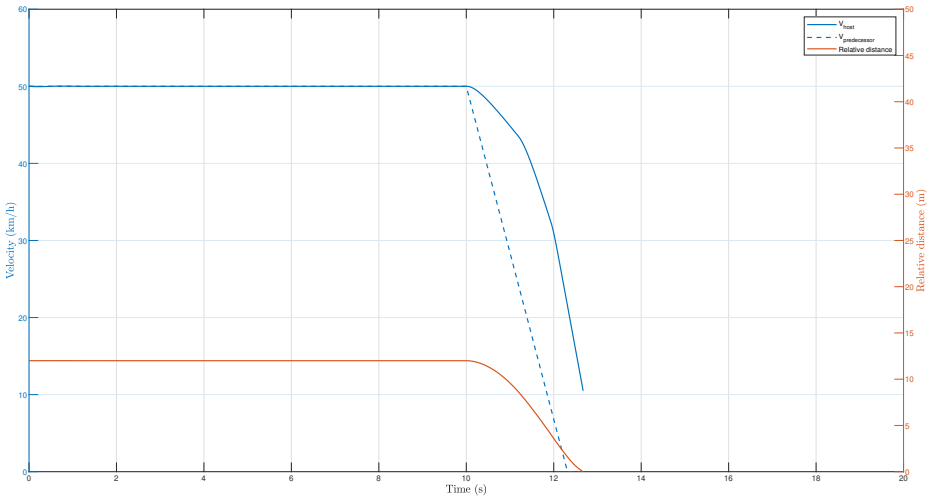

Figure 6.9: Simulation results of unified AEB and ACC CCR braking Scenario 4.

6.2 ACC performance

In order to evaluate the functionality of the ACC controller a scenario is designed with a set of 6 distinct situations to encompass the total envelope of working conditions. The six situations with their respective performance criteria are described below.

1. **Accelerating at a traffic light S1**

   This situation is defined as a fast drive away of the preceding vehicle from standstill.

   Performance criteria: The host vehicle should reach the desired relative distance D_{ref} and desired velocity with a comfortable acceleration $\dot{v_h}$ and jerk j_h.

2. **Decelerating to standstill S2**

   The host vehicle is following the preceding vehicle with the desired velocity and distance. At a certain moment in time, the preceding vehicle starts decelerating till standstill.

   Performance criteria: At standstill the error in the desired relative distance should be as low as possible, therefore no overshoot is allowed.

3. **Traffic jam velocity profile S3**

   In this situation the preceding vehicle is decelerating and accelerating at a low level with a sinusoidal movement.

   Performance criteria: Low level of acceleration $\dot{v_h}$ and jerk j_h, it is also desirable if the host vehicle is not copying the sinusoidal behavior of the preceding vehicle.

4. **Cut-in of preceding vehicle with a negative velocity difference S4**

   In this situation the vehicle is following a preceding vehicle with a certain velocity. At a certain moment in time, another vehicle is cutting in between the two vehicles. The new preceding vehicle has a lower velocity than the host vehicle.

   Performance criteria: The maximum deceleration which is limited for the ACC system to -2 $\frac{m}{s^2}$ must be achieved quickly to avoid a collision and to reach the desired distance and desired velocity as quickly as possible.

5. **Cut-in of preceding vehicle with a positive velocity difference S5**

   In this situation the vehicle is following a preceding vehicle with a certain velocity. At a certain moment in time, another vehicle is cutting in between the two vehicles. The new preceding vehicle has a higher velocity than the host vehicle.

   Performance criteria: Since the velocity of the cut-in vehicle it is desired to reach the desired distance without the of a braking input.

6. **Cut-out of preceding vehicle which lead to an ACC to CC switch S6**

   In this situation the vehicle is following a preceding vehicle with a certain velocity. At a certain moment in time, the preceding vehicle is switching lanes which will lead to an ACC to CC switch.

   Performance criteria: The cruise control velocity v_{CC} should be achieved in a comfortable manner. Therefore the acceleration $\dot{v_h}$ and jerk j_h should be low.

A test scenario is designed which includes the six situations S1 to S6. This test scenario is simulated and the results are evaluated in this section.

The desired velocity and the actual velocity are shown in Figure 6.10, the corresponding acceleration and jerk is shown in Figure 6.11. The desired distance and actual distance is depicted in Figure 6.12.

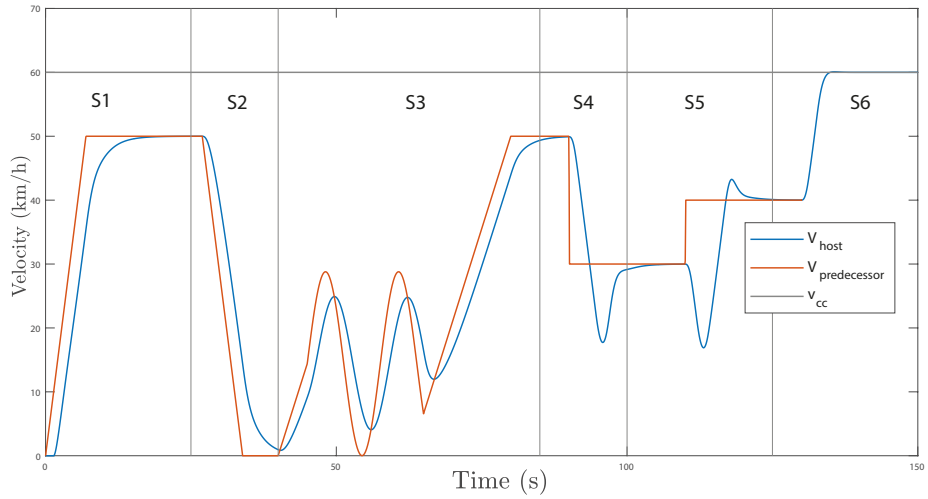

Figure 6.10: The desired velocity and the actual velocity during the simulation scenario.

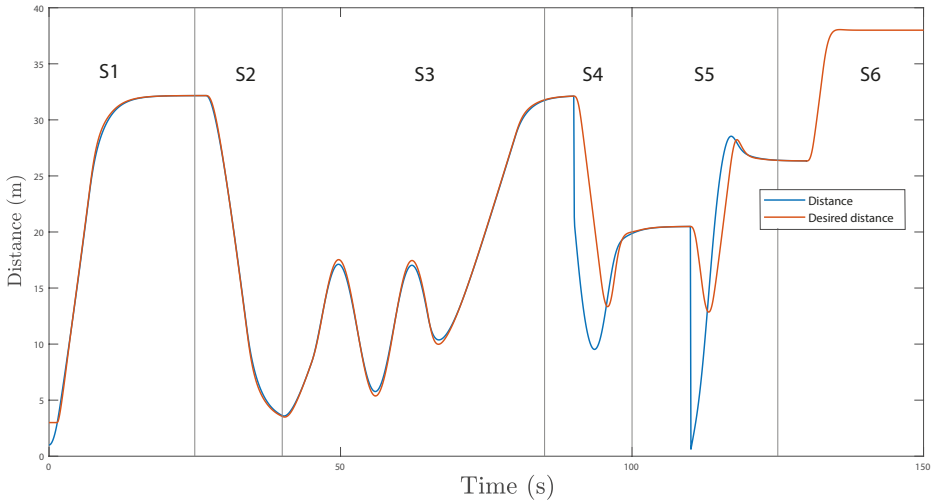

Figure 6.12: The desired distance and actual distance during the simulation scenario.

In the following list, the presented results are shortly discussed.

6.2.1 Situation 1

Accelerating at a traffic light: As can be seen from the results the initial distance between the host and preceding vehicle is 1 meter. The distance buffer between two vehicles in order to avoid a collision which is used in Constant-Time headway definition is set to 3 meters therefore the initial desired distance is 3 meters. The preceding vehicle starts to accelerate with 2 $[\frac{m}{s^2}]$ when the traffic lights turn green. It is concluded that the performance of the distance and velocity tracking controller is very good. Furthermore it can be seen that the ACC did stay between its operational limits as defined in section C.2.1.3. The acceleration during ACC scenarios should be between [-2 2] $[ms^{-2}]$ for comfort reasons. Furthermore the average negative jerk measured over 1 second shall not exceed 2.5 $[ms^{-3}]$. The maximum positive jerk is around 4 $[ms^{-3}]$, however the average over one second is around 2, which is acceptable.

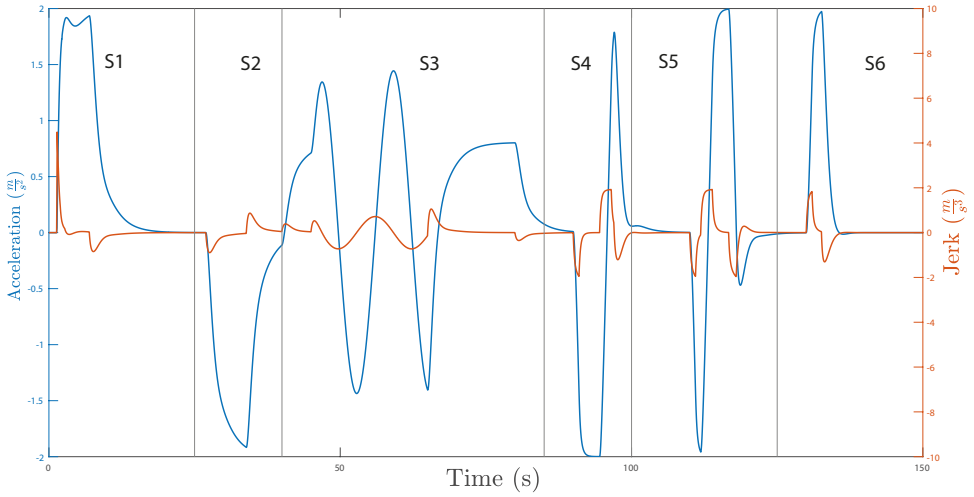

Figure 6.11: The acceleration and jerk during the simulation scenario.

6.2.2 Situation 2

Decelerating to standstill: It can be seen that the desired distance is tracked very well. The performance criteria for this scenario is that there should be no overshoot in the desired distance tracking. It can be concluded that the performance is good enough to avoid a collision. However the preceding vehicle decelerated with -2 $[ms^{-2}]$, if a higher deceleration is used the ACC could not avoid a collision anymore, since the ACC deceleration is limited to -2 $[ms^{-2}]$.

6.2.3 Situation 3

Traffic jam: The results show that the behavior is quite comfortable since both the jerk and acceleration levels are low, however this scenario could still be improved. The sinusoidal behavior is copied. A more advanced path planning method could overcome this problem.

6.2.4 Situation 4

Cut-in with a negative velocity difference: This scenario showed a situation where the host vehicle is following the preceding vehicle with a desired distance of approx. 32 meters. A vehicle cut in with a velocity of 30 km/h at a distance of 20 meters from the host vehicle. As can be seen the ACC system ensures safe behavior, the difference in velocity disappeared very quickly, however as can be seen the velocity tracking controller has some overshoot. The overshoot is caused by the desired distance error, therefore it is concluded that this is overshoot is desirable.

6.2.5 Situation 5

Cut-in with a negative velocity difference: This scenario showed a situation where the host vehicle is following the preceding vehicle with a desired distance of approx. 28 meters. A vehicle cut in with a velocity of 40 [km/h] at a distance of 3 meters from the host vehicle. The ACC system decides that this is a dangerous situation and start to brake, however this is not desirable, since the velocity of the preceding vehicle is already higher than the velocity of the host. This problem could be solved by using a control logic which ensures no deceleration if the relative velocity is positive.

6.2.6 Situation 6

Cut-out of preceding vehicle which lead to an ACC to CC switch: This scenario showed a situation where the preceding vehicle switched lanes and therefore the sensors detected a free lane. The vehicle is accelerated to the cruise control velocity which is set to 60 [km/h]. The results show that the ACC stayed between its operational limits and therefore its comfort requirements. No overshoot is seen in the velocity tracking controller. Therefore it is concluded that the performance of the ACC for this scenario is very good.

6.3 Discussion

In this chapter, a quantitative evaluation is conducted to research the impact of implementing information about the road conditions in the upper-level controller.

It is concluded that the number of collisions on low friction surfaces is clearly decreased. AEB systems without information were able to avoid a collision with standstill objects on a snowy road until starting velocities up to 35 km/h, while the AEB system with road information is able to avoid a collision with speeds up to 70 km/h. A collision is unavoidable with the current AEB settings for an initial velocity of 80 km/h; however the speed at impact is still acceptable according to Euro NCAP [26]. Furthermore, it is concluded that the ACC system is working well. However, some details could be improved. The ACC system does not benefit as much from the added road information as the AEB system. The only difference is that the host vehicle is following the preceding vehicle at larger relative distances on lower friction surfaces compared to high friction surfaces.

In this research, a maximum road friction estimator is developed which is able to monitor the road conditions in a virtual environment. Future research is needed with real vehicle measurements to conclude if the method as described in this research is practical feasible. Concluding, it is believed that enabling road information in the upper-level controller can have positive impact on safety.

7. Conclusions and recommendations

In this research a unified AEB and ACC system is developed which is able to have robust performance considering the variation of the road conditions in a simulation environment. Therefore a non-linear tyre model which can simulate different road conditions is employed and validated with a vehicle model from Siemens Simcenter Amesim. Subsequently, an overall control architecture is proposed to control the acceleration of the vehicle including the following elements: a slip controller which considers delayed actuator dynamics. A neural network, which is trained with simulation data to predict the maximum road friction coefficient and a slip control algorithm which is used to determine a stable setpoint for the slip controller based on the desired acceleration and the maximum road friction coefficient.

The predicted value of the maximum road friction coefficient is also used in the upper-level controller of the AEB algorithm.

In this section, the main findings and answers to the research questions as introduced in section 1.3 are provided. The five sub-questions are addressed individually which lead to the answer of the main research question:

How can we design an unified AEB and ACC system which is able to have robust performance considering the variation of the road conditions?

The answer to this main research questions lies directly in the answer to the sub-questions. First the summarized answers to the sub-questions are provided in Section 7.1.6, thereafter a recommendation for Siemens and the limitations of this research are provided in Section 7.2 and finally possible directions for future research is suggested in Section 7.3.

7.1 Research questions

7.1.1 Vehicle model

The first sub-question aimed at constructing a vehicle model that is able simulate the vehicle behavior on different road surfaces. Furthermore the vehicle model should govern the complex physics of a vehicle. Road variations such as different road conditions can influence the tyre-road friction and therefore adversely affect the function of an AEB system. An elaborate literature study is conducted in Chapter 2 to identify the different vehicle models that are used in the design of ADAS systems. It is concluded that a dynamic model with a non-linear tyre model should be used to model the vehicle dynamics. In Chapter 3 three vehicle models are described. At first the double-corner vehicle model from [54] is adapted to fit a vehicle model from Amesim. This model is used since it can simulate the longitudinal dynamics with a non-linear Pacejka tyre model known as the Magic Formula from 1989 and it had the same components as the model from Amesim. The model from [54] is expanded with a reset integrator friction model to have good behavior for low velocities. Thereafter this model is simplified to a control oriented vehicle model, which is still able to simulate the non linear tyre behavior, however this model is easier to linearize, since it is neglecting some dynamics such as the rolling resistance and aerodynamic forces. Finally, the roll axis vehicle model from [49] is adapted by expanding this model with a reset friction integrator model to be able to simulate the lateral (steering) dynamics of the vehicle.

7.1.2 Vehicle control

The seconds sub-question focused on identifying current methods to control the vehicle. As long as wheeled vehicles have , skidding and slipping has been a problem. Its effect is usually a total or partial loss of control of the vehicle. These problems can be prevented by means of active braking control systems. Most modern road vehicles are equipped with electronic ABS. An ABS could improve the safety of a vehicle in severe circumstances. An ABS ensures a maximum longitudinal tyre-road friction while keeping large lateral forces. The braking system characteristics and

actuator performance have a great influence on the design of automatic braking control systems. From the literature study is concluded that classical ABS systems use rule-based control logics to control vehicles equipped with traditional hydraulic actuators. Recent technologies lead to new braking systems, such as electro-hydraulic and electro-mechanical braking systems, which enabled a continuous modulation of the braking torque.

In this research is chosen to control a vehicle with a electro-mechanical brake with a Youla parameterized controller by using information about the road conditions. The Youla parameterization approach provided stability and performance for a broader range of operational conditions compared to a single linear PID controller. The maximum road friction coefficient μ_{max} is used in the slip control algorithm to define a stable set point for the slip controller. The slip controller is used for both the acceleration and deceleration. The limitations of this proposed method are described in section 7.2.

7.1.3 Unification of the AEB and ACC system

The third sub-question aims to unify the AEB and ACC system. It is concluded that the unified AEB and ACC system as shown in Figure 4.18 can be seen as two independent systems running simultaneously. However the system is optimized to work fluently by setting the constant-time headway to $f1$ the TTC flag of the forward collision warning system. Both systems have a positive influence on each other. The ACC system is maintaining the desired relative distance D_{ref} and tracks the preceding vehicle's speed v_p, therefore the ACC system can be seen as another pre-braking stage in some situations as is concluded in Chapter 6, which can lead to more comfort and less interventions from the AEB system. On the other hand the AEB system improves the safety of the driver by avoiding collision that can not be prevented by a standalone ACC.

7.1.4 Maximum road friction estimator

The fourth sub-question aimed at designing a maximum road friction estimator. From the literature study is concluded that a neural network could be a suitable approach to estimate the maximum road friction coefficient. In this study an ANN is trained with data that is obtained from the roll axis vehicle model in combination with a Pacejka tyre model.

The estimation algorithm is evaluated in Chapter 5 on varying road surfaces and shows a good accuracy. It is concluded that the maximum road friction estimator is able to accurately predict the maximum road friction coefficient μ_{max} if the vehicle is driving on a straight road with a nonzero constant acceleration or deceleration. The predicted μ_{max} can be used in the upper level controller of the ADAS systems to improve the performance on different road conditions. However it is not recommended to use this information in the design of a slip controller, since it is very important to always be able to have full control of the vehicle. If the estimation fails to detect μ_{max} for example during a sensor fail, the well-trained neural network may not be able to accurately estimate and therefore, which can lead to unstable control behavior.

Furthermore it is concluded that a very good knowledge about the tyre dynamics is needed. The trained data is now obtained from a mathematical tyre model. The proposed method is only analyzed theoretically and validated via simulation and therefore subsequent work is needed to validate the ANN with real world tyre data.

7.1.5 Stability

The fifth sub-question concerned the stability of the closed loop system as shown in Figure 4.1. In Chapter 4 a stability analysis is presented. It is concluded that the closed loop stability depends on the prediction accuracy of the maximum road friction μ_{max}. The results in Chapter 5 show a good overall accuracy, however in some scenarios the accuracy is not good enough.

If you know the maximum error of the estimator a robustness margin can be built into the slip control algorithm which limits the maximum deceleration and acceleration for different road conditions. This will prevent the system from going unstable. A drawback of this method is that the maximum deceleration can therefore not be achieved. As discussed before the estimator can also fail because of failing sensors. It is concluded that the stability can be guaranteed in the ideal simulation environment, however future research is needed to conclude on the stability in real world simulations.

7.1.6 Impact

The last sub-question focused on determining the expected impact of implementing information about the road conditions in the upper level controller of the AEB system. A quantitative evaluation is conducted in Chapter 6. The number of collisions on low friction surfaces is clearly decreased. AEB systems without information were able to avoid a collision with standstill objects on a snowy road until starting velocities up to 35 km/h, while the AEB system with road information is able to avoid a collision with speeds up to 70 km/h. A collision is unavoidable with the current AEB settings for an initial velocity of 80 km/h, however the speed at impact is still acceptable according to Euro NCAP [26]. As discussed in Chapter 1 to improve the SAE level 2 AEB system to an SAE level 3 AEB system, the environment such as the road condition should be monitored by the system. In this research a maximum road friction estimator is developed which is able to monitor the road conditions in a virtual environment. Future research is needed with real vehicle measurements to conclude if the method as described in this research is practical feasible. Concluding, it is believed that enabling road information in the upper level controller of an AEB system can have positive impact.

7.2 Recommendations and limitations

A practical (business) goal for Siemens was introduced in Section 1.2.1. This goal stated that this research should provide an unified AEB and ACC system which is able to have robust performance considering the variation of the road conditions as encountered in practice, furthermore a vehicle model which can simulate the different road conditions should be provided. The insights that were found indicate that the unified AEB and ACC system is able to have robust performance on different road conditions, however the model has a big limitation. The roll axis vehicle model was modelled very late in this research. The roll axis vehicle model was added to include lateral dynamics and enable the possibility to validate our designed ADAS in PreScan. The double corner model can also be used to validate our designed ADAS in PreScan, however the implementation of the roll axis vehicle model in PreScan is easier, since the current vehicle models that are used in PreScan demos have the same degrees of freedom as the roll axis vehicle model. Furthermore for demo purposes it is better to use a vehicle model which can simulate steering behavior. Since the roll axis vehicle model was modelled very late in this research all the other components in this research are based on longitudinal dynamics only. First the slip controller is based on tyre dynamics where the side slip angle $\alpha = 0$, therefore higher side slip angles can lead to unstable behavior. Secondly the maximum road friction estimator is trained with longitudinal data only, a state machine is designed to only estimate the μ_{max} on straight roads and lastly the TTC which is used to determine the threat level is calculated for straight roads only.

A second limitation is that the neural network is trained with data which is obtained from the Pacejka tyre model. A Pacejka tyre model can simulate tyre behavior quite accurately, however tyre dynamics are highly non linear. Further research is needed to conclude if the Pacejka tyre model can simulate a tyre accurate enough to be able to estimate the maximum road friction coefficient. It is also possible to directly train the neural network with real vehicle data which can also be a goal for a future research project.

A third limitation is that the closed loop stability of the Youla parameterized controller can only be guaranteed if the accuracy of the maximum road friction estimator is high enough. Surely this control problem can be solved in multiple other ways, however one of the contributions of this research is that it showed that knowing the road conditions could be beneficial in the design of ABS systems.

The last limitation is that all systems are validated without any sensor uncertainty or parameter uncertainty. The systems are validated for different operational working conditions, however it is expected that sensor and parameter uncertainty can also have a big influence. Both the Youla parameterized controller and the maximum road friction estimator are designed for a specific tyre, very good knowledge of the parameters is needed. The wheel slip κ is estimated with a kinematic model with the vehicle velocity u and the rotational wheel velocity ω as input. Wheel encoders give in general quite accurate results, however to measure the vehicle's velocity with good accuracy a good sensor fusion is needed.

7.3 Future research

The scientific goal of the research entailed providing insights in the usage of a neural network to estimate the maximum road friction coefficient μ_{max}. From the limitations several research directions were found that can be explored in the future.

During development of the neural network only longitudinal inputs are used. Future research could expand the estimator with lateral dynamics. Moreover, the neural network is trained with simulated data obtained from a Pacejka tyre model. Future research could be in the direction of determining if a neural network could be trained directly with real simulation data. Furthermore it can be validated if the current trained neural network is robust enough to estimate μ_{max} during real vehicle tests.

Subsequently, both the slip controller and the maximum road friction estimator are validated without any sensor uncertainty or parameter uncertainty. Future research must conclude if both these systems are suitable for real vehicle implementation by encompassing parameter and sensor uncertainty in the design and validation of these systems.

Finally, a goal of this research is to implement and validate the designed systems in PreScan. The results of this validation are not shown in this report, however some results may be included during the presentation.

Bibliography

[1] Road fatality statistics in the EU (infographic) — News — European Parliament. v, 1

[2] Simcenter Amesim Delivering engineering innovation with system simulation. Technical report. 19

[3] Verkehrsunfälle - Fachserie 8 Reihe 7 - 2011. Technical report. 1

[4] White paper – 'European transport policy for 2010: time to decide' — Mobility and Transport. v, 1

[5] Leonardo Gonzalez Alarcon, Myriam Elizabeth Vaca Recalde, Mauricio Marcano, and Enrique Marti. Adaptable Emergency Braking Based on a Fuzzy Controller and a Predictive Model. *2018 IEEE International Conference on Vehicular Electronics and Safety, ICVES 2018*, pages 1–6, 2018. 11

[6] Mohammad Ali, Esteban R. Gelso, and Jonas Sjöberg. Automotive threat assessment design for combined braking and steering maneuvers. *IEEE Transactions on Vehicular Technology*, 62(4):1519–1526, 2013. 9

[7] Alberto Bemporad, Manfred Morari, N Lawrence Ricker, and MathWorks. Model Predictive Control Toolbox ™ User ' s Guide How to Contact MathWorks. *The Mathworks*, 2015. 111

[8] Johan Bengtsson. Adaptive Cruise Control and Driver Modeling. *Thesis*, 2001. 14, 15

[9] Karl Berntorp, Tru Hoang, Rien Quirynen, and Stefano Di Cairano. Control Architecture Design for Autonomous Vehicles. *2018 IEEE Conference on Control Technology and Applications, CCTA 2018*, pages 404–411, 2018. 13

[10] R a P M Van Den Bleek. *Design of a Hybrid Adaptive Cruise Control Stop- & -Go system.* PhD thesis, University of Technology Eindhoven, 2007. 14

[11] Mattias Brännström, Erik Coelingh, and Jonas Sjöberg. Model-based threat assessment for avoiding arbitrary vehicle collisions. *IEEE Transactions on Intelligent Transportation Systems*, 11(3):658–669, 2010. 8

[12] B Breuer, U Eichhorn, and J Roth. Measurement of tyre/road-friction ahead of the car and inside the tyre. sep 1992. 16

[13] Merry Cherian and S. Paul Sathiyan. Neural Network based ACC for Optimized safety and comfort. *International Journal of Computer Applications*, 42(14):1–4, 2012. 15

[14] Jessica B. Cicchino. Effectiveness of forward collision warning and autonomous emergency braking systems in reducing front-to-rear crash rates. *Accident Analysis and Prevention*, 2017. 1

[15] Canadian Standards Association (CSA). ISO 15622, 2009. xvi, xvi, xvi, xvi, xvi, 110, 111, 112, 113

[16] Lian Cui, Jia Hu, B. Brian Park, and Pavle Bujanovic. Development of a simulation platform for safety impact analysis considering vehicle dynamics, sensor errors, and communication latencies: Assessing cooperative adaptive cruise control under cyber attack. *Transportation Research Part C: Emerging Technologies*, 97:1–22, dec 2018. 13

[17] John Dahl, Gabriel Rodrigues de Campos, Claes Olsson, and Jonas Fredriksson. Collision Avoidance: A Literature Review on Threat-Assessment Techniques. *IEEE Transactions on Intelligent Vehicles*, 4(1):101–113, 2018. 7, 10, 52

[18] WERNER DAMM, HANS-JÖRG PETER, JAN RAKOW, and BERND WESTPHAL. Can we build it: formal synthesis of control strategies for cooperative driver assistance systems. *Mathematical Structures in Computer Science*, 23(4):676–725, 2013. 9

[19] TNO DelftTyre. MF-Tyre/MF-Swift 6.2. *Mechanical Simulation*, 2013. 13

[20] Yongqiang DIng, Huiyan Chen, Jianwei Gong, Guangming Xiong, and Gang Wang. Model Predictive Enhanced Adaptive Cruise Control for Multiple Driving Situations. *IEEE Intelligent Vehicles Symposium, Proceedings*, 2018-June(Iv):1717–1722, 2018. 9, 11, 16

[21] Tobias Dirndorfer and Michael Botsch. Model-Based Analysis of Sensor-Noise in Predictive Passive Safety Algorithms. *22nd International Technical Conference on the Enhanced Safety of Vehicles (ESV)*, 2011. 13

[22] Tannenbaum Doyle, Francis. Feedback Control Theory. pages 17–48. Dover Publications, New York, NY, 1990. 42, 43

[23] Dr. Ir. I.J.M. Besselink. Vehicle Dynamics - 4AT000 lecture notes 2017, 2017. vi, 5, 18, 19, 26

[24] H Dugoff, P S Fancher, and L Segel. TIRE PERFORMANCE CHARACTERISTICS AFFECTING VEHICLE RESPONSE TO STEERING AND BRAKING CONTROL INPUTS. aug 1969. 13

[25] ENCAP. EUROPEAN NEW CAR ASSESSMENT PROGRAMME (Euro NCAP) TES PROTOCOL – AEB systems. (July), 2017. vi, 1, 7, 51, 69, 108

[26] Euro NCAP. Euro NCAP 2025 Roadmap. pages 1–19, 2017. xv, xv, xv, xvi, 70, 72, 74, 80, 83, 110

[27] FRICTI@N. EUROPA - On-board Measurement of Friction and Road Slipperiness to Enhance the Performance of Integrated and Cooperative Safety Systems — TRIMIS - European Commission. 16

[28] Matthias Gerdts and Ilaria Xausa. Avoidance trajectories using reachable sets and parametric sensitivity analysis. In Dietmar Hömberg and Fredi Tröltzsch, editors, *System Modeling and Optimization*, pages 491–500, Berlin, Heidelberg, 2013. Springer Berlin Heidelberg. 9

[29] Gene Grimm, Michael J. Messina, Sezai E. Tuna, and Andrew R. Teel. Examples when nonlinear model predictive control is nonrobust. *Automatica*, 40(10):1729–1738, oct 2004. 11

[30] C Grover, I Knight, F Okoro, I Simmon, G Couper, P Maddie, and B Smith. Automated Emergency Brake Systems: Technical requirements, costs and benefits by. *TRL Limited*, 1(1):109, 2008. 108

[31] L Guo, Z J Ren, P S Ge, and J Chang. Advanced Emergency Braking Controller Design for Pedestrian Protection Oriented Automotive Collision Avoidance System. *Scientific World Journal*, 2014, 2014. 12

[32] Fredrik Gustafsson. Tire-road friction is estimated using the wheel-slip computed from standard sensor signals . A parametric model is estimated using an adaptive lter supported by a fault detector . Results from extensive eld trials are presented . (November 1996):1–29, 1996. 16

[33] David A. Haessig and Bernard Friedland. On the modeling and simulation of friction. In *Proceedings of the American Control Conference*, pages 1256–1261. Publ by American Automatic Control Council, 1990. 22

[34] Xiangkun He, Xuewu Ji, Kaiming Yang, Yulong Liu, Jian WU, and Yahui Liu. Autonomous Emergency Braking Control Based on Hierarchical Strategy Using Integrated-Electro-Hydraulic Brake System. *SAE Technical Paper Series*, 1:1–8, 2017. 12

[35] Seyedmehrdad Hosseini, Nikolce Murgovski, Gabriel Rodrigues De Campos, and Jonas Sjoberg. Adaptive forward collision warning algorithm for automotive applications. *Proceedings of the American Control Conference*, 2016-July:5982–5987, 2016. 8

[36] Constantin Hubmann, Jens Schulz, Marvin Becker, Daniel Althoff, and Christoph Stiller. Automated Driving in Uncertain Environments: Planning With Interaction and Uncertain Maneuver Prediction. *IEEE Transactions on Intelligent Vehicles*, 3(1):5–17, mar 2018. 10

[37] Mark Hudson, Beale Martin, T Hagan, and Howard B Demuth. Deep Learning Toolbox™ User's Guide. Technical report, 1992. 61

[38] Hyunkyu Kim, Kyungsik Shin, Iljoon Chang, and Kunsoo Huh. Autonomous Emergency Braking Considering Road Slope and Friction Coefficient. *International Journal of Automotive Technology*, 19(6):1013–1022, dec 2018. 1, 7, 11

[39] Markus Koschi and Matthias Althoff. SPOT: A tool for set-based prediction of traffic participants. *IEEE Intelligent Vehicles Symposium, Proceedings*, pages 1686–1693, 2017. 10

[40] D.S. Laila, P. Shakouri, A. Ordys, and M. Askari. Longitudinal vehicle dynamics using Simulink/Matlab. *UKACC International Conference on CONTROL 2010*, pages 955–960, 2010. v, 19

[41] Cornelia Lex. Estimation of the Maximum Coefficient of Friction between Tire and Road Based on Vehicle State Measurements, 2015. xiv, 2, 8, 17, 57

[42] Yixuan Liu, Ying Zhao, Zhen Hu, Zissimos P. Mourelatos, and Dimitrios Papadimitriou. Collision-Avoidance Reliability Analysis of Automated Vehicle Based on Adaptive Surrogate Modeling. *ASCE-ASME J. Risk and Uncert. in Engrg. Sys., Part B: Mech. Engrg.*, 5(2):020906, 2019. 10

[43] Lghani Menhour, Brigitte D'Andrea-Novel, Michel Fliess, Dominique Gruyer, and Hugues Mounier. An Efficient Model-Free Setting for Longitudinal and Lateral Vehicle Control: Validation Through the Interconnected Pro-SiVIC/RTMaps Prototyping Platform. *IEEE Transactions on Intelligent Transportation Systems*, 19(2):461–475, 2018. 13

[44] Vicente Milanés, Jorge Villagrá, Jorge Godoy, and Carlos González. Comparing fuzzy and intelligent PI controllers in stop-and-go manoeuvres. *IEEE Transactions on Control Systems Technology*, 20(3):770–778, 2012. 15

[45] Gerrit Naus, Roel van den Bleek, Jeroen Ploeg, Bart Scheepers, Rene van de Molengraft, and Maarten Steinbuch. Explicit MPC design and performance evaluation of an ACC Stop-&-Go. In *2008 American Control Conference*, pages 224–229. IEEE, jun 2008. 14, 110

[46] Balázs Németh, Péter Gáspár, Rodolfo Orjuela, and Michel Basset. Robust H-infinity design of an automotive cruise control system. *IFAC-PapersOnLine*, 28(15):341–346, 2015. 15

[47] Jonas Nilsson, Anders C E Odblom, and Jonas Fredriksson. Worst-case analysis of automotive collision avoidance systems. *IEEE Transactions on Vehicular Technology*, 65(4):1899–1911, 2016. 8, 13

[48] Samyeul Noh and Woo Yong Han. Collision avoidance in on-road environment for autonomous driving. *International Conference on Control, Automation and Systems*, pages 884–889, 2014. 8, 10

[49] H. B. Pacejka and Igo. Besselink. *Tire and vehicle dynamics*. Butterworth-Heinemann, 2012. vi, 13, 14, 19, 20, 26, 28, 81

[50] Andrea Raffin, Michele Taragna, and Michele Giorelli. Adaptive longitudinal control of an autonomous vehicle with an approximate knowledge of its parameters. *11th International Workshop on Robot Motion and Control, RoMoCo 2017 - Workshop Proceedings*, pages 1–6, 2017. 13, 15

[51] Laura R. Ray. Nonlinear Tire Force Estimation and Road Friction Identification: Simulation and Experiments. *Automatica*, 33(10):1819–1833, oct 1997. 17

[52] Marcello Restelli. POLITECNICO DI MILANO DEEP FEATURE EXTRACTION FOR SAMPLE-EFFICIENT REINFORCEMENT LEARNING. Technical report, 2016. xiv, 61

[53] Alexandre M. Ribeiro, Alexandra Moutinho, André R. Fioravanti, and Ely C. de Paiva. Estimation of tire–road friction for road vehicles: a time delay neural network approach. *Journal of the Brazilian Society of Mechanical Sciences and Engineering*, 42(1):1–10, 2020. 3, 17, 57

[54] Sergio Savaresi and Mara Tanelli. *Active Braking Control Systems Design for Vehicles*, volume 53. IEEE, 2013. v, vi, 19, 81

[55] H E Schouten. Research on the vehicle dynamics of a loaded vehicle. Technical report, 2005. xiii, xiii, 26, 27

[56] Payman Shakouri, Jacek Czeczot, and Andrzej Ordys. Simulation Validation of Three Nonlinear Model-Based Controllers in the Adaptive Cruise Control System. *Journal of Intelligent and Robotic Systems: Theory and Applications*, 80(2):207–229, 2015. xiii, 13, 14, 15, 54

[57] PreScan — TASS International. 1

[58] Kanwar Bharat Singh and Saied Taheri. Estimation of tire–road friction coefficient and its application in chassis control systems. *Systems Science & Control Engineering*, 3(1):39–61, jan 2015. 3

[59] Amirmasoud Soltani and Francis Assadian. New Slip Control System Considering Actuator Dynamics. *SAE International Journal of Passenger Cars - Mechanical Systems*, 8(2):512–520, 2015. 12, 37

[60] Jan Erik Stellet, Patrick Vogt, Jan Schumacher, Wolfgang Branz, and J. Marius Zollner. Analytical derivation of performance bounds of autonomous emergency brake systems. *IEEE Intelligent Vehicles Symposium, Proceedings*, 2016-Augus(Iv):220–226, 2016. 10, 13

[61] Christoph Stockle, Wolfgang Utschick, Stephan Herrmann, and Tobias Dirndorfer. Robust Design of an Automatic Emergency Braking System Considering Sensor Measurement Errors. *IEEE Conference on Intelligent Transportation Systems, Proceedings, ITSC*, 2018-Novem:2018–2023, 2018. 7, 10, 11, 13

[62] Taku Takahama and Daisuke Akasaka. Model Predictive Control Approach to Design Practical Adaptive Cruise Control for Traffic Jam. *SAE international Japan*, pages 1–6, 2017. 14

[63] Antonino Trotta, Andrea Cirillo, and Michele Giorelli. A feedback linearization based approach for fully autonomous adaptive cruise control. *2019 18th European Control Conference, ECC 2019*, pages 2614–2619, 2019. 11

[64] Ari J. Tuononen, Panu Sainio, Christian Hartweg, Thomas Hüsemann, Stefan Nord, Anssi Rautiainen, Andrea Nepote, Federico Mancosu, and Mikko Liukkula. Tyre sensing approach for friction estimation in Fricti@n project, 2008. 16

[65] J. M. Twomey and A. E. Smith. Performance measures, consistency, and power for artificial neural network models. *Mathematical and Computer Modelling*, 21(1-2):243–258, jan 1995. 62

[66] Michael Robert Uchanski. Road Friction Estimation for Automobiles Using Digital Signal Processing Methods. Technical report, 2001. xiii, 17

[67] Liuhui Wang, Zhenfei Zhan, Xin Yang, Qingmiao Wang, Yufeng Zhang, Ling Zheng, and Gang Guo. Development of BP Neural Network PID Controller and Its Application on Autonomous Emergency Braking System. *IEEE Intelligent Vehicles Symposium, Proceedings*, 2018-June(Iv):1711–1716, 2018. 12

[68] Yizhen Zhang, E.K. Antonsson, and K. Grote. A new threat assessment measure for collision avoidance systems. *2006 IEEE Intelligent Transportation Systems Conference*, pages 968–975, 2008. 8, 11

[69] Ronghui Zhang, Kening Li, Zhaocheng He, Haiwei Wang, and Feng You. Advanced Emergency Braking Control Based on a Nonlinear Model Predictive Algorithm for Intelligent Vehicles. *Applied Sciences*, 7(5):504, 2017. 9, 12

A. Simulation results

A.1 Amesim validation

In this section the simulation results of the double corner model are compared with the simulation results of the Amesim model. The simulation results are shown in Appendix A. The vehicle is accelerated with a front wheel torque input, the rear wheel torque input is zero. After 12 seconds the vehicle is decelerated with a brake input on both the front and rear wheel, which can be seen in Figures A.1 and A.3. Figure A.1 shows the input torques, where Figure A.3 shows the velocity outputs. In Figure A.4 the front and rear wheel velocities are compared. In Figure A.5 and A.8 the front and rear longitudinal forces and the front and rear vertical forces are compared.

From Figures A.3 and A.4 it can be seen that the vehicle velocity and angular wheel velocities yield almost similar results as Amesim. Around 13.2 seconds, the front and rear wheel rotational velocities are slightly different. It is suspected that this difference is caused by a discontinuity in the longitudinal force from the Amesim simulation, which can be seen in Figure A.7.

From Figures A.5 , it can be seen that during acceleration the front wheel slip from the Simulink model is different compared with Amesim. The reason for this is that Amesim does not make a distinction between slip calculation during braking or accelerating.

The normal force comparison is shown in Figures A.8. It can be seen that during braking and steady state, the behavior is similar, however during the acceleration stage there is a static difference in force. The normal force is derived from three components: an aerodynamic moment, an acceleration moment and the gravitational force. The gravitational force is matching and the aerodynamic moment is neglectable. The difference during the acceleration stage originates from the acceleration moment ($mh\dot{u}$). However, the acceleration, the mass and the height of the center of gravity are similar between Amesim and the Simulink model. It seems that Amesim has an extra unexplained component for the normal force derivation. Another explanation could be that Amesim is changing the height where the acceleration force acts during acceleration and deceleration. In the end this difference does not affect the important vehicle dynamics (velocity characteristics) for an ACC and AEB system, since the acceleration is a function of the sum of the longitudinal forces with $F_x = F_z\mu(\kappa)$.

The difference in longitudinal force which is shown in Figures A.6 is neglectable apart from the difference which is caused by the discontinuities as discussed before.

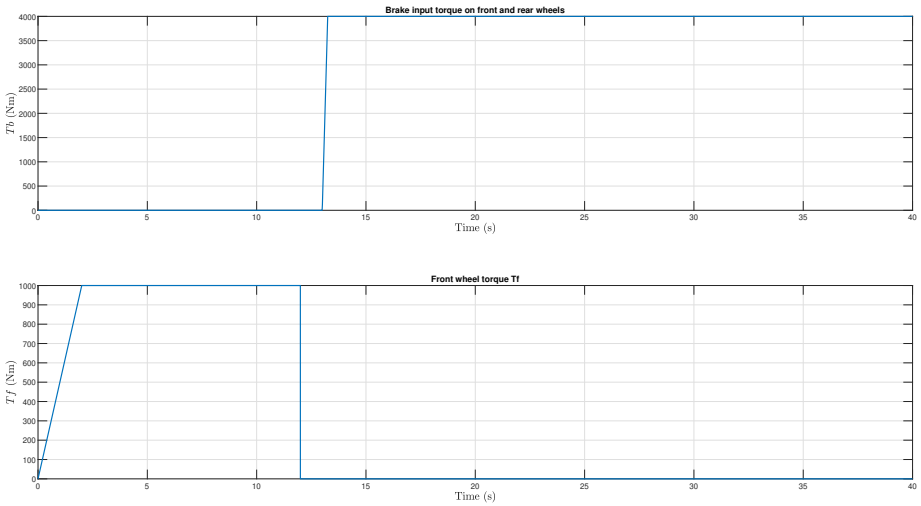

Figure A.1: Input signal for a Amesim and Simulink validation.

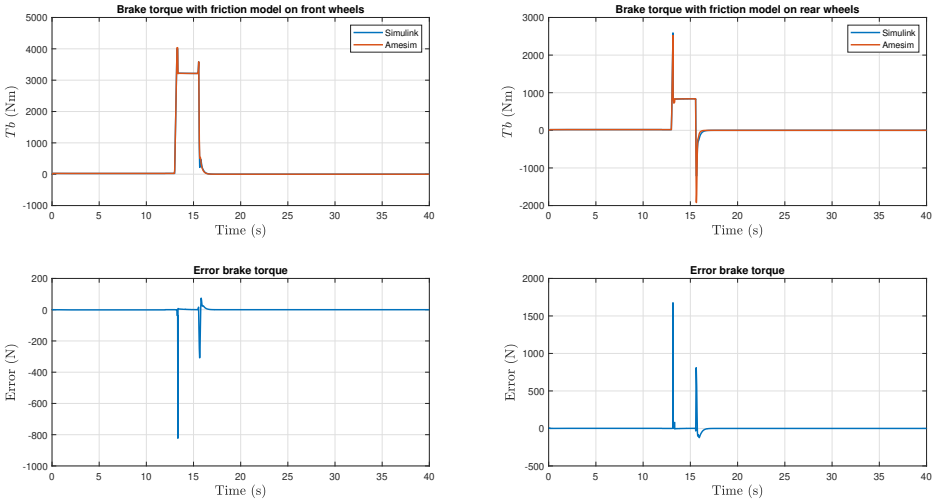

Figure A.2: Comparison of braking torque after friction model between Amesim and Simulink model.

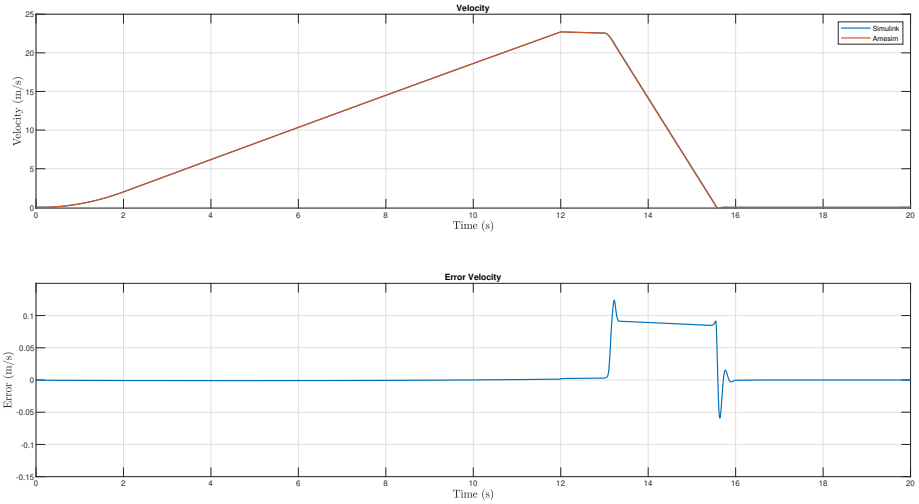

Figure A.3: Comparison of velocity between Amesim and Simulink model.

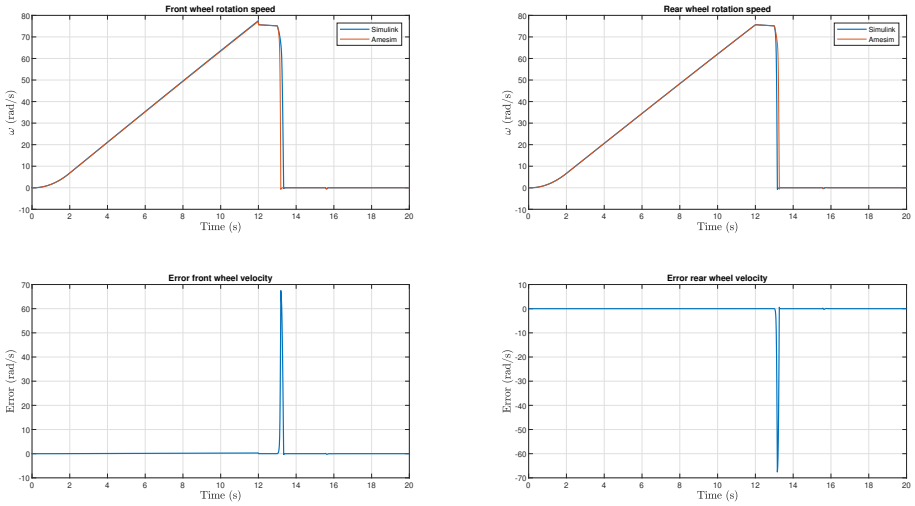

Figure A.4: Comparison of front and rear wheel rotational velocity ω_f and ω_r between Amesim and Simulink model.

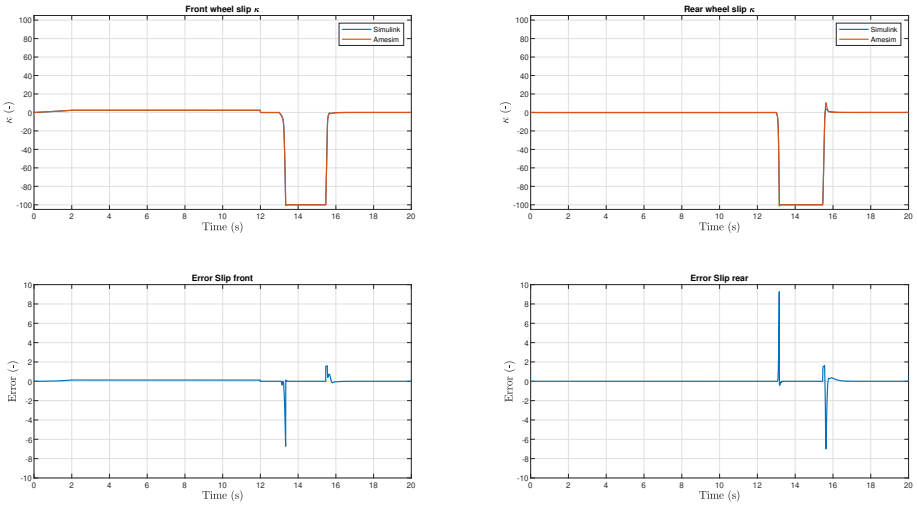

Figure A.5: Comparison of front and rear wheel slips κ_f and κ_r between Amesim and Simulink model.

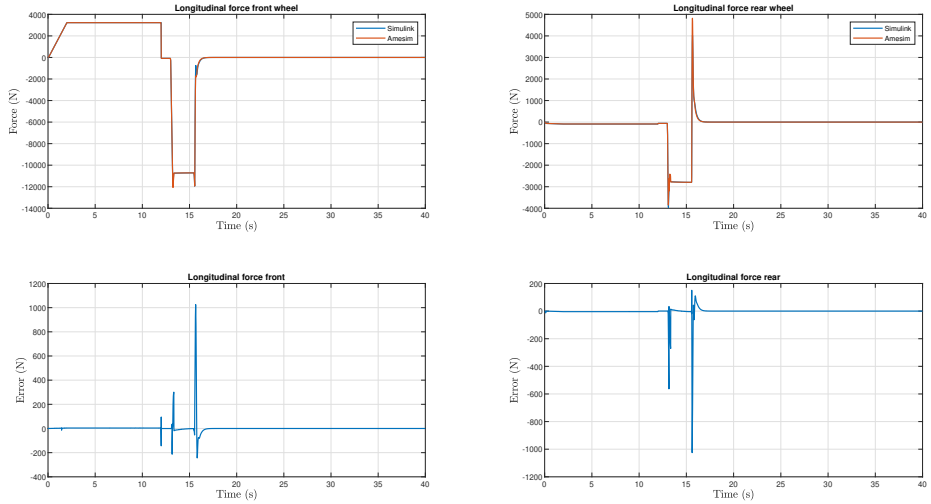

Figure A.6: Comparison of front and rear longitudinal forces F_{x_f} and F_{x_r} between Amesim and Simulink model.

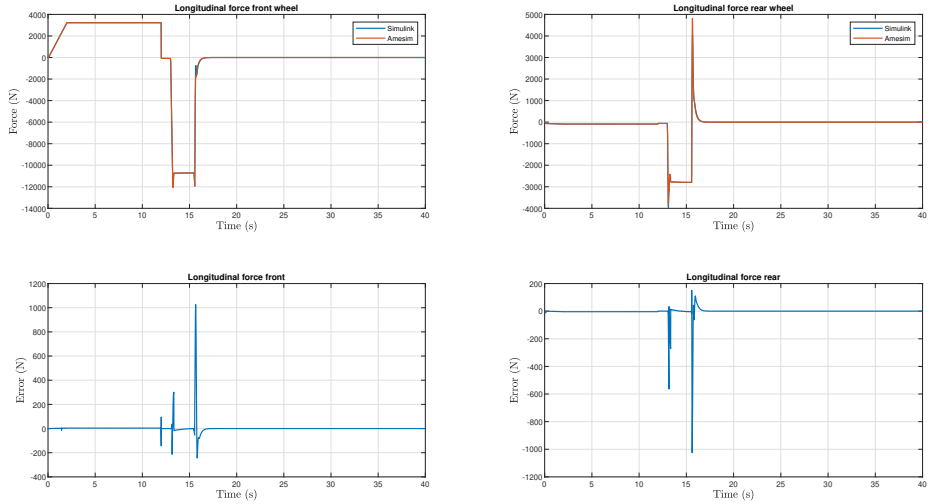

Figure A.7: A zoomed plot from Figure A.5

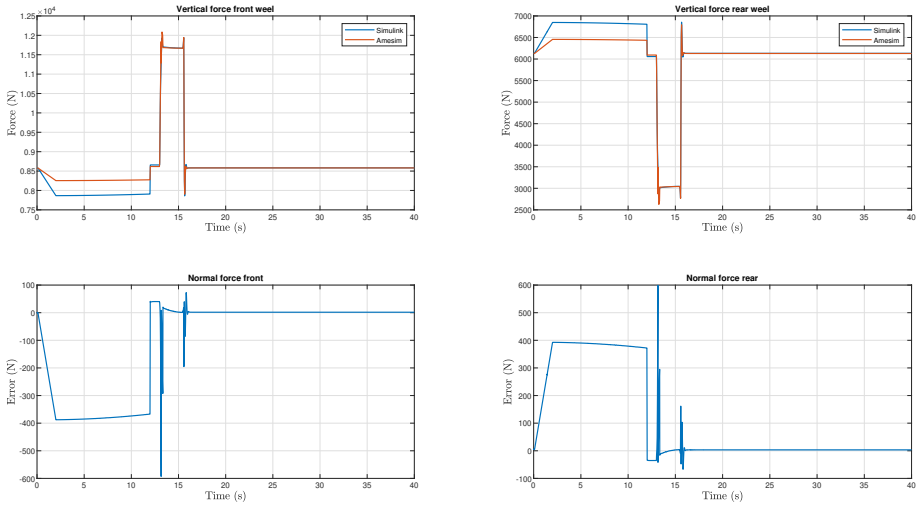

Figure A.8: Comparison of front and rear vertical forces F_{z_f} and F_{z_r} between Amesim and Simulink model.

A.2 Control

A.2.1 Open loop simulation

To investigate if a brake controller is needed an open-loop simulation is performed with different braking inputs. In Figures A.9, A.10, A.11 and A.12 the most important outputs of this simulation are presented. The brake force is distributed evenly over the front and rear axles. It can be seen that an input of 3500 Nm leads to the shortest stopping distance. When the input force is further increased the front wheel is slipping, which is not beneficial.

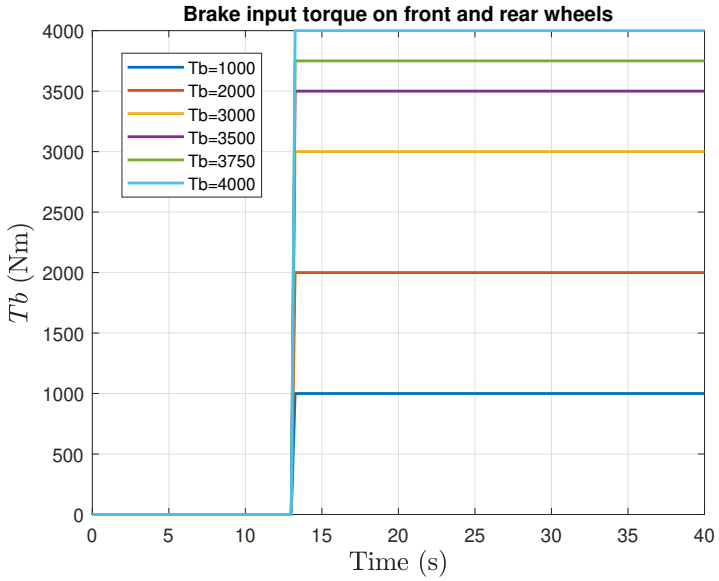

Figure A.9: Input torque of open loop simulation without controller on dry asphalt.

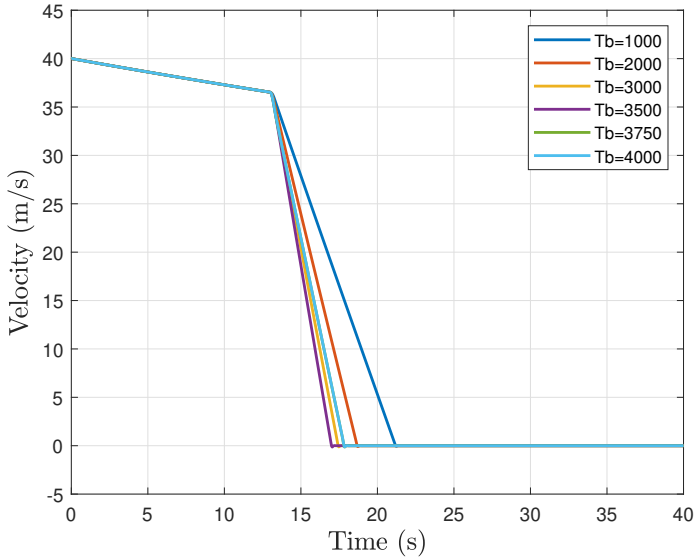

Figure A.10: Velocity result of open loop simulation without controller on dry asphalt for different input torques.

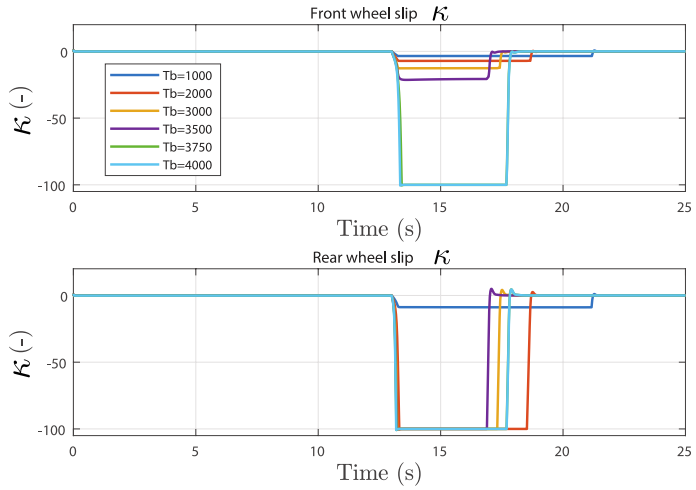

Figure A.11: Slip ratio result of open loop simulation without controller on dry asphalt for different input torques.

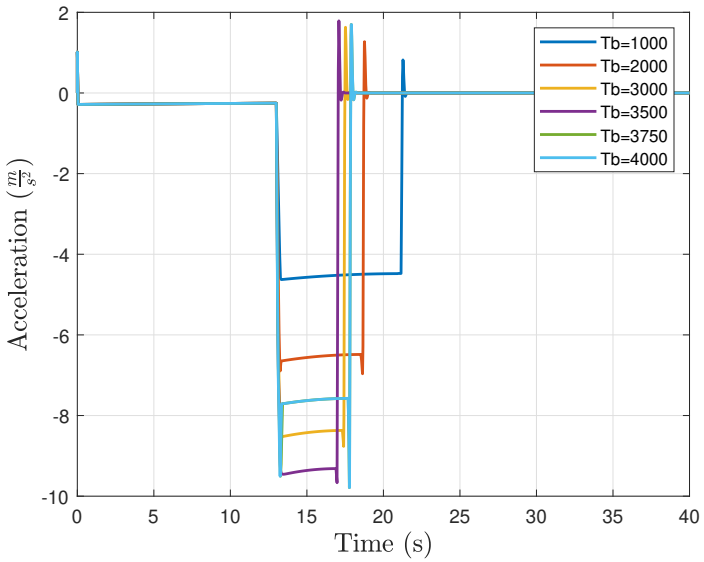

Figure A.12: Acceleration result of open loop simulation without controller on dry asphalt for different input torques.

A.2.2 PI control

Now a slip controller is designed that can achieve good dynamic performance, to be as follows: ensure asymptotic tracking of a constant wheel slip set-point for all admissible speed values. The aim is to design a controller with a bandwidth between 1 to 10 Hz, with a maximum overshoot of 15%. Furthermore the nominal robustness margins are used, which are a modulus margin lower than 6 dB, a phase margin higher than 30 degrees and a gain margin higher than 6 dB. For controller design we will work with linearized plant model $G_\kappa(s, \bar{u})$, linearized around a vertical load of of $F_z = mg$ and a wheel slip ratio of $\kappa = 0.5$. The transfer function is given by

$$G_\kappa(s, \bar{u}) = \frac{\frac{0.6}{\bar{u}}}{s - \frac{259}{\bar{u}}}. \tag{A.1}$$

Before moving to the design of a dynamic controller, first recall that it is shown that with an appropriate choice of the controller gain value, a proportional controller which guarantees closed-loop stability for all working conditions can be found. To ensure, asymptotic tracking of a constant set-point an integral control action is added to the proportional controller. The PI-controller that is designed is given by

$$R_{PI}(s) = K\frac{(\tau s + 1)}{s} \tag{A.2}$$

with a gain value K of 1750 and τ is 5. This controller is validated on the nonlinear vehicle model which is described in Section 3.1. In Figures A.13 and A.14 the simulation results are shown.

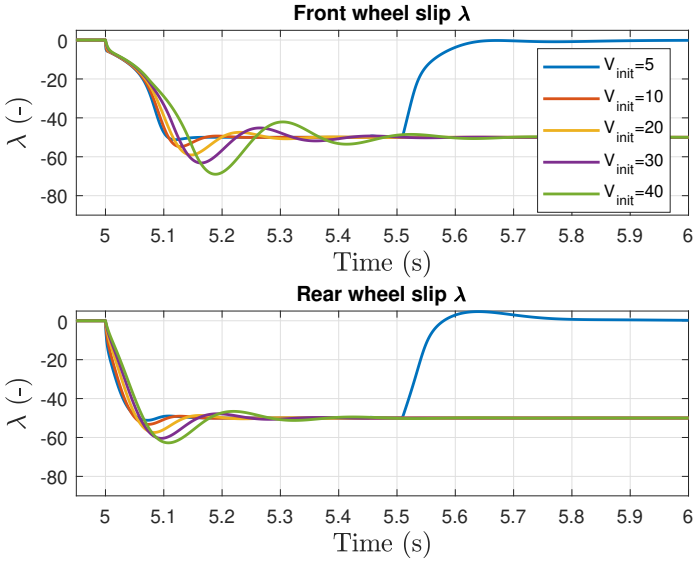

Figure A.13: Slip ratio result of closed loop simulation with controller on dry asphalt for different velocities.

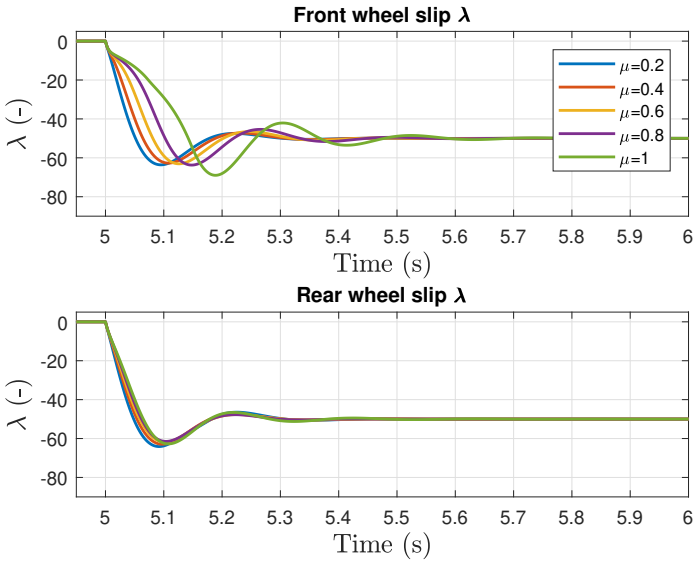

Figure A.14: Slip ratio result of closed loop simulation with controller on different road conditions.

The wheel slip set-point is, without controller, an unstable equilibrium, however it can be seen that a single controller controller is able to stabilize the wheel slip for different velocities and for different road conditions. The performance is dependent on $\bar{u}$ and $\bar{\kappa}$, however the performance is satisfactory under all possible conditions. A situation where it is possible to control the system with a single controller with this performance would be an ideal situation, however to move toward a more realistic situation, the actuator dynamics of the brakes should be considered. The transfer function of the brake actuator dynamics which is a first-order linear time-invariant system is given by

$$G_{\text{actuator}}(s) = G_{act}(s)G_d(s) = \frac{\omega_{\text{act}}}{s+\omega_{\text{act}}}e^{-s\tau} \tag{A.3}$$

with a pole at ω_{act} and a pure delay of τ. Nominal values for these kind of brake actuators are ω_{act}=70 rad/s with a delay of τ=20 ms. In the more realistic situation where a delay is added to the actuator dynamics, it is impossible to ensure closed-loop stability with good performance margins with a single controller for all velocities, since the system dynamics become faster as speed decreases. To show this, the controller as discussed before is now validated with the delay. In Figure A.15 the Nyquist diagram of $K(s)G_{actuator}(s)G_{\kappa}(s,u)$ is shown for a velocity of 25 [m/s]. It can be seen that the closed loop is now unstable, since there are two RHP closed-loop poles due to one RHP open-loop pole and one positive encirclement's around the point -1 in the Nyquist plot.

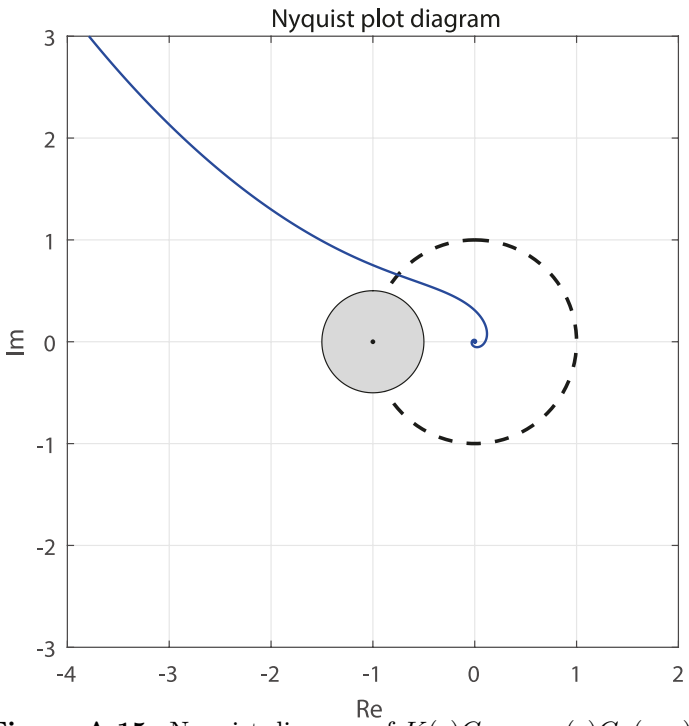

Figure A.15: Nyquist diagram of $K(s)G_{actuator}(s)G_{\kappa}(s,u)$.

A.2.3 Validation

The simulation results for K_2 are shown in Figure A.16 and A.17. It can be seen that the controller is less robust for different road conditions, since the performance is worsened. However, from Figure A.17 it can be seen that the stability region (the velocity where the dynamics become unstable) is slightly improved for a stable setpoint.

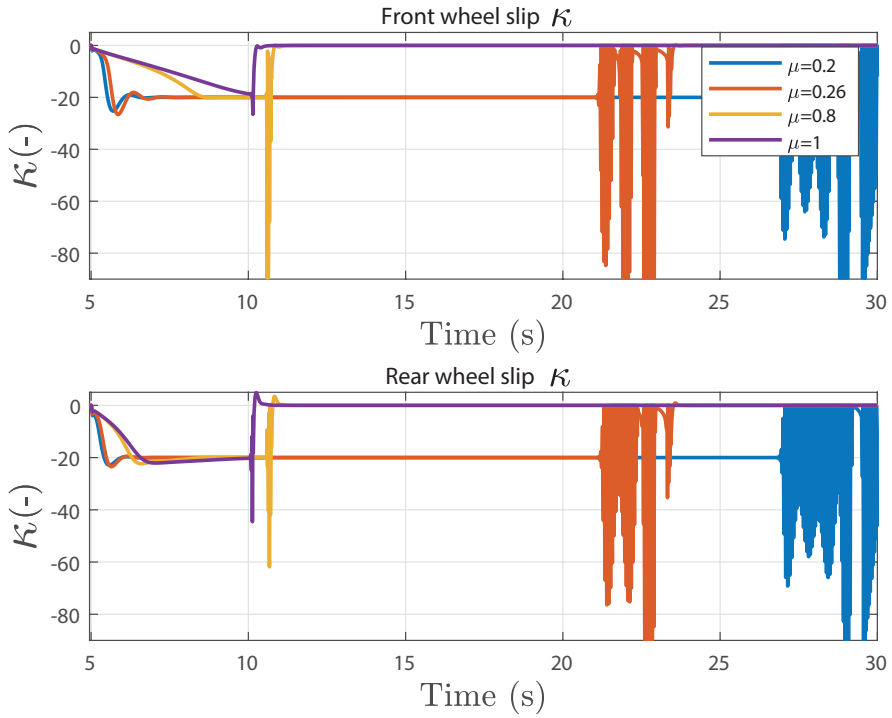

Figure A.16: The controlled front and rear wheel slip κ_f and κ_r for different road conditions with initial velocity $u_{init} = 40$. Controller: K_2. Slip setpoint $\kappa = 20$.

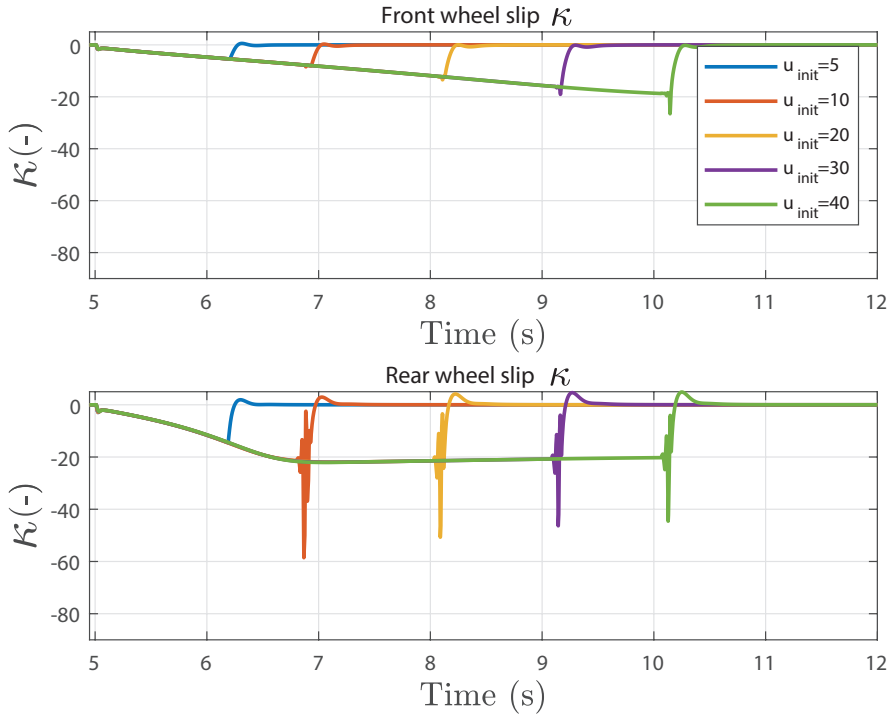

Figure A.17: The controlled front and rear wheel slip κ_f and κ_r for different initial velocities on dry surface $\mu_{max} = 1$. Controller: K_2. Slip setpoint $\kappa = 20$.

In Figure A.18 and A.19 the simulation results for K_3 are shown. The purple line in Figure A.18 corresponds to the green line in Figure 4.15. It can be seen that K_3 is also able to stabilize κ in the unstable region ($\mu_{max} < 0.8$), however for low velocities the dynamics are still unstable. However, in Figure A.19 the results are shown for a stable setpoint, these results confirms the hypothesis that a Youla controller is able to stabilize the plant with actuator dynamics and delay for all velocities.

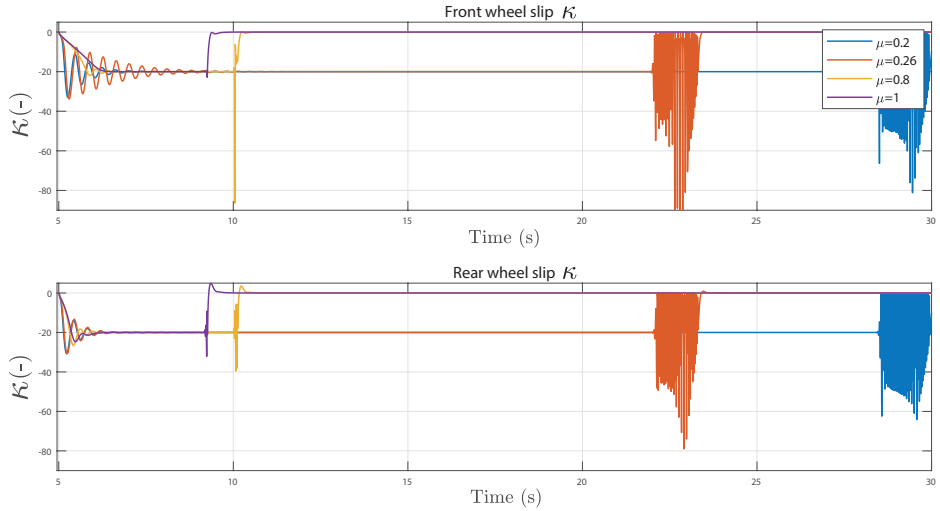

Figure A.18: The controlled front and rear wheel slip κ_f and κ_r for different road conditions with initial velocity $u_{init} = 40$. Controller: K_3. Slip setpoint $\kappa = 20$.

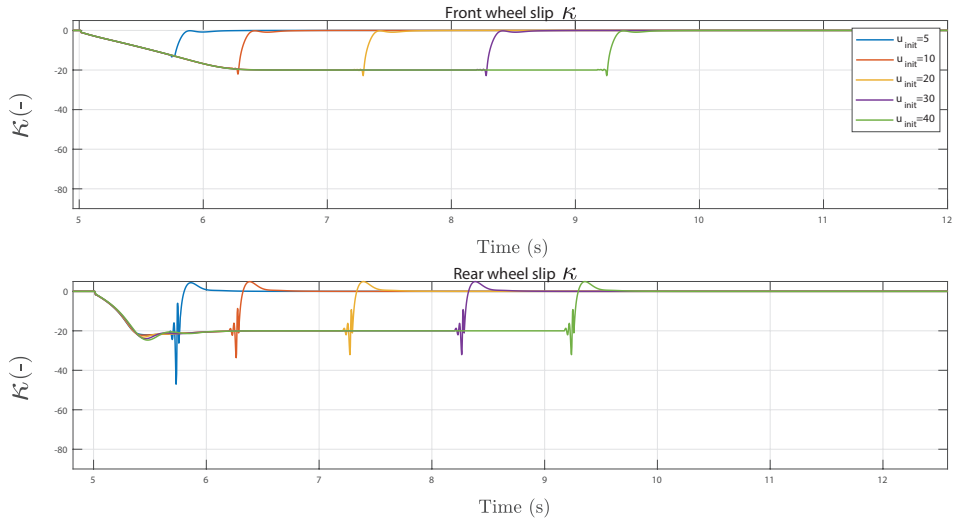

Figure A.19: The controlled front and rear wheel slip κ_f and κ_r for different initial velocities on dry surface $\mu_{max} = 1$. Controller: K_3. Slip setpoint $\kappa = 20$.

A.3 Neural network

	One hidden layer	Two hidden layers	Three hidden layers
5 Neurons	0.1615	0.1015	0.1152
10 Neurons	0.1010	0.0631	0.1683
13 Neurons	0.0980	0.0616	0.1808
14 Neurons	0.0954	0.0601	0.1765
15 Neurons	0.0932	0.0592	0.1582
16 Neurons	0.0921	0.0598	0.1893
17 Neurons	0.0889	0.0621	0.1921
20 Neurons	0.0758	0.0645	0.1363
25 Neurons	0.0915	0.0721	0.1533

Table A.1: Root mean squared error for different configurations.

B. Parameters

B.1 Magic formula 1989

Parameter	Value
b_0	1.6
b_1	0
b_2	1000
b_3	0
b_4	100
b_5	0
b_6	0
b_7	0
b_8	0
b_9	0
b_{10}	0
b_{11}	0
b_{12}	0
λ_{cx}	1
λ_{kx}	1
λ_{hx}	1
λ_{cx}	1
λ_{ex}	1

Table B.1: Magic formula 1989 parameters.

B.2 Magic formula 2002

B.2.1 Longitudinal force F_x

$$F_x = (D_x \sin(C_x \arctan(B_x\kappa_x - E_x(B_x\kappa_x - \arctan(B_x\kappa_x)))) + S_{Ix}) \cdot G_{x\alpha}$$

with pure slip coefficients

$$\begin{aligned}
C_x &= p_{Cx1} \cdot \lambda_{Cx} \\
D_x &= \mu_x \cdot F_z \\
\mu_x &= (p_{Dx1} + p_{Dx2} df_z) \cdot \lambda_{\mu x} \\
E_x &= \left(p_{Ex1} + p_{Ex2} df_z + p_{Ex3} df_z^2\right) \leq 1 \\
K_x &= F_z \cdot (p_{Kx1} + p_{Kx2} df_z) \cdot \exp\left(p_{Kx3} df_z\right) \cdot \lambda_{Kx} \\
B_x &= \frac{K_x}{C_x D_x}
\end{aligned}$$

and combined slip coefficients

$$\begin{aligned}
G_{x\alpha} &= \cos(C_{x\alpha} \arctan(B_{x\alpha}\alpha)) \\
B_{x\alpha} &= r_{Bx1} \cos(\arctan(r_{Bx2}\kappa)) \\
C_{x\alpha} &= r_{Cx1}
\end{aligned}$$

B.2.2 Longitudinal force F_y

$F_y = G_{y\kappa} F_{yz}$

with pure slip coefficients

$$
\begin{aligned}
F_{yp} &= D_y \sin(C_y \arctan(B_y\alpha_y - E_y(B_y\alpha_y - \arctan(B_y\alpha_y)))) + S_{Vy\gamma} \\
S_{Hy} &= p_{Hy3} \cdot \gamma \\
S_{Vy\gamma} &= F_z \left(p_{Vy3} + p_{Vy4} df\right) \cdot \gamma \cdot \lambda_{\mu y} \\
\alpha_y &= \alpha + S_{Hy} \\
B_y &= \frac{K_{y\alpha}}{C_y D_y} \\
C_y &= p_{Cy1} \lambda_{Cy} \\
D_y &= \mu_y \cdot F_z \cdot \\
\mu_y &= \left(p_{Dy1} + p_{Dy2} df_z\right) \cdot \left(1 - p_{Dy3}\gamma^2\right) \cdot \lambda_{\mu y} \\
E_y &= \left(p_{Ey1} + p_{Ey2} df_z\right) \cdot \left(1 - p_{Ey4}\gamma\right) \operatorname{sgn}\left(\alpha_y\right)) \lambda_{Ey} \leq 1 \\
K_{y\alpha} &= p_{Ky1} \cdot F_{z0} \cdot \sin\left[p_{Ky4} \arctan\left\{\frac{F_z}{\left(p_{Ky2} + p_{Ky5}\gamma^2\right) F_{z0}}\right\}\right] \cdot \left(1 - p_{Ky3}|\gamma|\right) \cdot \lambda_{Ky\alpha}
\end{aligned}
$$

and combined slip coefficients

$$
\begin{aligned}
G_{y\kappa} &= cos(C_{y\kappa} \cdot \arctan(B_{y\kappa}\kappa)) \\
C_{y\kappa} &= r_{Cy1} \\
B_{y\kappa} &= r_{By1} \cdot cos(\arctan(r_{By2}\alpha))
\end{aligned}
$$

B.2.3 Self aligning moment M_z

$M_z = -t \cdot (F_y - S_{iyx}) + M_{zr} + s \cdot F_x$

where the pneumatic trail t can be calculated with

$$
\begin{aligned}
t &= D_t \cos\left[C_t \arctan\left\{B_t\alpha_{t,eq} - E_t\left(B_t\alpha_{t,eq} - \arctan\left(B_t\alpha_{t,eq}\right)\right)\right\}\right] \cdot \cos\left(\alpha_M\right) \\
B_t &= \left(q_{Bz1} + q_{Bz2} df_z + q_{Bzz} df_z^2\right) \cdot \left(1 + q_{Bz4}\gamma + q_{Bzs}|\gamma|\right) \cdot \frac{\lambda_{Ky\alpha}}{\lambda_{\mu y}} \\
C_t &= q_{Cz1} \\
D_t &= F_z \cdot \left(q_{Dz1} + q_{Dz2} df_z\right) \cdot \left(1 + q_{Dz3}\gamma + q_{Dz4}\gamma^2\right) \cdot \frac{R_0}{F_{z0}} \cdot \lambda_t \\
E_t &= \left(q_{Ez1} + q_{Ez2} df_z + q_{Ez3} df_z^2\right) \cdot \left(1 + \left(q_{Ez4} + q_{Ez5}\gamma\right) \cdot \left(\frac{2}{\pi}\right) \cdot \arctan\left(B_t C_t \alpha_t\right)\right) \leq 1
\end{aligned}
$$

for combined slip:

$$
\begin{aligned}
\alpha_{t,eq} &= \arctan \sqrt{\tan^2\left(\alpha_t\right) + \left(\frac{K_{xx}}{K_{y\alpha}}\right)^2 \kappa^2} \operatorname{sgn}\left(\alpha_t\right) \\
\alpha_{r,eq} &= \arctan \sqrt{\tan^2\left(\alpha_r\right) + \left(\frac{K_{x\kappa}}{K_{y\alpha}}\right)^2 \kappa^2} \operatorname{sgn}\left(\alpha_r\right) \\
s &= \left(s_{sz2}\left(\frac{F_y}{F_{z0}}\right) + \left(s_{sz3} + s_{sz4} df_z\right)\gamma\right) R_0 \lambda_s
\end{aligned}
$$

with

$$
\begin{aligned}
\alpha_t &= \alpha_M + S_{Ht} \\
\alpha_r &= \alpha_F + S_{Hy} + \frac{S_{Vy\gamma}}{K_{y\alpha}} \\
S_{Ht} &= q_{Hz1} + q_{Hz2} df_z + \left(q_{Hz3} + q_{Hz4} df_z\right) \cdot \gamma
\end{aligned}
$$

The residual moment M_{zr}

$$M_{zr} = D_r \cos\left[\arctan\left(B_r \alpha_{r,eq}\right)\right]$$
$$D_r = F_z R_0 cos(\alpha)(q_{Dz8} + q_{Dz9} df_z \cdot \gamma) \cdot \lambda_{Kzy}) \cdot \lambda_{\mu y}$$
$$B_r = q_{Bz9} \cdot \frac{\lambda_{Ky\alpha}}{\lambda_{\mu y}} + q_{Bz10} \cdot B_y \cdot C_y$$

C. requirements

C.1 AEB

Autonomous Emergency Braking (AEB) is braking that is applied automatically by the vehicle in response to the detection of a likely collision. The primary goal of AEB technology is to prevent crashes by detecting a potential conflict and alerting the driver, and, in many systems, aiding in brake application or automatically applying the brakes. Systems that work mostly at lower speed are referred to as AEB City systems, those that function at higher speeds, AEB Inter-Urban systems. [25]

C.1.1 Requirements

In [30] the characteristics of AEB systems that were identified as being in current production vehicles at the time the literature review and industry surveys were carried out are identified. The requirements are derived from these characteristics. A distinction is made between different requirement categories. The control strategy requirements, general requirements, operational limit requirements and the sensor system are given respectively in Sections C.1.1.1, C.1.1.2, C.1.1.3 and C.1.1.4.

C.1.1.1 Control strategy requirements

The AEB system can be toggled on and of manually. However the system is automatically deactivated when;

- The sensor view is 'blinded' during periods of heavy rain, snow etc.
- The sensor head is impaired because of debris build-up.
- A system fault is detected.

The system is ineffective under the following circumstances:

- There is a sudden encounter such as a vehicle cutting immediately in front.
- Sudden acceleration is applied and the preceding vehicle is becoming too close.
- The distance between vehicles is extremely short.
- The overlap with the preceding vehicle is small.

It can be seen that the circumstances in which an AEB system is fully effective is quite limited. Effectively, the AEB system is only fully functional in front to rear collisions on straight roads in good weather conditions, where both vehicles are in the same lane.

C.1.1.2 General requirements

An AEB shall satisfy the following general requirements:

- The AEB system is able to identify a front to rear shunt collision on a straight road.
- Collision risk judgment algorithm update frequency is approximately 50 Hz.
- The AEB system is able to identify all moving and stationary vehicles, including motorcycles travelling centrally in lane; excluding pedestrians and smaller two wheeled vehicles travelling in edge of lane.

C.1.1.3 Operational limit requirements

- Operative velocity range is between 10 and 180 km/h, or $\leq$ 70 km/h if approaching a stationary obstacle.
- Relative velocity between preceding vehicle and subject vehicle for activation AEB is $>$ 10 km/h.
- Maximum achievable deceleration depending on surface conditions for light vehicle are approximately: Dry surface 1g; Wet surface 0.65g and icy surface 0.20g.
- Brake system reaction time 0.2 to 0.3 seconds.

C.1.1.4 Sensor system

The allowed sensors camera, LIDAR and RADAR should satisfy the following requirements:

- Sensor range ahead of vehicle(m): short range 30; long range 200;
- Horizontal field of view: 16.9 $\pm$ 3.8 degrees
- Vertical field of view: 4 $\pm$ 1.5 degrees
- Sensor scanning rate: 10 Hz

C.1.1.5 Performance

Euro NCAP rates AEB systems of cars based on their performance on their test scenarios. There are three scenarios namely CCRs, CCRm and CCRb:

Car-to-Car Rear Stationary (CCRs) – a collision in which a vehicle travels forwards towards another stationary vehicle and the frontal structure of the vehicle strikes the rear structure of the other.
Car-to-Car Rear Moving (CCRm) – a collision in which a vehicle travels forwards towards another vehicle that is travelling at constant speed and the frontal structure of the vehicle strikes the rear structure of the other.
Car-to-Car Rear Braking (CCRb) – a collision in which a vehicle travels forwards towards another vehicle that is travelling at constant speed and then decelerates, and the frontal structure of the vehicle strikes the rear structure of the other.

All three scenarios are illustrated in Figure C.1. The vehicle sponsor will fund 10 verification tests per scenario, where applicable. For AEB City, 10 tests in CCRs (10-50km/h). For AEB Inter-Urban, 10 tests for AEB (CCRm). The end of a test is considered when one of the following occurs:

- Velocity subject vehicle is 0 km/h.
- Velocity subject vehicle is lower than preceding vehicle.
- A collision between subject vehicle and preceding vehicle.

When a collision occurs the relative velocity is measured. Based on these measurements the performance is rated.

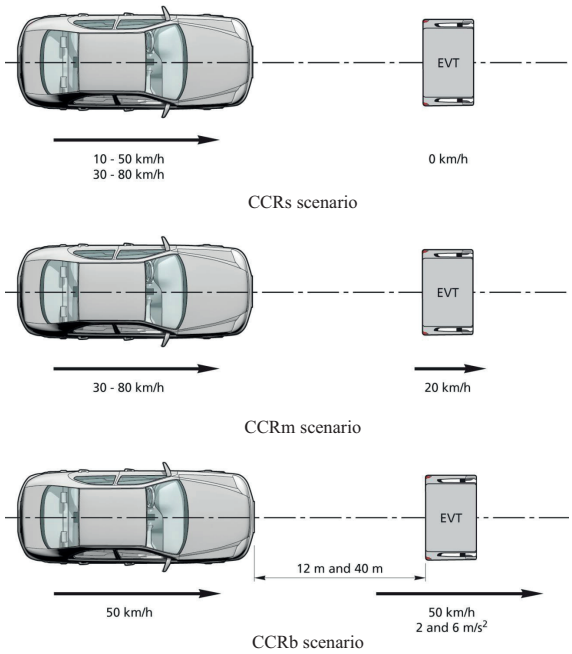

Figure C.1: Test scenarios. [26]

C.2 ACC

Adaptive cruise control(ACC) originates from Cruise Control(CC), which today is a widespread functionality in modern vehicles. CC controls the vehicle speed actuating the throttle only, via tracking of speed v that is set by the driver. ACC automatically adapts the vehicle's speed depending on a predecessor's behavior, actuating the throttle as well as the brake system.[45] The goal of ACC is a partial automation of the longitudinal vehicle control and the reduction of the workload of the driver with the aim of supporting and relieving the driver in a convenient manner. The main system function of Adaptive Cruise Control is to control vehicle speed adaptively to a preceding vehicle by using information about: the distance from the ACC equipped vehicle to the preceding vehicle in the same lane, the motion of the ACC equipped vehicle and the preceding vehicle and lastly the driver commands (see Figure C.2). Based upon the information acquired, the controller sends commands to actuators for carrying out its longitudinal control strategy and it also sends status information to the driver.

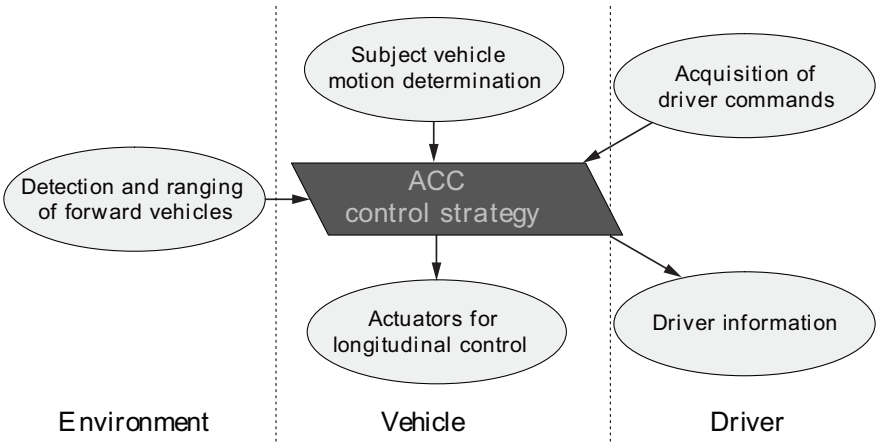

Figure C.2: Functional ACC elements[15]

C.2.1 Requirements

In this section all requirements for an "Adapative Cruise Control" system following the ISO 15622 [15] are presented. A distinction is made between different requirement categories. The control strategy, following capability and operational limit requirements are given respectively in Sections C.2.1.1, C.2.1.2 and C.2.1.3.

C.2.1.1 Control strategy requirements

An ACC system shall, as a minimum, provide the following control strategy and state transitions shown in Figure C.3. The following requirements constitutes the fundamental behaviour of ACC systems:

- When the ACC is active, the vehicle speed shall be controlled automatically either to maintain a clearance (distance from the preceding vehicle to the subject vehicle), or to maintain the set speed, whichever speed is lower. The change between these two control modes is made automatically by the ACC system.
- The steady-state clearance may be either self-adjusting by the system or adjustable by the driver.
- The transition from "ACC stand-by" to "ACC active" shall be inhibited if the subject vehicle's speed is below a minimum operational speed, v_{low}. Additionally, if the vehicle's speed drops below v_{low} while the system is in the "ACC active" state, automatic acceleration shall be inhibited. Optionally, the ACC system may drop from "ACC active" to "ACC stand-by"
- If there is more than one forward vehicle, the one to be followed shall be selected automatically.

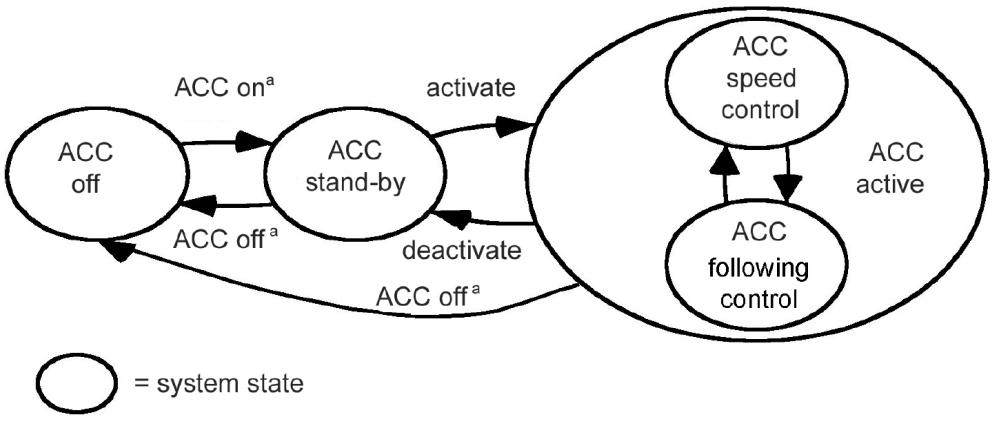

Figure C.3: ACC states and transitions. [a] is manual switching [15]

The decision which mode to use based on real-time radar measurements shall be made automatically by the ACC system . For example, if the lead car is too close, the ACC system switches from speed control to spacing control. Similarly, if the lead car is further away, the ACC system switches from spacing control to speed control. In other words, the ACC system makes the ego car travel at a driver-set speed as long as it maintains a safe distance.[7]

C.2.1.2 Following capability requirements

- τ_{min} shall be the minimum selectable time gap for following control mode under steady-state conditions for all speeds v. τ_{min} shall be $>$ 0,8 s. The time gap is calculated from vehicle speed v and clearance c by: $\tau = \frac{c}{v}$.

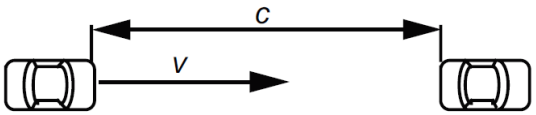

Figure C.4: Illustration of clearance. [15]

- At least one time gap setting τ in the range of 1,5 s to 2,2 s shall be provided.
- Under steady-state conditions the minimum clearance shall be τ_{min} times v.
- Under transient conditions, the clearance may temporarily fall below the minimum clearance. If such a situation occurs, the system shall adjust the clearance to attain the desired clearance.

The ACC shall have detection range, target discrimination and curve capabilities as specified in the following sections:

Detection range

- If a forward vehicle is present within the distance range d_1 to d_{max} which is illustrated in Figure C.5, the ACC system shall measure the range between the forward and subject vehicles.
- If a forward vehicle is present within the distance range d_0 to d_1, the ACC system shall detect the presence of the vehicle but is not required to measure the range to the vehicle nor the relative speed between the forward and subject vehicles.
- If a forward vehicle is present at a distance less than d_0, the ACC system is not required to detect the presence of the vehicle.

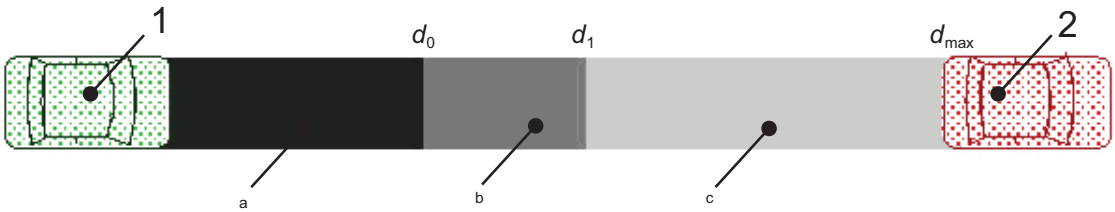

Figure C.5: Zones of detection. zone a: Detection not required, zone b: Detection of vehicles required and zone c: Determination of range required. [15]

Curve capability The ACC system shall enable a steady-state vehicle following with a time gap of $\tau_{max}(v_{circle})$, on straight roads and curves with a radius down to $R_{min} = 125m$. Therefore the system shall be capable of following a preceding vehicle with the steady-state time gap $\tau_{max}(vcircle)$, if the preceding vehicle cruises on a constant curve radius R_{min} with a constant speed v_{circle}.

Target discrimination If there is more than one preceding vehicle on straight or steady state curved roads, the preceding vehicle(red) in the subject vehicle's(green) path as shown in Figure C.6 shall be selected for ACC control.

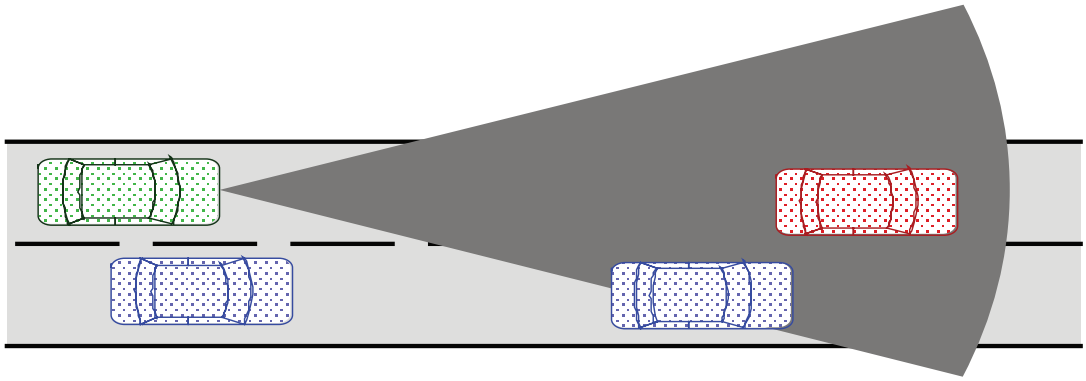

Figure C.6: Target detection. [15]

C.2.1.3 Operational limit requirements

- Automatic positive acceleration of ACC requires a vehicle speed v_{low} of at least 5 m/s.
- There shall not be a sudden brake force release in the case of an automatic deactivation of the ACC system below v_{low}.
- The minimum set speed shall be $v_{set_min} \geq 7m/s$ and $v_{set_min} \geq v_{low}$.
- The average automatic deceleration of ACC systems shall not exceed 3,5 m/s^2 (average over 2 s).
- The average rate of change of automatic deceleration (negative jerk) shall not exceed 2,5 m/s^3 (average over 1 s).
- Automatic acceleration of ACC systems shall not exceed $a_{max} \leq 2{,}0\ m/s^2$.
- If a forward vehicle is detected within the distance range d_0 to d_1 and the distance cannot be determined, the system shall inhibit automatic acceleration.